# STRESS-FUNCTION VARIATIONAL METHOD FOR STRESS ANALYSIS OF ADHESIVELY BONDED JOINTS

A Thesis
Submitted to the Graduate Faculty
of the
North Dakota State University
of Agriculture and Applied Science

By

Youhao Zhao

In Partial Fulfillment of the Requirements
for the Degree of
MASTER OF SCIENCE

Major Department:
Mechanical Engineering

May 2014

Fargo, North Dakota

# North Dakota State University
## Graduate School

Title

Stress-Function Variational Method for Stress Analysis of Adhesively Bonded Joints

By

YouHao Zhao

The Supervisory Committee certifies that this *disquisition* complies with North Dakota State University's regulations and meets the accepted standards for the degree of

MASTER OF SCIENCE

SUPERVISORY COMMITTEE:

Dr. Xiangfa Wu
Chair

Dr. Long Jiang

Dr. Majura Selekwa

Dr. Mijia Yang

Approved:

| 10/10/2014 | Dr. Alan Kallmeyer |
|---|---|
| Date | Department Chair |

## ABSTRACT

Recently, adhesively bonded joints (ABJs) has found more rapidly increasing applications in aerospace and aeronautical structures, ground vehicles, and flexible electronics than mechanical fastening and welding technologies. However, outstanding issues still exist.

This work was to develop a systematic semi-analytic method for accurate prediction of the interfacial shear and normal stresses of ABJs. Two unknown shear and peeling stress functions at each interface was first introduced in formulation, which satisfies all the traction boundary conditions. A set of governing ordinary differential equations (ODEs) was determined via triggering the theorem of minimum complimentary strain energy. Matlab® code was programmed to execute the proposed method. Furthermore, the present method was validated by finite element method and compared with those models in the literature.

The present method is applicable for convenient scaling analysis and optimal design of ABJs and other types of ABJs such as adhesively bonded tubular and composite joints, etc.

## ACKNOWLEDGMENTS

I would like to express my sincere gratitude to my advisor, Dr. Xiangfa Wu, whose expertise, guidance and support added considerably to my graduate experiences at NDSU. I appreciate his in-depth understanding and insight in this field, scientific seriousness in my thesis research, and helpful and constructive criticism in my thesis writing. I would like to thank the other members of my graduate study supervisory committee: Dr. Long Jiang, Dr. Majura Selekwa, and Dr. Mijia Yang for the assistance they provided.

I recognize that this research of the thesis would not be possible finished without the support of NSF, ND NASA EPSCoR, the Faculty Research Initiative Grant, and the Department of Mechanical Engineering at NDSU.

In the last, I would like to thank my parents for instilling in my confidence and a drive for pursuing my Master Degree.

**TABLE OF CONTENTS**

## LIST OF FIGURES

# 1. INTRODUCTION

In the past five decades, adhesively bonded joints (ABJs) have been successfully structured in broad fields with the developments in adhesive chemistry and joining technology. Today, high-performance ABJs with compact design, high load-carrying capacity, and high mechanical strength and durability have been successfully integrated into broad primary structures in aerospace, aeronautic, and ground vehicles. The technology of ABJs has also been utilized in microelectronic packaging and personal electronic devices such as built-in contact lenses in camera, foldable cell phones, smart skin temperature monitors, etc.

Due to the unique features of adhesive bonding, it is crucial to understand the mechanical behavior of ABJs such as the mechanical strength, durability, and environmental (e.g., temperature, humidity, corrosion, etc.) response when integrated in structures. It is the common sense that stress concentrations exist at the edges of the overlap bonding lines due to the mismatch of mechanical properties of neighboring adherends. It has been well studied in the literature that shear stress of ABJs concentrates at the edges of overlap bonding lines; however, only a small portion of load is carried by the region far away the edges (Suo, 2012), so does the normal stress. Such high interfacial stresses near the free edges of the adherends are responsible for the debonding failure of ABJs in reality. In addition, more complicated stress field could arise in ABJs under the action of combined mechanical or thermomechanical loads. It is essential to gain an accurate stress analysis of ABJs for improving structural design and prediction of the mechanical durability of ABJs. Therefore, efficient, high-accuracy models of ABJs that are capable of comprehensively taking into account the effects of material properties (Young's modulus, Poisson's ratio, coefficients of

thermal expansion, etc.), design parameters, and external mechanical and thermomechanical loadings are still highly desired.

Substantial investigations on the stress and strength analysis of ABJs have been performed and reported in the literature in the past five decades. In the view of engineering, most of the pioneering works on stress analysis of ABJs carried their technical deficiencies due to their oversimplifications of the analytic models of ABJs. First of all, the stress fields derived from these joint models do not accurately satisfy the traction boundary conditions at the free edges of the adherends and adhesive layers. In fact, there are supposed to be shear-free at the free-edges of the adherends and adhesive layers. However, most of the analytic models reported in the literature, even including those well documented in some major engineering textbooks, simply indicated that the maximum value of shear stresses appears at the edge of adherends. Secondly, in these ABJ models, stresses and strains of the adhesive layers do not obey the generalized Hooke's law, which also violate the assumption of small stress and strain variation across the adhesive layers as commonly adopted in almost all the literature models of ABJs.

The purpose of this thesis work was to extend the stress-function variational method developed recently by Wu and Jenson (2011) in the research group for accurately determining the stress field in ABJs. In this approach, in the typical case of adhesively bonded strap joints in planar stress state, two unknown interfacial shear and normal stress functions are introduced at each adherend/adhesive interface. The axial normal stresses in the adherends and adhesive layer are assumed to vary linearly, following the elementary *Euler-Bernoulli* beam theory. The transverse normal stress and shear stress in the adherends and adhesive layer are determined according the stress equilibrium equations of two-dimensional (2D) elasticity. With the aid of the theorem of minimum complementary strain energy, a set of four coupled $4^{th}$-order ordinary

differential equations (ODEs) is derived for determining the unknown interfacial stress functions. The gained set of governing ODEs is further solved efficiently by using eigenfunctions of the resulting eigenvalue problem. Correspondingly, a robust, efficient, compact MATLAB™ code is developed for determining the entire stress field in ABJs with varying geometries, material properties, and external loadings. Detailed finite element analysis (FEA) based on commercial software package (i.e., ANSYS™) is performed to validate the numerical accuracy of the present semi-analytic ABJ models. These results show a major advantage of the proposed method for scaling analysis of stress variation and optimal design of ABJs.

# 2. LITERATURE REVIEW

## 2.1. Structural Joining Technology

Joining technology could be first invented by human ancestor in making spear that typically consisted of stone flakes bonded to a wood handle by tar for hunting (Mazza et al., 2006). After thousands of years of development, joining technology has been finding rapidly expanding applications in civil structures, aerospace, aeronautical and ground vehicles, and microelectronics (e.g., microchip packaging). Compared to mechanical bolts, rivets, and welds, ABJs are overwhelmingly welcome due to their compact design, low manufacturing cost, enhanced mechanical durability, sound noise suppression, and obvious reduction of weight (Tomblin & Davies, 2004). ABJs have been widely accepted and increasingly used for the purpose of load transfer and structural connection in civil structures (Goncalves et al., 2002). In aerospace engineering, for instance, stringers and metallic honeycomb assemblies are made of multiple ABJs, which are economically preferable (Higgins, 2000). ABJs have also made a significant impact to weight reduction of a variety of joint structures, especially for spacecrafts and aircrafts. A typical example is the birth of Airbus A300 (Racker, 2004), in which ABJs have been used in the primary structures. ABJs also play an essential role in flexible electronics, where thermomechanical stresses are a common factor causing the structural failure. (Timoshenko, 1915; Chen & Nelson, 1979; Suhir, 1989). The problem of function degradation in microelectronics has attracted growing technical concern over the past three decades (Eischen et al., 1990; Suo, 2003). It is technically important to understand the high interfacial stresses near the free edges of stiff silicon microchips bonded onto compliant polymeric substrate (Lu et al., 2007; Kim & Rogers, 2008; Suo, 2012). Bonded joints are better employed in the applications of flexible

electronics due to their high mechanical durability (Jiang & Khang, 2008; Sun, 2013). Therefore, it is recommendable for structural analysts to wisely select the types of adhesives, which have high strength and mechanical durability under various loading and thermal conditions (Wu et al , 2014).

## 2.2. Current Understanding

In the past six decades, a significant number of theoretical and experimental investigations have been made on the mechanical strength and durability of ABJs. Fig. 2.1 illustrates the typical failure modes of ABJs. Historically, Volkersen (1938) was the first to consider the adhesive layer in ABJs as a continuously shear spring and find the maximum singular stresses at the edges. Volkersen's ABJ model has the advantage of simplicity but it ignores the role of normal stress in the failure criterion. An improved approach was fulfilled by Goland and Reissner (1944) with the assumption of uniform distribution of the peeling and shear stresses across the adhesive layer, which became one of classic models of adhesively bonded single-lap joints extensively cited in the literature since then. Volkersen's and Goland and Reissner's ABJ models and their interfacial stress solutions have been adopted in many popular textbooks for design and strength analysis of ABJs. Yet, two obvious limitations can be easily identified from these ABJs as follows. Firstly, the peak shear stress appears at the adherend ends, which conflicts with the shear-free condition at the free-ends; secondly, the stress variation across the adhesive layer is neglected due to ignorance of the thin adhesive layer. After the above two classic ABJ models, a significant number of theoretical follow-ups have been made. To mention a few, Delale et al. (1981) formulated an efficient ABJ model based on elementary *Euler-Bernoulli* beam theory to take into account all the mechanical properties and geometries of the ABJs, in which they treated the adherends as *Euler-Bernoulli* beams and the adhesive

layer was ignored due to its negligible deformation across the thickness. However, the interfacial shear stress determined by this ABJ model does not satisfy the shear-free condition at the adherend ends. Chen and Cheng (1983) developed an innovative ABJ model within the framework of 2D elasticity. In this ABJ model, the stress fields in the upper and lower adherends are expressed in terms of two unknown peeling stresses according to the elementary *Euler-Bernoulli* beam theory and the stress equilibrium equations of 2D elasticity, while the stress variation across the adhesive layer is ignored. A gained set of governing ODEs of the peeling stresses along the interface was determined via triggering the theorem of complementary strain energy. This model is capable of predicting the reasonable location of the peak interfacial shear stress, which is located at a distance about 20% from the free end of adherend. In addition, Frostig (1997) used a high-order theory to overcome the limitations of the elastic foundation formulation. Her (1999) constructed several analytic models for stress analysis of adhesively bonded single-lap joints as well as double lap joints based on a simple tension-bar approach. Mortensen and Thomsen (2002) carried on the study of stress distribution in adhesively bonded composite joints. Kadioglu (2003) discovered that the environmental temperature had a proportional relation in load transfer through adhesive joints. Keller (2004) developed an analytical solution of stress-strain relation in an ABJ, from which a parameter study of the overlap length and thickness of layers was demonstrated. In addition, classical laminate plate theory was also introduced for stress analysis of ABJs including adhesively bonded composite joints (Xiao, 2004). da Silva and Adams (2006) further developed a numerical analysis based on Kadioglu's study in double lap joints. Chataigner (2010) formulated an improved method based on Volkersen's shear-lag theory for stress analysis of double-lap joints. Recently, Sayman (2012) proposed an analytical elastoplastic model of ABJs, which was verified by FEA. Finally, Sayman also conducted an analytic study and concluded that the

strength of ABJs can be increased via introducing proper residual stresses. Kumar and Scanlan (2013) developed a stress function method for stress analysis of adhesively bonded tubular joints. Yousefsani and Tahani (2013) formulated a model of layerwise ABJs, from which the divided sub-layers were treated as field variables and solved through a set of governing ODEs by evoking the theorem of minimum strain energy. Nevertheless, outstanding issues still exist when applying the above ABJ models for determining the stress field in adhesively bonded composite joints, in which stress singularity occurs at the end of binding lines and laminate interfaces. In fact, transverse deformation plays an essential role in delamination failure of composite joints, in which the transverse modulus of composite laminates is very low. Technically, the classic and high order laminated plate theories are unable to successfully predict the high stress concentration in composite joints due to the nature of laminated structures and limitation of the classic laminated plate theory (Renton & Vinson, 1975; Yang & Pang, 1996; Seltzer & Klang, 2003; Yang, 2004). Owing mainly to the technical compromises in the above models, the shear-free condition at adherend ends, the stress continuity across the bonding lines, and the stress variation between the adhesive layers were not well satisfied. Theoretically speaking, the interfacial shear and peeling stresses predicted by FEA (Diaz, 2009) had the singular values near the adherend ends, which tended to higher and higher in a way of refining the mesh in FEA process. With the aid of FEA, computational stress field indicated that both the shear and normal stresses reached the maximum values at the ends of bonding lines, and these stresses declined and tended to almost zero at the middle portion of the bonding lines (Ozel, 2014).

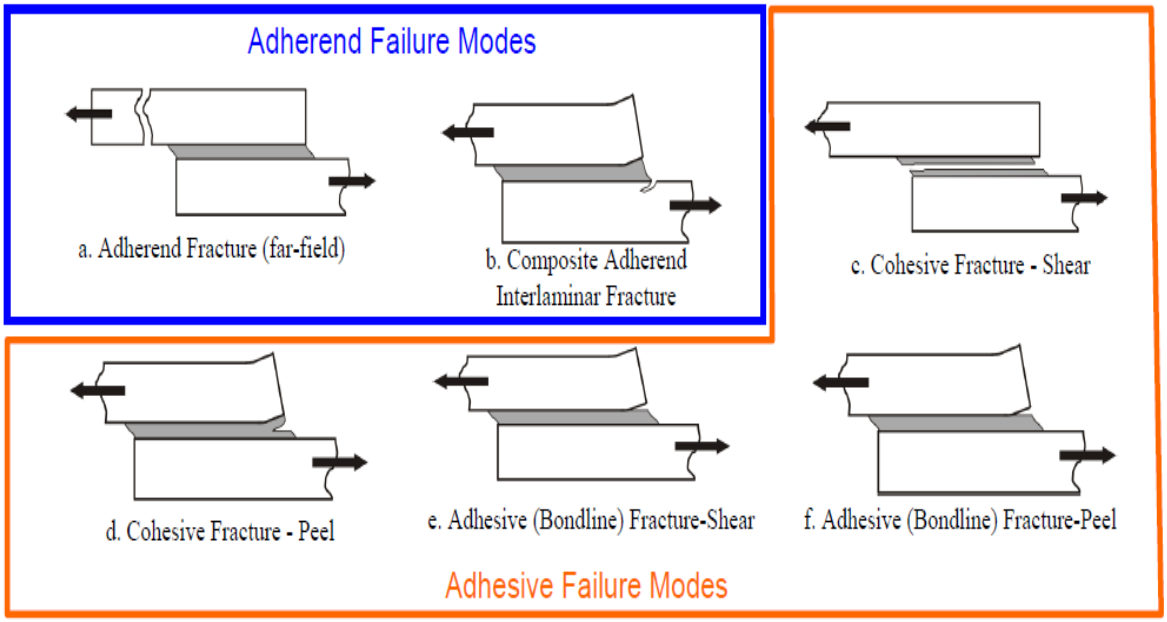


Figure 2.1. Typical failure modes of adhesively bonded joints (Heslehurst & Hart-Smith, 2002).

Recently, a systematic semi-analytic method was developed for accurate prediction of the interfacial stresses of bonded joints subjected to external mechanical and/or thermomechanical loadings (Wu & Jenson, 2011). In this method, two unknown interfacial shear and peeling stress functions were first introduced independently. By adopting the elementary *Euler-Bernoulli* beam theory, the axial normal stress was approached varying linearly across the adherend layers. The transverse normal stress and shear stress were determined to satisfy the static equilibrium equations, traction boundary conditions at the top and bottom surfaces of adherends, and stress continuity across adhesive layer. Furthermore, the entire stress field in the joint was expressed in terms of the unknown interfacial stress functions. Followed by the theorem of minimum complimentary strain energy of the joint, a set of governing ODEs in terms of two interfacial normal and shear stress functions was established, and an efficient eigenfunction method was used to solve the set of the resulting ODEs. The entire solving process was finally implemented via

designing a robust efficient MATLAB$^{TM}$ code that involved all the mechanical properties, geometries and external mechanical or thermomechanical loads of the joint. As a result, the entire stress field of the bonded joints can be determined accurately, which was validated by using FEM based on a commercial FEA software package (ANSYS$^{TM}$)

## 2.3. Outstanding Problems in Stress Analysis of Bonded Joints and ABJs

To date, considerable research has been conducted for determination of the interfacial shear and normal stress distribution in ABJs made of dissimilar adherends. By manipulating the geometry and loading of the ABJs, there are five typically structural ABJs, as illustrated in Fig. 2.2, which will be demonstrated for determining the interfacial shear and normal stresses by extending Wu and Jenson's (2011) stress-function variational method for bonded joints in this thesis study. The stress-field results of these typical ABJs will be validated by using FEM and comparing with literature ABJ models.

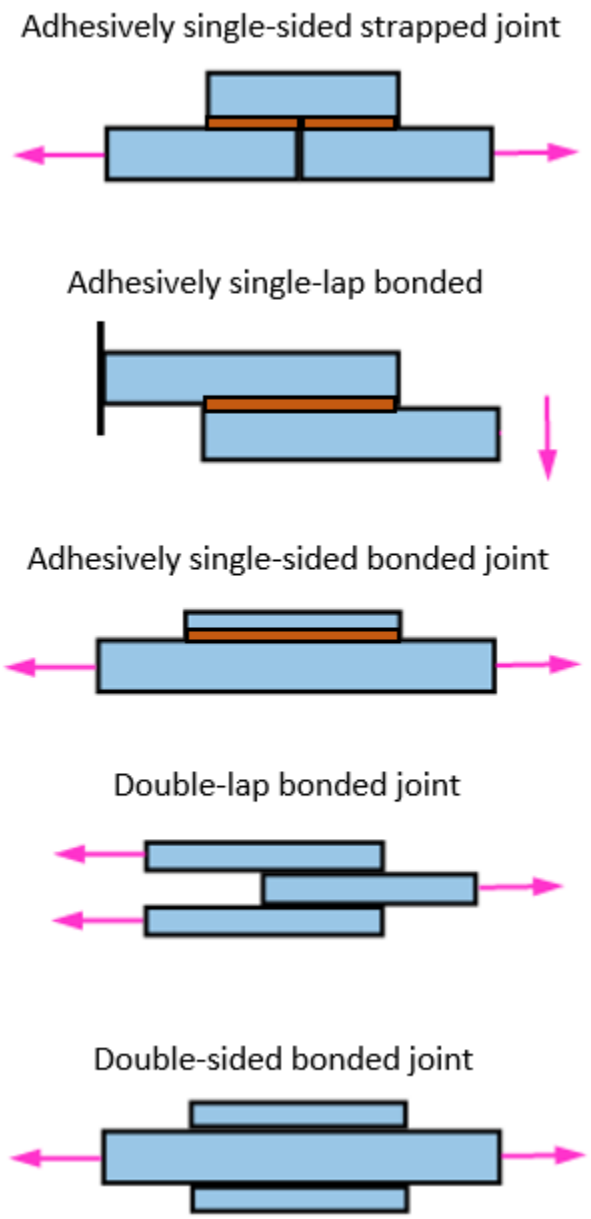


Figure 2.2. Typical adhesively bonded joints (ABJs) and bonded joints.

To further extend the work of stress-function variational method (Wu & Jenson, 2011), Chapter 3 is going to demonstrate the formulation of extended stress-function variational method in details for stress analysis of adhesively single-sided strap joint consisting of two slender substrate layers (adherends) and a slender cover layer, which are bonded with an adhesive layer. The joint under consideration is assumed

under action of a uniform axial tension along the substrate layers. Due to the structural and load symmetries of the joint, the entire stress analysis is implemented on the half-joint model subjected to uniform axial tension far away on the substrate layer. Four unknown interfacial shear and normal stress functions are introduced for the model formulation. A set of four coupled $4^{th}$-order ODEs is set up, which is solved numerically by designing an efficient MATLAB™ code. Furthermore, comparison of the stress results yielded from the present ABJ model with those obtained by ANSYS™ is demonstrated. Moreover, the effectiveness of temperature change in determining the stress field of the joint is further given. This generalized method is also applicable for stress analysis of a wide variety of other joined structures (Wu & Zhao, 2013).

In Chapter 4, the stress-function variational method is further applied for stress analysis of adhesively bonded single-lap joint comprising of a slender upper adherend layer and a slender bottom adherend layer bonded with an adhesive layer under shear traction. In this chapter, the model results not only show a very good agreement of the newly obtained ABJ results with those gained by ANSYS™, but also are compared with those given by Erdogan's simple joint model (Delale et al., 1981).

Chapter 5 further extends the stress-function variational method developed in Chapter 3 for stress analysis of adhesively bonded single-sided joint, double lap bonded joint, and double-sided bonded joint. Corresponding FEA models are formulated to validate these semi-analytic joint models by comparing the distributions of interfacial stresses.

Chapter 6 summaries the current research and expects the future work following the thesis work.

# 3. GENERALIZED STRESS-FUNCTION VARIATIONAL METHOD FOR STRESS ANALYSIS OF ADHESIVELY BONDED JOINTS

## 3.1. Problem Formulation—Adhesively Single-sided Strap Joints

### 3.1.1. Model Formulation

In this chapter, a generalized stress-function variational method is to be formulated for determination of the stress field in an adhesively single-sided strap joint (ASSJ) subjected to mechanical and/or thermomechanical loadings. The stress field in an ASSJ determined by the proposed method can be expressed explicitly, which will be further validated via comparison with those obtained by commercial FEA software package (ANSYS$^{TM}$). Due to the mismatch of material properties across the bonding interfaces, high interfacial stresses in a complicated three-dimensional (3D) stress state occur near the free edges of bonding patch. To simplify the process of stress analysis, the ASSJ under consideration is dealt in two-dimensional (2D) stress/strain state by assuming that the joint width to be infinitely long. During the formulation of the ASSJ model for stress analysis, a representative segmental element of the ASSJ consists of a cover layer, adhesive layer, and substrate layer in 2D.

The configuration of ASSJ is illustrated in Fig. 3.1(*a*), where the overlap bonding length is denoted as $L$. For the convenience of the model formulation, subscripts 1, 0, and 2 are attached to the cover, adhesive, and substrate layers, respectively. These three layers have the geometrical parameters of thicknesses $h_i$ ($i$ = 1,0,2) and mechanical properties of Young's moduli $E_i$ ($i$ =1,0,2), Poisson's ratios $\nu_i$ ($i$ = 1,0,2), and coefficients of thermal expansion $\alpha_i$ ($i$ = 1,0,2). The width $b$ is assumed to be unit width. The $x$-coordinate in a 2D ASSJ model is chosen from the symmetric mid-span of the system; the $y$-coordinate is chosen

perpendicular to the *x*-coordinate and along the layer edge. As aforementioned, the external loading can be axial tension, shear traction, bending moment, or temperature change, or their combination. In this upcoming derivation, the ASSJ is treated in *plane-stress* state and subjected to a uniform tensile traction $p_0$ far away the substrate layer; meanwhile the joint has a uniform temperature change $\Delta T$ from the reference temperature. Furthermore, stress analysis of the ASSJ is made on the right half-portion as shown in Fig. 3.1 (*b*); the mechanical and thermomechanical loadings can be treated separately due to the nature of linear stress analysis according to the method of superposition. From Fig. 3(*c*), it can be expected that interfacial shear and normal stresses are caused by the mismatch of material properties along the bonding lines; lateral deflection can be induced since the joint is not laterally symmetric. In the formulation, all the joint layers are treated as isotropic, linearly thermoelastic materials. Furthermore, to convert the results in the *plane-stress* state to those in the *plane-strain* state, it needs to replace the Young's moduli $E_i$ ($i$ = 1,0,2) by $(1-\upsilon_i^2)/E_i$, Poisson's ratios $\upsilon_i$ ($i$ = 1,0,2) by $\upsilon_i/(1-\upsilon_i)$, and coefficients of thermal expansion $\alpha_i$ ($i$ = 1,0,2) by $(1+\upsilon_i)\alpha_i$.

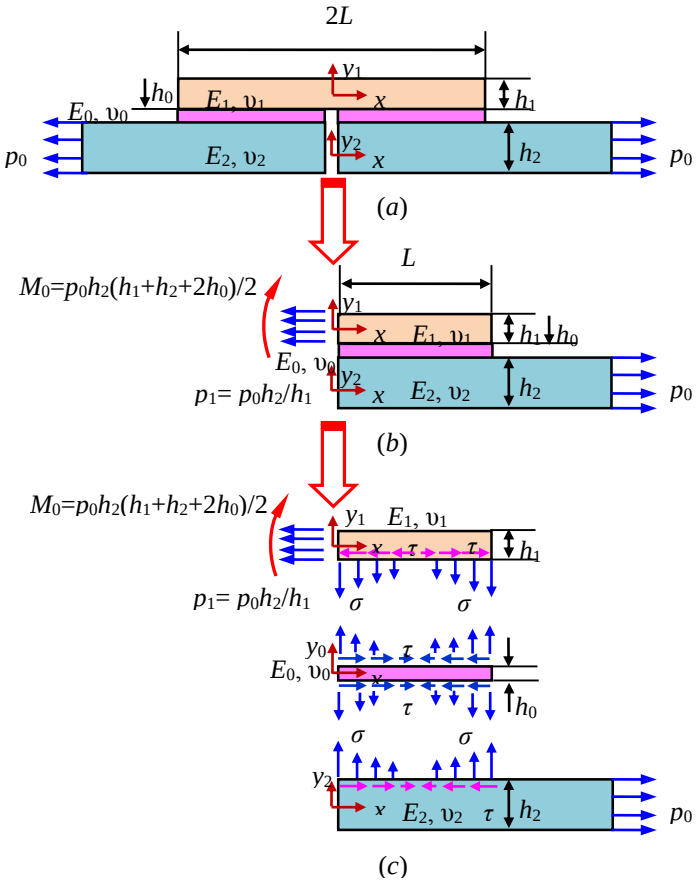


Figure 3.1. Schematic of an adhesively single-sided strap joint: (*a*) Structural configuration consisting of two identical substrate layers, two adhesive layers, and a slender cover layer, (*b*) reduced right symmetric half-joint, (*c*) distribution of the interfacial stresses in the joint.

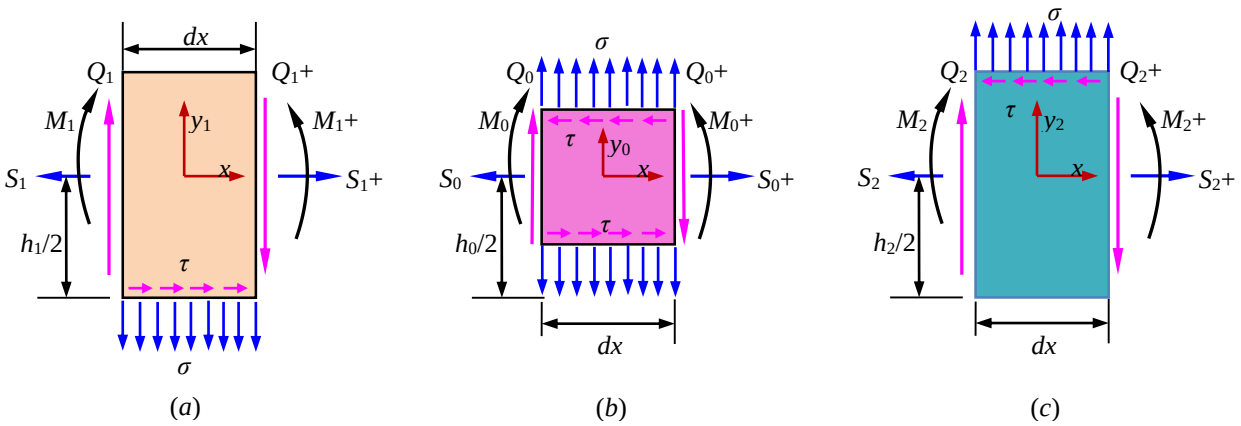


Figure 3.2. Free body diagrams of representative segmental elements of (*a*) the cover layer, (*b*) the adhesive layer, and (*c*) the substrate layer.

3.1.2. Static Equilibrium Equations

The purpose of this work is to find the stress field in the entire ASSJ, particularly the interfacial shear and peeling stresses at the interface between the upper adherend and the adhesive layer as well as the adhesive layer and the lower adherend, which can be expressed in terms of four independent unknown functions as:

$$\tau_1 = f_1(x), \text{ and } \sigma_1 = g_1(x), \tag{3.1}$$

$$\tau_2 = f_2(x), \text{ and } \sigma_2 = g_2(x), \tag{3.2}$$

As aforementioned, the free-shear at the adherend edges $x$=0 and $L$ can be expressed as:

$$f_1(0) = f_1(L) = f_2(0) = f_2(L) = 0, \tag{3.3}$$

Fig. 3.2(*a*)-(*c*) show the typical representative segmental elements, where the shear and normal (peeling) stresses can be fully determined with the static equilibrium equations in 2D elasticity with the given axial force $S_i$ ($i$ = 1,0,2), shear force $Q_i$ ($i$ = 1,0,2), and bending moment $M_i$ ($i$ = 1,0,2), which are defined according to the standard sign conventions of elementary Mechanics of Materials (Beer et al., 2011).

For the representative segmental element of the cover layer as shown in Fig. 3.2(*a*), the static equilibrium equations can be obtained as:

$$\Sigma F_x = 0 : \frac{dS_1}{dx} = -b\tau_1, \tag{3.4}$$

$$\Sigma F_y = 0 : \frac{dQ_1}{dx} = -b\sigma_1, \tag{3.5}$$

$$\Sigma M = 0 : \frac{dM_1}{dx} = Q_1 - \frac{h_1 b \tau_1}{2}. \tag{3.6}$$

Meanwhile, the static equilibrium equations of the representative segmental element of the adhesive layer [Fig. 3.2(*b*)] are expressed as

$$\Sigma F_x = 0 : \frac{dS_0}{dx} = b(\tau_1 - \tau_2)\,, \tag{3.7}$$

$$\Sigma F_y = 0 : \frac{dQ_0}{dx} = b(\sigma_1 - \sigma_2), \tag{3.8}$$

$$\Sigma M = 0 : \frac{dM_0}{dx} = Q_0 - \frac{h_0 b}{2}(\tau_1 + \tau_2). \tag{3.9}$$

Accordingly, the static equilibrium equations of the representative segmental element of the substrate layer [Fig. 3.2(*c*)] are written as

$$\Sigma F_x = 0 : \frac{dS_2}{dx} = b\tau_2\,, \tag{3.10}$$

$$\Sigma F_y = 0 : \frac{dQ_2}{dx} = b\sigma_2\,, \tag{3.11}$$

$$\Sigma M = 0 : \frac{dM_2}{dx} = Q_2 - \frac{h_2 b\tau_2}{2}. \tag{3.12}$$

3.1.3. Stress Resultants

Under the action of uniaxial tension $p_0$ far away the substrate layer, the physical conditions of the axial force, shear traction, and bending moment at the ends of the upper adherend, adhesive layer, and lower adherend are expressed respectively as:

$$S_1(0) = p_0 b h_2\,, \tag{3.13a}$$

$$S_1(L) = 0, \tag{3.13b}$$

$$Q_1(0) = 0, \tag{3.13c}$$

$$Q_1(L) = 0, \tag{3.13d}$$

$$M_1(0) = bm_0 = p_0 bh_2(h_1 + 2h_0 + h_2)/2, \tag{3.13e}$$

$$M_1(L) = 0, \tag{3.13f}$$

$$S_2(0) = 0, \tag{3.13g}$$

$$S_2(L) = p_0 bh_2, \tag{3.13h}$$

$$Q_2(0) = 0, \tag{3.13i}$$

$$Q_2(L) = 0, \tag{3.13j}$$

$$M_2(0) = 0, \tag{3.13k}$$

$$M_2(L) = 0, \tag{3.13l}$$

$$S_0(0) = 0, \tag{3.13m}$$

$$S_0(L) = 0, \tag{3.13n}$$

$$Q_0(0) = 0, \tag{3.13o}$$

$$Q_0(L) = 0, \tag{3.13p}$$

$$M_0(0) = 0, \tag{3.13q}$$

$$M_0(L) = 0. \tag{3.13r}$$

In this case, given a pure temperature change $\Delta T$ ($p_0$=0) from the reference temperature of free thermomechanical stresses, it needs to adjust all the terms involving $p_0$ to satisfy the traction-free boundary conditions (BCs) such as Eq. (3.13*a*), Eq. (3.13*e*) and Eq. (3.13*h*).

In addition, all the stress resultants for the segmental elements of the three layers can be expressed in terms of $f_i$ ($i$ = 1,2) and $g_i$ ($i$ = 1,2) as followings. With BC (3.13*i*) and integration of Eq. (3.4) with respect to $x$ from $x$ = 0, peeling-force of the cover layer yields as:

$$\int_0^x dS_1 = -\int_0^x b f_1(\xi) d\xi, \tag{3.14}$$

$$S_1(x) = p_0 b h_2 - b\int_0^x f_1(\xi) d\xi, \tag{3.15}$$

Meanwhile, shear-force of the cover layer can be written by using BC (3.13*c*) and integration of Eq. (3.5):

$$\int_0^x dQ_1 = -\int_0^x b g_1(\xi) d\xi, \tag{3.16}$$

$$Q_1(x) = -b\int_0^x g_1(\xi) d\xi, \tag{3.17}$$

Moreover, bending moment of the cover layer is expressed based on BC (3.13*e*) and integration of Eq. (3.6):

$$\int_0^x dM_1 = \int_0^x [Q_1(\xi) - \frac{h_1 b \tau_1}{2}] d\xi, \tag{3.18}$$

$$M_1(x) = m_0 b - b\int_0^x \int_0^\zeta g_1(\zeta) d\zeta d\xi - \frac{b h_1}{2}\int_0^x f_1(\xi) d\xi. \tag{3.19}$$

According to the same procedure above, the stress resultants in the adhesive layer with respect to *x* from *x*=0 can be asserted with BCs [Eq. (3.13*m*), Eq. (3.13*o*), and Eq. (3.13*q*)] and integration of Eqs. (3.7-9):

$$\int_0^x dS_0 = \int_0^x b[f_1(\xi) - f_2(\xi)] d\xi, \tag{3.20}$$

$$S_0(x) = b\int_0^x [f_1(\xi) - f_2(\xi)] d\xi, \tag{3.21}$$

$$\int_0^x dQ_0 = \int_0^x b[g_1(\xi) - g_2(\xi)] d\xi, \tag{3.22}$$

$$Q_0(x) = b\int_0^x [g_1(\xi) - g_2(\xi)] d\xi, \tag{3.23}$$

$$\int_0^x dM_0 = \int_0^x [Q_0(\xi) - \frac{h_0 b}{2}(\tau_1 + \tau_2)] d\xi, \tag{3.24}$$

$$M_0(x) = b\int_0^x \int_0^\zeta [g_1(\zeta) - g_2(\zeta)] d\zeta d\xi - \frac{b h_0}{2}\int_0^x [f_1(\xi) + f_2(\xi)] d\xi. \tag{3.25}$$

Similarly, the stress resultants in the substrate layer with respect to $x$ from $x = 0$ can be determined with BCs [Eq. (3.13*g*), Eq. (3.13*i*), and Eq. (3.13*k*)] and integration of Eqs. (3.10-12):

$$\int_0^x dS_2 = \int_0^x b f_2(\xi) d\xi, \tag{3.26}$$

$$S_2(x) = b\int_0^x f_2(\xi) d\xi, \tag{3.27}$$

$$\int_0^x dQ_2 = \int_0^x b g_2(\xi) d\xi, \tag{3.28}$$

$$Q_2(x) = b\int_0^x g_2(\xi) d\xi, \tag{3.29}$$

$$\int_0^x dM_2 = \int_0^x [Q_2(\xi) - \frac{h_2 b \tau_2}{2}] d\xi, \tag{3.30}$$

$$M_2(x) = b\int_0^x \int_0^\zeta g_2(\zeta) d\zeta d\xi - \frac{bh_2}{2}\int_0^x f_2(\xi) d\xi. \tag{3.31}$$

3.1.4. Stress Components

Due to the bending moment superimposed with a uniform axial traction $p_1$ on the cover layer, the axial normal stress can be assumed to follow the flexural stress formula according to the *Euler-Bernoulli* beam theory as:

$$\sigma_{xx}^{(1)} = \frac{S_1}{bh_1} - \frac{M_1 y_1}{I_1} = p_1 - \frac{1}{h_1}\int_0^x f_1(\xi) d\xi + \frac{12 y_1}{h_1^3}[-m_0 + \int_0^x \int_0^\zeta g_1(\zeta) d\zeta d\xi + \frac{h_1}{2}\int_0^x f_1(\xi) d\xi], \tag{3.32}$$

where, $p_1 = p_0 h_2 / h_1$. Moreover, the shear stress of the cover layer can be determined by integrating the 2D static equilibrium equation:

$$\frac{\partial \sigma_{xx}^{(1)}}{\partial x} + \frac{\partial \tau_{y_1 x}^{(1)}}{\partial y_1} = 0, \tag{3.33}$$

with respect to $y_1$ from an arbitrary point in the cover layer to the top surface $y_1 = h_1/2$ and taking into account the traction-free BC $\tau_{y_1x}^{(1)}(h_1/2)=0$, which leads to

$$\tau_{y_1x}^{(1)} = \frac{1}{h_1}[(\frac{h_1}{2}-y_1)-\frac{3}{h_1}(\frac{h_1^2}{4}-y_1^2)]f_1(x)-\frac{6}{h_1^3}(\frac{h_1^2}{4}-y_1^2)\int_0^x g_1(\xi)d\xi, \tag{3.34}$$

Furthermore, the transverse normal stress of the cover layer can be determined by integrating the 2D static equilibrium equation:

$$\frac{\partial\sigma_{y_1y_1}^{(1)}}{\partial y_1}+\frac{\partial\tau_{xy_1}^{(1)}}{\partial x}=0, \tag{3.35}$$

with respect to $y_1$ from an arbitrary point to the top surface $y_1=h_1/2$ and using the traction-free BC $\sigma_{y_1y_1}^{(1)}(h_1/2)=0$, which yields

$$\begin{aligned}\sigma_{y_1y_1}^{(1)} = &-\frac{1}{h_1}\{\frac{h_1}{2}(\frac{h_1}{2}-y_1)-\frac{1}{2}(\frac{h_1^2}{4}-y_1^2)-\frac{3}{h_1}[\frac{h_1^2}{4}(\frac{h_1}{2}-y_1)-\frac{1}{3}(\frac{h_1^3}{8}-y_1^3)]\}f_1'(x)\\ &+\frac{6}{h_1^3}[\frac{h_1^2}{4}(\frac{h_1}{2}-y_1)-\frac{1}{3}(\frac{h_1^3}{8}-y_1^3)]g_1(x).\end{aligned} \tag{3.36}$$

For the adhesive layer, given the classic *Euler-Bernoulli* beam theory and 2D static equilibrium equation, with the aid of $\tau_{y_0x}^{(0)}(h_0/2)=-f_1(x)$, $\tau_{y_0x}^{(0)}(-h_0/2)=-f_2(x)$, $\sigma_{y_0y_0}^{(0)}(h_0/2)=g_1(x)$, and $\sigma_{y_0y_0}^{(0)}(-h_0/2)=g_2(x)$, the axial, shear, and normal stress can be determined correspondingly such that

$$\begin{aligned}\sigma_{xx}^{(0)} = &\frac{S_0}{bh_0}-\frac{M_0y_0}{I_0}=\frac{1}{h_0}\int_0^x[f_1(\xi)-f_2(\xi)]d\xi\\ &-\frac{12y_0}{h_0^3}\{\int_0^x\int_0^\zeta[g_1(\zeta)-g_2(\zeta)]d\zeta d\xi-\frac{h_0}{2}\int_0^x[f_1(\xi)+f_1(\xi)]d\xi\},\end{aligned} \tag{3.37}$$

$$\begin{aligned}\tau_{y_0x}^{(0)} = &-f_2(x)-\frac{1}{h_0}(y_0+\frac{h_0}{2})[f_1(x)-f_2(x)]-\frac{3}{h_0^2}(y_0^2-\frac{h_0^2}{4})[f_1(x)+f_2(x)]\\ &+\frac{6}{h_0^3}(y_0^2-\frac{h_0^2}{4})\int_0^x[g_1(\xi)-g_2(\xi)]d\xi,\end{aligned} \tag{3.38}$$

$$\sigma_{y_0y_0}^{(0)} = g_2(x) + (y_0 + \frac{h_0}{2}) f_2'(x) + \frac{1}{h_0}[\frac{1}{2}(y_0^2 - \frac{h_0^2}{4}) + \frac{h_0}{2}(y_0 + \frac{h_0}{2})][f_1'(x) - f_2'(x)]$$
$$+ \frac{3}{h_0^2}[\frac{1}{3}(y_0^3 + \frac{h_0^3}{8}) - \frac{h_0^2}{4}(y_0 + \frac{h_0}{2})][f_1'(x) + f_2'(x)] \quad (3.39)$$
$$- \frac{6}{h_1^3}[\frac{1}{3}(y_0^3 + \frac{h_0^3}{8}) - \frac{h_0^2}{4}(y_0 + \frac{h_0}{2})][g_1(x) - g_1(x)].$$

For the substrate layer, with the aid of the classic *Euler-Bernoulli* beam theory and 2D static equilibrium equation, the axial, shear, and normal stresses can also be determined as

$$\sigma_{xx}^{(2)} = \frac{S_2}{bh_2} - \frac{M_2 y_2}{I_2} = \frac{1}{h_2}\int_0^x f_2(\xi)d\xi - \frac{12y_2}{h_2^3}[\int_0^x \int_0^\zeta g_2(\zeta)d\zeta d\xi - \frac{h_2}{2}\int_0^x f_2(\xi)d\xi], \quad (3.40)$$

$$\tau_{y_2x}^{(2)} = -\frac{1}{h_2}[(y_2 + \frac{h_2}{2}) + \frac{3}{h_2}(y_2^2 - \frac{h_2^2}{4})] f_2(x) + \frac{6}{h_2^3}(y_2^2 - \frac{h_2^2}{4})\int_0^x g_2(\xi)d\xi, \quad (3.41)$$

$$\sigma_{y_2y_2}^{(2)} = \{\frac{1}{h_2}[\frac{1}{2}(y_2^2 - \frac{h_2^2}{4}) + \frac{h_2}{2}(y_2 + \frac{h_2}{2}) + \frac{3}{h_2^2}[\frac{1}{3}(y_1^3 + \frac{h_2^3}{8}) - \frac{h_1^2}{4}(y_2 + \frac{h_2}{2})]\} f_2'(x)$$
$$- \frac{6}{h_1^3}[\frac{1}{3}(y_2^3 + \frac{h_2^3}{8}) - \frac{h_2^2}{4}(y_2 + \frac{h_2}{2})]g_2(x). \quad (3.42)$$

With the axial normal stresses varying linearly across the adherends and adhesive layer, the corresponding shear and transverse normal (peeling) stresses vary in parabolic and cubical functions, respectively. As the matter of fact, the stress field satisfies all the traction BCs and stress continuity across the interfaces.

### 3.1.5. Governing Equations of Interfacial Stresses

In the view of mathematics, complimentary strain energy is an energy functional with respect to the four unknown interfacial stress functions $f_i$ ($i$ = 1,2) and $g_i$ ($i$ = 1,2) defined above, which were

introduced to determine the interfacial stress distribution of ASSJ. To achieve the set of governing ODEs of the interfacial stress functions, the entire strain energy of the ASSJ can be determined by integrating the strain energy density (per unit length) with respect to the length variable $x$ from $x = 0$ to $x = L$ such that

$$\begin{aligned} U = & b\int_0^L \int_{-h_1/2}^{h_1/2} \{\frac{1}{2}[\sigma_{xx}^{(1)}\varepsilon_{xx}^{(1)} + \sigma_{yy}^{(1)}\varepsilon_{yy}^{(1)}] + \frac{1+\upsilon_1}{E_1}[\tau_{xy_1}^{(1)}]^2\} dy_1 dx \\ & + b\int_0^L \int_{-h_0/2}^{h_0/2} \{\frac{1}{2}[\sigma_{xx}^{(0)}\varepsilon_{xx}^{(0)} + \sigma_{yy}^{(0)}\varepsilon_{yy}^{(0)}] + \frac{1+\upsilon_0}{E_0}[\tau_{xy_0}^{(2)}]^2\} dy_0 dx \\ & + b\int_0^L \int_{-h_2/2}^{h_2/2} \{\frac{1}{2}[\sigma_{xx}^{(2)}\varepsilon_{xx}^{(2)} + \sigma_{yy}^{(2)}\varepsilon_{yy}^{(2)}] + \frac{1+\upsilon_2}{E_2}[\tau_{xy_2}^{(2)}]^2\} dy_2 dx. \end{aligned} \tag{3.43}$$

where $\varepsilon_{xx}^{(i)}$ and $\varepsilon_{yy}^{(i)}$ ($i$ = 1,0,2) are the axial and transverse strains of the cover, adhesive, and lower layer, respectively. Based on the generalized Hooke's law of linearly thermoelectric solids, the strains can be expressed as:

$$\varepsilon_{xx}^{(i)} = \frac{1}{E_i}\sigma_{xx}^{(i)} - \frac{\upsilon_i}{E_i}\sigma_{yy}^{(i)} + \alpha_i \Delta T, \tag{3.44}$$

$$\varepsilon_{yy}^{(i)} = \frac{1}{E_i}\sigma_{yy}^{(i)} - \frac{\upsilon_i}{E_i}\sigma_{xx}^{(i)} + \alpha_i \Delta T, \tag{3.45}$$

where $\alpha_i$ ($i$ = 1,0,2) are coefficients of thermal expansion of the cover, adhesive, substrate layers, respectively, and $\Delta T$ is the uniform temperature change from the reference temperature of free thermomechanical stresses. According to the theorem of minimum complimentary strain energy, mathematical variation of the strain energy functional (3.43) with respect to any of the four interfacial stress functions reaches a stationary state such that

$$\delta U = b\int_0^L \int_{-h_1/2}^{h_1/2} \{\frac{1}{2}[\sigma_{xx}^{(1)}\delta\varepsilon_{xx}^{(1)} + \delta\sigma_{xx}^{(1)}\varepsilon_{xx}^{(1)} + \sigma_{yy}^{(1)}\delta\varepsilon_{yy}^{(1)} + \delta\sigma_{yy}^{(1)}\varepsilon_{yy}^{(1)}] + \frac{2(1+\upsilon_1)}{E_1}\tau_{xy_1}^{(1)}\delta\tau_{xy_1}^{(1)}\}dy_1 dx$$
$$+ b\int_0^L \int_{-h_0/2}^{h_0/2} \{\frac{1}{2}[\sigma_{xx}^{(0)}\delta\varepsilon_{xx}^{(0)} + \delta\sigma_{xx}^{(0)}\varepsilon_{xx}^{(0)} + \sigma_{yy}^{(0)}\delta\varepsilon_{yy}^{(0)} + \delta\sigma_{yy}^{(0)}\varepsilon_{yy}^{(0)}] + \frac{2(1+\upsilon_0)}{E_0}\tau_{xy_0}^{(0)}\delta\tau_{xy_0}^{(0)}\}dy_0 dx \quad (3.46)$$
$$+ b\int_0^L \int_{-h_2/2}^{h_2/2} \{\frac{1}{2}[\sigma_{xx}^{(2)}\delta\varepsilon_{xx}^{(2)} + \delta\sigma_{xx}^{(2)}\varepsilon_{xx}^{(2)} + \sigma_{yy}^{(2)}\delta\varepsilon_{yy}^{(2)} + \delta\sigma_{yy}^{(2)}\varepsilon_{yy}^{(2)}] + \frac{2(1+\upsilon_2)}{E_2}\tau_{xy_2}^{(2)}\delta\tau_{xy_2}^{(2)}\}dy_2 dx = 0.$$

where δ is the mathematical variational operator with respect to either $f_i$ ($i$ = 1,2) or $g_i$ ($i$ = 1,2).

By plugging the stress resultants [Eq. (3.32), Eq. (3.34), and Eqs. (3.36-42)] and normal strains (Eq. (3.44) and Eq. (3.45)] into (Eq.3.46), it yields a set of 4th-order ODEs with respect to $f_i$ ($i$ = 1,2) and $g_i$ ($i$ = 1,2) as

$$[\mathrm{A}]\{\Phi^{(IV)}\} + [\mathrm{B}]\{\Phi''\} + [\mathrm{C}]\{\Phi\} + \{\mathrm{D}\} = \{0\}. \quad (3.47)$$

where $\{\Phi\} = \{F_1(\xi), G_1(\xi), F_2(\xi), G_2(\xi)\}^T$ is a column of the dimensionless interfacial stress functions with the components defined as

$$F_1(\xi) = F_1(x/h_2) = -\frac{1}{p_0 h_2}\int_0^x f_1(\zeta)d\zeta, \quad (3.48)$$

$$F_2(\xi) = F_2(x/h_2) = -\frac{1}{p_0 h_2}\int_0^x f_2(\zeta)d\zeta, \quad (3.49)$$

$$G_1(\xi) = G_1(x/h_2) = \frac{1}{p_0 h_2^2}\int_0^x \int_0^\zeta g_1(\eta)d\eta d\zeta, \quad (3.50)$$

$$G_2(\xi) = G_2(x/h_2) = \frac{1}{p_0 h_2^2}\int_0^x \int_0^\zeta g_2(\eta)d\eta d\zeta. \quad (3.51)$$

In addition, [*A*], [*B*], and [*C*] are four square symmetric coefficient matrices relating the geometric properties of ASSJ as

$$[\mathrm{A}]=\begin{bmatrix} \frac{1}{105}(h_{02}^3e_{20}+h_{12}^3e_{21}) & \frac{11}{210}(h_{02}^2e_{20}-h_{12}^2e_{21}) & -\frac{1}{140}h_{02}^3e_{20} & \frac{13}{420}h_{02}^2e_{20} \\ & \frac{13}{35}(h_{02}e_{20}+h_{12}e_{21}) & -\frac{13}{420}h_{02}^2e_{20} & \frac{9}{70}h_{02}e_{20} \\ & & \frac{1}{105}(1+h_{02}^3e_{20}) & \frac{11}{210}(1-h_{02}^2e_{20}) \\ \text{Sys} & & & \frac{13}{35}(1+h_{02}e_{20}) \end{bmatrix}, \quad (3.52)$$

$$[\mathrm{B}]=\begin{bmatrix} -\frac{4}{15}(h_{02}e_{20}+h_{12}e_{21}) & (-\frac{1}{5}+\upsilon_0)e_{20}+(\frac{1}{5}-\upsilon_1)e_{21} & \frac{1}{15}h_{02}e_{20} & \frac{1}{5}e_{20} \\ & -\frac{12}{5}(h_{02}^{-1}e_{20}+h_{12}^{-1}e_{21}) & -\frac{1}{5}e_{20} & \frac{12}{5}h_{02}^{-1}e_{20} \\ & & -\frac{4}{15}(1+h_{02}e_{20}) & (\frac{1}{5}-\upsilon_0)e_{20}-\frac{1}{5}+\upsilon_2 \\ \text{Sys} & & & -\frac{12}{5}(1+h_{02}^{-1}e_{20}) \end{bmatrix}, \quad (3.53)$$

$$[C]=\begin{bmatrix} 4(h_{02}^{-1}e_{20}+h_{12}^{-1}e_{21}) & 6(h_{02}^{-2}e_{20}-h_{12}^{-2}e_{21}) & 2h_{02}^{-1}e_{20} & -6h_{02}^{-2}e_{20} \\ & 12(h_{02}^{-3}e_{20}+h_{12}^{-3}e_{21}) & 6h_{02}^{-2}e_{20} & -12h_{02}^{-3}e_{20} \\ & & 4(1+h_{02}^{-1}e_{20}) & 6(1-h_{02}^{-2}e_{20}) \\ \textit{Sys} & & & 12(1+h_{02}^{-3}e_{20}) \end{bmatrix}, \quad (3.54)$$

where $h_{02} = h_0/h_2$, $h_{12} = h_1/h_2$, $e_{20} = E_2/E_0$, and $e_{21} = E_2/E_1$ are four parameters related to the geometrical dimensions and mechanical properties of the ASSJ.

The column $\{D\}$ is related to the external mechanical and thermomechanical loads, whose actual expression depends upon the types of external loads.

In the case of the ASSJ subjected to external mechanical and thermomechanical loads, a dimensionless force column $\{D\}_{4\times1}$ can be expressed as

$$
\begin{aligned}
D_1 &= \frac{h_{12}^{-1} + 3p_0(1+2h_{02}+h_{12})h_{12}^{-3}}{E_1} + \frac{\Delta T}{2}(-\alpha_0 + \alpha_1),\\
D_2 &= -\frac{6p_0(1+2h_{02}+h_{12})h_{12}^{-3}}{E_1},\\
D_3 &= \frac{\Delta T}{2}(-\alpha_2 + \alpha_0),\\
D_4 &= 0.
\end{aligned}
\tag{3.55}
$$

The solution to the set of resulting ODEs described in Eq. (3.47) can be determined with the general solution $\{\Psi\}$ superimposed with a particular solution $\{\Phi_0\}$ such that

$$\{\Phi\} = \{\Psi\} + \{\Phi_0\}, \tag{3.56}$$

where $\{\Psi\}$ is the general solution of the corresponding set of homogenous ODEs:

$$[\mathrm{A}]\{\Psi^{(IV)}\} + [\mathrm{B}]\{\Psi^{//}\} + [\mathrm{C}]\{\Psi\} = \{0\}, \tag{3.57}$$

and

$$\{\Phi_0\} = -[\mathrm{C}]^{-1}\{\mathrm{D}\}. \tag{3.58}$$

In order to efficiently solve the resulting homogenous Eq. (3.57), with the aid of eigenfunctions, a general solution can be assumed as

$$\{\Psi\} = \{\Psi_0\}\exp(\lambda\xi), \tag{3.59}$$

where $\{\Psi_0\}$ and $\lambda$ are respectively the eigenvector and eigenvalue of the set of homogenous ODEs in Eq. (3.57).

Hence,

$$\lambda^4[\mathrm{A}]\{\Psi_0\} + \lambda^2[\mathrm{B}]\{\Psi_0\} + [\mathrm{C}]\{\Psi_0\} = \{0\}. \tag{3.60}$$

To reduce the above generalized eigenvalue problem into a standard eigenvalue problem by adopting $\{\Psi_1\} = \lambda^2\{\Psi_0\}$, the resulting standard eigenvalue problem is

$$\begin{bmatrix} \mathrm{I} & 0 \\ 0 & \mathrm{A} \end{bmatrix} \begin{Bmatrix} \Psi_0 \\ \Psi_1 \end{Bmatrix} = -\lambda^{-2} \begin{bmatrix} 0 & -\mathrm{I} \\ \mathrm{C} & \mathrm{B} \end{bmatrix} \begin{Bmatrix} \Psi_0 \\ \Psi_1 \end{Bmatrix}, \tag{3.61}$$

where I is a 8×8 identity. Eigenvalue problem (3.61) can be solved by using robust, efficient numerical algorithms offered by MATLAB™. The final expression of the homogenous solution to Eq. (3.47) can be expressed as

$$\{\Phi\} = \sum_{k=1}^{8} [c_k \{\Psi_0^k\} \exp(\lambda_k \xi) + d_k \{\Psi_0^k\} \exp(-\lambda_k \xi)] + \{\Phi_0\}, \tag{3.62}$$

where $\{\Psi_0^k\}$ ($k$ = 1, 2, …, 8) are the eigenvectors corresponding to eigenvalues $\lambda_k$ ($k$ = 1, 2, …, 8), respectively, and $c_k$ and $d_k$ ($k$ = 1, 2, …, 8) are the coefficients (may be real or complex) to satisfy the traction BCs in Eq. (3.3) and Eqs. (3.13*a*-*r*). In the present case, the linearly independent BCs can be extracted from Eqs. (3.13*a*-*p*) accordingly such that

$$F_1(0) = 0, \tag{3.63a}$$

$$F_1(L/h_2) = -1, \tag{3.63b}$$

$$F_1'(0) = 0, \tag{3.63c}$$

$$F_1'(L/h_2) = 0, \tag{3.63d}$$

$$G_1(0) = 0, \tag{3.63e}$$

$$G_1(L/h_2) = 1/2 + h_{02}, \tag{3.63f}$$

$$G_1'(0) = 0, \tag{3.63g}$$

$$G_1'(L/h_2) = 0, \tag{3.63h}$$

$$F_2(0) = 0, \tag{3.63i}$$

$$F_2(L/h_2) = -1, \tag{3.63j}$$

$$F_2'(0) = 0, \tag{3.63k}$$

$$F_2'(L/h_2) = 0, \tag{3.63l}$$

$$G_2(0) = 0, \tag{3.63m}$$

$$G_2(L/h_2) = 1/2, \tag{3.63n}$$

$$G_2'(0) = 0, \tag{3.63o}$$

$$G_2'(L/h_2) = 0. \tag{3.63p}$$

Consequently, a set of simultaneous linear algebraic equations can be formulated with the BCs [Eqs. (3.63*a-p*) and formal solution (3.62)]:

$$\sum_{k=1}^{8} c_k \Psi_0^{k,1} + \sum_{k=1}^{8} d_k \Psi_0^{k,1} = -\Phi_0^{(1)}, \tag{3.64a}$$

$$\sum_{k=1}^{8} c_k \Psi_0^{k,1} \exp(\lambda_k L/h_2) + \sum_{k=1}^{8} d_k \Psi_0^{k,1} \exp(-\lambda_k L/h_2) = -[1+\Phi_0^{(1)}], \tag{3.64b}$$

$$\sum_{k=1}^{8} c_k \lambda_k \Psi_0^{k,1} - \sum_{k=1}^{8} d_k \lambda_k \Psi_0^{k,1} = 0, \tag{3.64c}$$

$$\sum_{k=1}^{8} c_k \lambda_k \Psi_0^{k,1} \exp(\lambda_k L/h_2) - \sum_{k=1}^{8} d_k \lambda_k \Psi_0^{k,1} \exp(-\lambda_k L/h_2) = 0, \tag{3.64d}$$

$$\sum_{k=1}^{8} c_k \Psi_0^{k,2} + \sum_{k=1}^{8} d_k \Psi_0^{k,2} = -\Phi_0^{(2)}, \tag{3.64e}$$

$$\sum_{k=1}^{8} c_k \Psi_0^{k,2} \exp(\lambda_k L/h_2) + \sum_{k=1}^{8} d_k \Psi_0^{k,2} \exp(-\lambda_k L/h_2) = 1/2 + h_{02} - \Phi_0^{(2)}, \tag{3.64f}$$

$$\sum_{k=1}^{8} c_k \lambda_k \Psi_0^{k,2} - \sum_{k=1}^{8} d_k \lambda_k \Psi_0^{k,2} = 0, \tag{3.64g}$$

$$\sum_{k=1}^{8} c_k \lambda_k \Psi_0^{k,2} \exp(\lambda_k L/h_2) - \sum_{k=1}^{8} d_k \lambda_k \Psi_0^{k,2} \exp(-\lambda_k L/h_2) = 0, \tag{3.64h}$$

$$\sum_{k=1}^{8} c_k \Psi_0^{k,3} + \sum_{k=1}^{8} d_k \Psi_0^{k,3} = -\Phi_0^{(3)}, \tag{3.64$i$}$$

$$\sum_{k=1}^{8} c_k \Psi_0^{k,3} \exp(\lambda_k L / h_2) + \sum_{k=1}^{8} d_k \Psi_0^{k,3} \exp(-\lambda_k L / h_2) = -[1 + \Phi_0^{(3)}], \tag{3.64 $j$}$$

$$\sum_{k=1}^{8} c_k \lambda_k \Psi_0^{k,3} - \sum_{k=1}^{8} d_k \lambda_k \Psi_0^{k,3} = 0, \tag{3.64$k$}$$

$$\sum_{k=1}^{8} c_k \lambda_k \Psi_0^{k,3} \exp(\lambda_k L / h_2) - \sum_{k=1}^{8} d_k \lambda_k \Psi_0^{k,3} \exp(-\lambda_k L / h_2) = 0, \tag{3.64$l$}$$

$$\sum_{k=1}^{8} c_k \Psi_0^{k,4} + \sum_{k=1}^{8} d_k \Psi_0^{k,4} = -\Phi_0^{(4)}, \tag{3.64$m$}$$

$$\sum_{k=1}^{8} c_k \Psi_0^{k,4} \exp(\lambda_k L / h_2) + \sum_{k=1}^{8} d_k \Psi_0^{k,4} \exp(-\lambda_k L / h_2) = 1/2 - \Phi_0^{(4)}, \tag{3.64$n$}$$

$$\sum_{k=1}^{8} c_k \lambda_k \Psi_0^{k,4} - \sum_{k=1}^{8} d_k \lambda_k \Psi_0^{k,4} = 0, \tag{3.64$o$}$$

$$\sum_{k=1}^{8} c_k \lambda_k \Psi_0^{k,4} \exp(\lambda_k L / h_2) - \sum_{k=1}^{8} d_k \lambda_k \Psi_0^{k,4} \exp(-\lambda_k L / h_2) = 0. \tag{3.64$p$}$$

where, $\Psi_0^{k,1}$, $\Psi_0^{k,2}$, $\Psi_0^{k,3}$, and $\Psi_0^{k,4}$ ($k$ = 1, 2, …, 8) are respectively the 1st to 4th elements of the $k$-th eigenvector, and $\Phi_0^{(1)}$, $\Phi_0^{(2)}$, $\Phi_0^{(3)}$, and $\Phi_0^{(4)}$ are the 1st to 4th elements of the particular solution vector $\{\Phi_0\}$. In the case of the stress field due to a pure temperature change, the above BCs [Eq. (3.63*b*), Eq. (3.63*f*), Eq. (3.63*j*), and Eq. (3.63*n*)] are needed to set as zeros, which further influence the right terms of the algebraic equations [Eq. (3.64*b*), Eq. (3.64*f*), Eq. (3.64*j*), and Eq. (3.64*n*)].

Once coefficients $c_k$ and $d_k$ have been determined by solving the resulting set of homogeneous algebraic equations (3.64*a*-*p*), the interfacial shear and peeling stresses at the upper and lower interfaces can be finalized according to expressions (3.48-51) as

$$f_1(x)/p_0 = -\sum_{k=1}^{8} c_k \lambda_k \Psi_0^{k,1} \exp(\lambda_k x/h_2) + \sum_{k=1}^{8} d_k \lambda_k \Psi_0^{k,1} \exp(-\lambda_k x/h_2), \tag{3.65}$$

$$g_1(x)/p_0 = \sum_{k=1}^{8} c_k \lambda_k^2 \Psi_0^{k,2} \exp(\lambda_k x/h_2) + \sum_{k=1}^{8} d_k \lambda_k^2 \Psi_0^{k,2} \exp(-\lambda_k x/h_2), \tag{3.66}$$

$$f_2(x)/p_0 = -\sum_{k=1}^{8} c_k \lambda_k \Psi_0^{k,3} \exp(\lambda_k x/h_2) + \sum_{k=1}^{8} d_k \lambda_k \Psi_0^{k,3} \exp(-\lambda_k x/h_2), \tag{3.67}$$

$$g_2(x)/p_0 = \sum_{k=1}^{8} c_k \lambda_k^2 \Psi_0^{k,4} \exp(\lambda_k x/h_2) + \sum_{k=1}^{8} d_k \lambda_k^2 \Psi_0^{k,4} \exp(-\lambda_k x/h_2). \tag{3.68}$$

## 3.2. Model Validation

### 3.2.1. Interfacial Stresses due to Mechanical Loads

FEM based on commercial FEA software package (ANSYS™) is used to validate the present stress function variational method for stress analysis of ABJs. Specifically, an ASSJ with unit width is chosen for such purpose, which is assumed to be subjected to uniform axial tension on the substrate layers in a general 2D plane-stress state. The geometrical parameters for the ASSJ are taken as: $L$ = 20 mm, $h_1$ = 2.0 mm (steel/cover), $h_2$ = 2.0 mm (aluminum/bottom), and $h_0$ = 0.2 mm (epoxy/adhesive). Material parameters are given as: $E_1$ = 210 GPa, $v_1$ = 0.293 (steel/cover), $E_2$ = 70 GPa, $v_2$ = 0.345 (aluminum/bottom), and $E_0$ = 10 GPa, $v_0$ = 0.40 (epoxy/adhesive). The given tension $p_0$ is assumed to be 1MPa.

During FEM simulation (ANSYS™) of the right half-symmetric ASSJ, four-node elements (PLANE182) and uniform quadrilateral meshes are employed. In their recent study, Wu and Jenson (2011) have determined the accurate stress field in a bonded joint without the adhesive layer using stress function varational method, which was validated by means of FEM (ANSYS™). To understand the trend of the singular stresses along the bonding lines, two different mesh sizes (0.05 × 0.05 mm and 0.01 × 0.01 mm)

are employed at the two ends of the overlap. Note that the right portion of ASSJ as shown in Fig. 3.1 (*b*) is utilized in FEM modeling, a uniform traction of 1MPa is applied as the axial load, and a single corner node is used to constrain the displacement in the vertical direction near the loading point so as to mimic the BCs under uniaxial tension. Fig. 3.3 shows the variations of the interfacial shear and normal stresses of the tested ASSJ model predicted by the present stress variational method, which are compared with those obtained by FEM (ANSYS$^{TM}$). Because of the existence of bending moment resultant at the middle of the joint [Fig. 3.1(*c*)], the interfacial shear and normal stresses at the free-edges of mid-span can be found in high values. Compared to the shear stress, the high normal stress mainly contributes to the debonding failure of ABJs. Obviously, the interfacial shear stresses predicted by the present method exactly satisfy the shear-free boundary condition in ABJs as required by the theoretical formulation. Even though the normal and shear stresses assume the very similar varying trends along the upper and lower bonding lines, the difference of these stresses does exist around the free edges, especially the interfacial normal stresses, which dominates the debonding failure of ABJs.

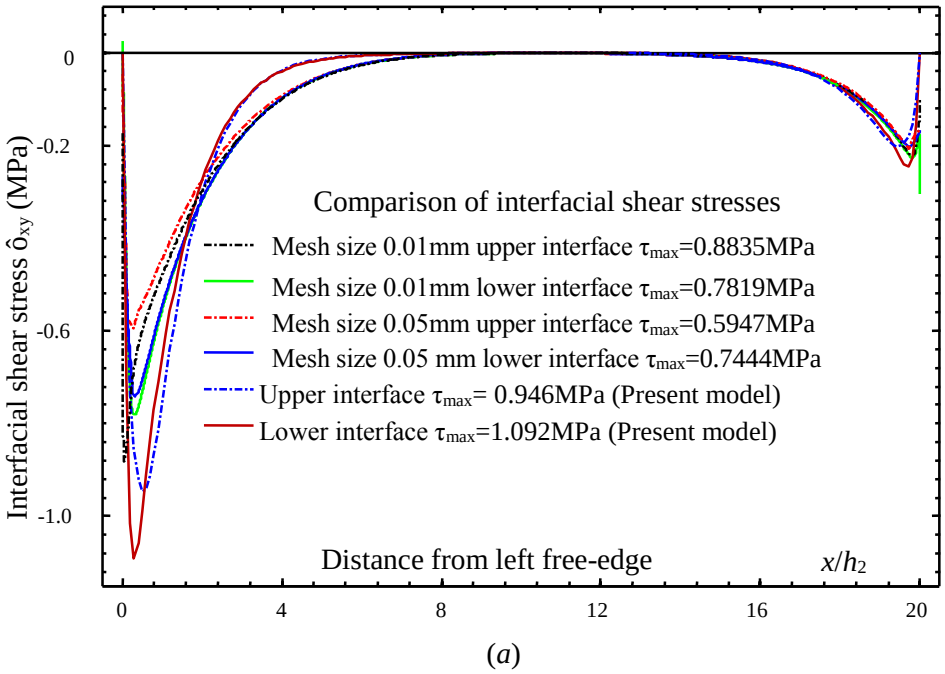


(*a*)

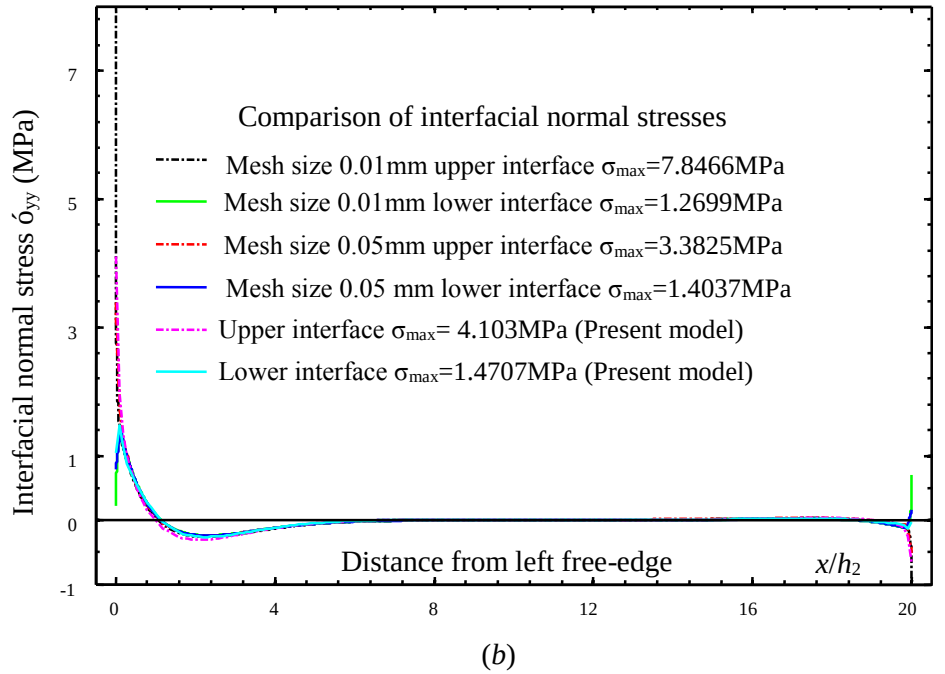


(*b*)

Figure 3.3. Validation of the stress-function variational method by FEM for interfacial shear and normal stresses in ASSJ subjected to uniaxial tension: (*a*) Interfacial shear stress and (*b*) interfacial normal stress.

To explain the difference between the interfacial stresses across the adhesive layer, let us consider a segmental element of the adhesive layer with the length $\Delta x$ as shown in Fig. 3.4. Assume $\bar{\sigma}_{yy}^{h_0/2}$ and $\bar{\sigma}_{yy}^{-h_0/2}$ are the average normal stresses at the top and bottom adhesive surface along the length $\Delta x$. Static equilibrium equation of the segmental element can be expressed as

$$(\bar{\sigma}_{yy}^{h_0/2} - \bar{\sigma}_{yy}^{-h_0/2})\Delta x - \tau_{xy} h_0 = 0, \tag{3.69}$$

The difference of the average normal stress can be obtained from Eq. (3.69) as

$$\Delta\sigma_{yy} = \bar{\sigma}_{yy}^{h_0/2} - \bar{\sigma}_{yy}^{-h_0/2} = \tau_{xy} h_0 / \Delta x. \tag{3.70}$$

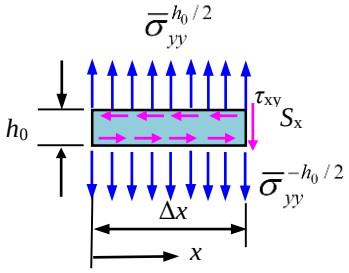


Figure 3.4. Free body diagram of a representative adhesive layer segment.

From Eq. (3.70), when $\Delta x$ is much smaller than the thickness of the adhesive layer $h_0$, the normal stress difference could be significantly large. Based on this, the common assumption that the normal and shear stresses do not change significantly across the adhesive layer as used in most literature ABJ models is not held.

### 3.2.2. Interfacial Stresses due to Thermal Loads

Thermomechanical stress analysis of an ASSJ subjected purely to uniform temperature change is analogous to that of an adhesively bonded thermostat. To simplify the process, the ASSJ is treated as no

residual stresses at the initial load-free state at the reference temperature, and the temperature change is assumed uniform throughout the joint. The structural and mechanical parameters of the present joint are given as: $h_1$ = 2.5 mm, $E_1$ = 70 GPa, $\upsilon_1$ = 0.345, $\alpha_1 = 23.6\times10^{-6}/^{o}C$, $h_2$ = 2.5 mm, $E_2$ = 325 GPa, $\upsilon_2$ = 0.293, $\alpha_2 = 4.9\times10^{-6}/^{o}C$, $L$ = 50.8 mm, $E_0$ = 10 GPa, $\upsilon_0$ = 0.40, and $\alpha_0 = 73.8\times10^{-6}/^{o}C$, and $\Delta T = 240^{o}C$. Two thicknesses of the adhesive layer are taken into comparison as: $h_0$ = 0.25 mm and 1.0 mm, respectively. Furthermore, *plane-strain* state from the precious studies is used in the present adhesively bonded thermostat.

Recent work in Dr. Wu's research group at NDSU has demonstrated the reliability of stress-function variational method for solving such type of problems (Wu and Jensen, 2011).

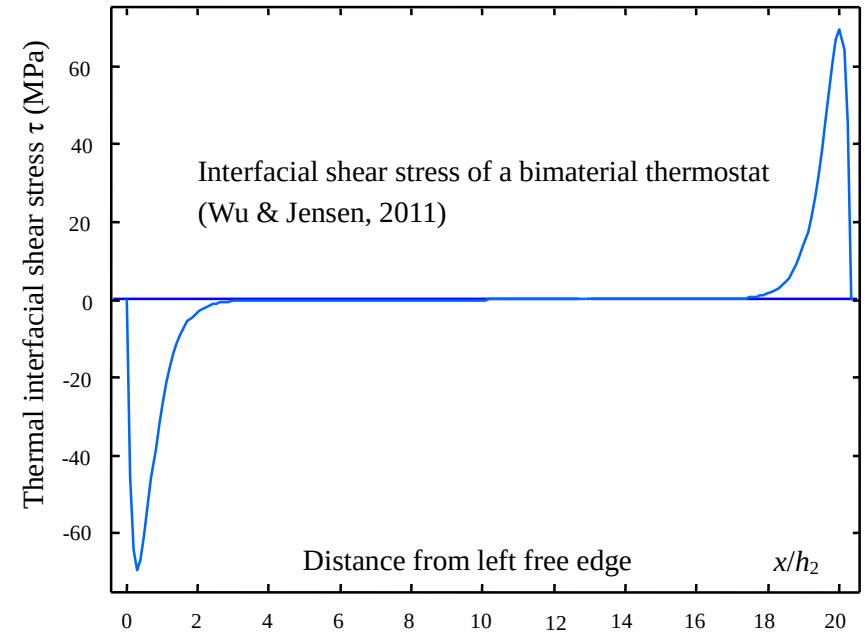


(*a*)

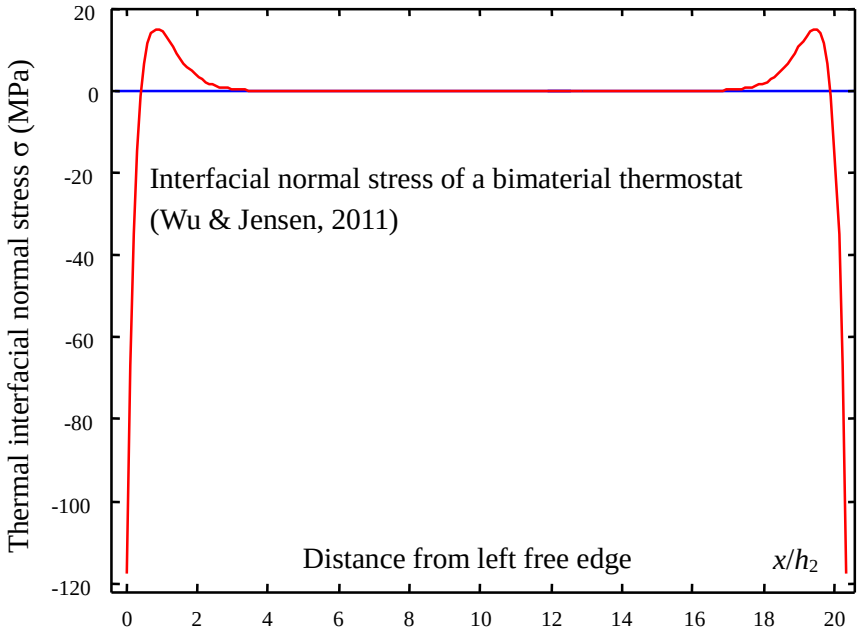


(*b*)

Figure 3.5. Thermomechanical shear and normal stresses along the interface of a bimaterial thermostat based on stress-function variational method (Wu & Jensen, 2011): (*a*) Interfacial shear stresses, (*b*) interfacial normal stresses.

In Fig. 3.5, predictions of the thermomechanical shear and normal stresses are pretty close to those obtained by Suhir (1989), Eischen et al. (1990), Ru (2002), etc. To better demonstrate the proposed stress-

function variational method for predicting the thermomechanical interfacial stresses in adhesively bonded thermostats, a thin adhesive layer is further introduced into Wu and Jenson's joint model (Wu & Jenson, 2011).

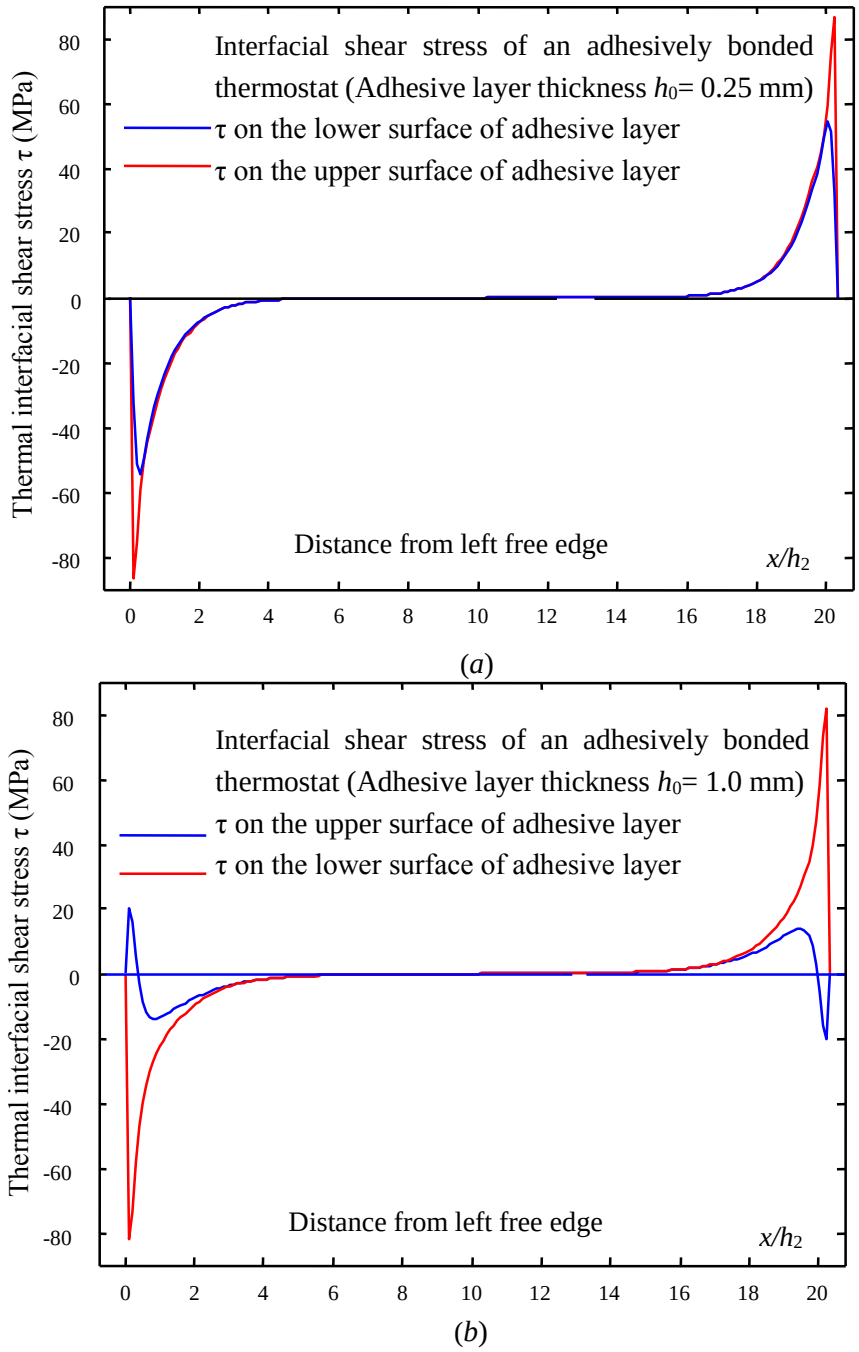


Figure 3.6. Variations of the dimensionless thermomechanical interfacial shear stresses in the adhesively single-sided strap joint over the dimensionless distance from the mid-span: (*a*) The interfacial shear stress for thickness $h_0$ = 0.25 mm, (*b*) the interfacial shear stress for thickness $h_0$ = 1 mm.

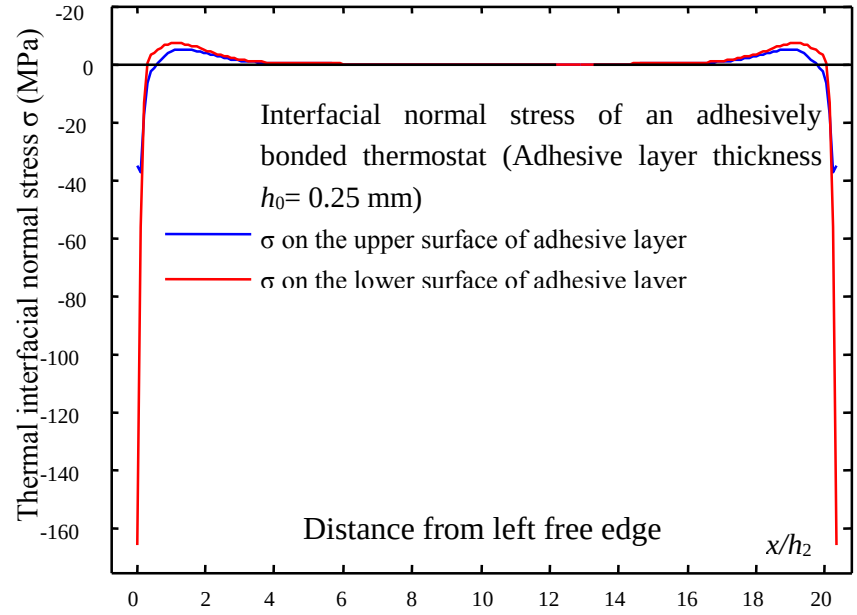


(*a*)

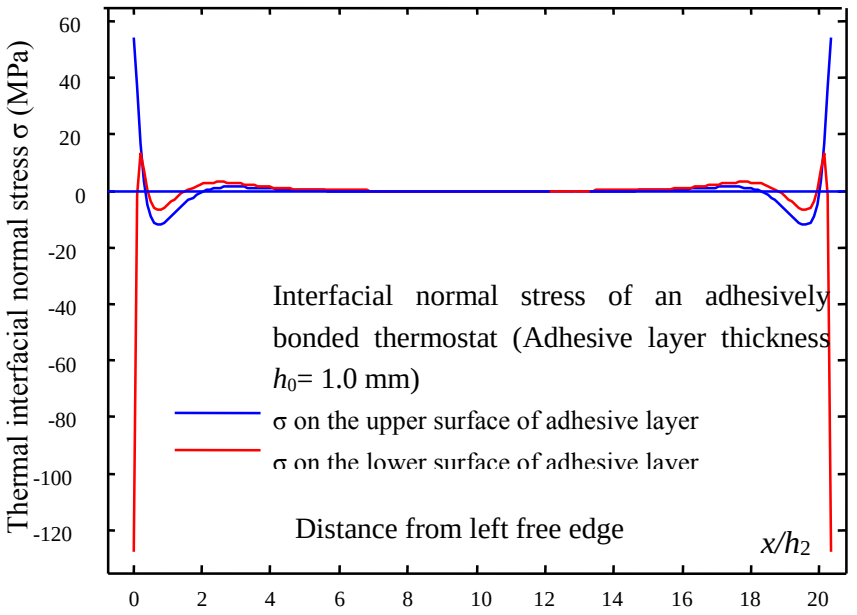


(*b*)

Figure 3.7 Variations of the dimensionless thermomechanical interfacial normal stresses in the adhesively single-sided strap joint over the dimensionless distance from the mid-span: (*a*) The interfacial normal stress for thickness $h_0$ = 0.25 mm, (*b*) the interfacial normal stress for thickness $h_0$ = 1 mm.

In the present semi-analytic stress-functional variational method, variations of the thermomechanical interfacial shear and normal stresses in the adhesively bonded thermostat at two different thicknesses ($h_0$ = 0.25 mm and 1.0 mm) are demonstrated in Fig. 3.6 and Fig. 3.7, respectively. Compared to Fig. 3.5 by Wu and Jenson (2011), the shear and normal stresses at the upper and lower interfaces in Fig. 3.6(*a*) and Fig. 3.7(*a*) with a relatively thin adhesive layer ($h_0$ = 0.25 mm) carry very similar varying trends. The peak values of both the shear and normal stresses at the lower surface of the adhesive layer are 40% higher than those of the biomaterial thermostat with the same geometries, material properties, and temperature change. However, the peak values of both the shear and normal stresses at the upper surface of the adhesive layer are lower than those of the biomaterial thermostat. Specifically, the peak value of shear stress is decreased about 20%, and that of normal stress is decreased around two-thirds. While applying a temperature change to the ASSJ with a relatively thin adhesive layer, the adhesive layer appears a large thermal expansion due to its large coefficient of thermal expansion and Poisson's ratio, which cause higher stresses at the interface to deform thermostat to the stiffer substrate layer.

In other case of a thick adhesive layer ($h_0$ = 1.0 mm), the shear and normal stresses at the lower interface as shown in Fig. 3.6(*b*) and Fig. 3.7(*b*) slightly decrease compared to those of a thinner adhesive layer as shown in Fig. 3.6(*a*) and Fig. 3.7(*a*). Relatively large mismatched deformations owing to the large thickness and low modulus of the adhesive layer between the upper and lower adherends are responsible for the inconsistent thermal expansion. In contrast, at the upper surface of the adhesive layer, the directions of both the shear and normal stresses are altered, corresponding to the change of the characteristic deflection of the upper adherend induced by the varying adhesive layer thickness. In this case, compared to the thinner

adhesive layer, the peak value of interfacial shear stress decreases nearly half, and the peak value of interfacial normal stress nearly doubles.

### 3.2.3. Scaling Analysis of Interfacial Stresses due to Mechanical Loads

A compact, efficient computational code has been designed to implement the present stress-function variational method for stress analysis of ABJs, which can be used to examine the dependencies of the interfacial shear and normal stresses upon all the geometrical and material parameters of the ABJs including the layer thickness ratios $h_0/h_2$ and $h_1/h_2$, length ratio $L/h_2$, modulus ratios $E_0/E_2$ and $E_1/E_2$, Poisson's ratios $\upsilon_1$, $\upsilon_2$ and $\upsilon_3$, and coefficients of thermal expansion $\alpha_0$, $\alpha_1$ and $\alpha_2$. In single-sided strap joints (Wu and Jensen, 2011), scaling parameter studies have been conducted to examine the effects of adherend thickness ratio $h_1/h_2$, length ratio $L/h_2$ and modulus ratio $E_1/E_2$ on the shear and normal stress variations along the interface.

The goal of this section is to examine the effects of thickness and modulus of the adhesive layer on the interfacial shear and normal stresses. In addition, it needs to be mentioned that the present ABJ model is established within the framework of linear elasticity. Thus, the stress fields in ABJs triggered by combined mechanical loads and temperature change can be dealt with separately based on the method of superposition. In this case, the adherend length and modulus ratios are fixed as $L/h_2 = 5$ and $E_1/E_2 = 3$, and Poisson's ratios of the upper and lower adherends are fixed as $\upsilon_1 = 0.293$ (steel) and $\upsilon_2 = 0.345$ (aluminum). For the adhesive layer, two thickness ratios ($h_0/h_2 = 0.2$, and 0.5) and two modulus ratios ($E_0/E_2 = 1/20$ and 1/10) are adopted, and the Poisson's ratio is fixed at $\upsilon_2 = 0.4$ (thermoset epoxy) in the calculations. The joint is treated in the state of *plane-stress*.

In comparison, the interfacial shear and normal stresses of a single-sided strap joint (Wu and Jenson, 2011) are shown in Figs. 3.8 (*a*) and (*b*).

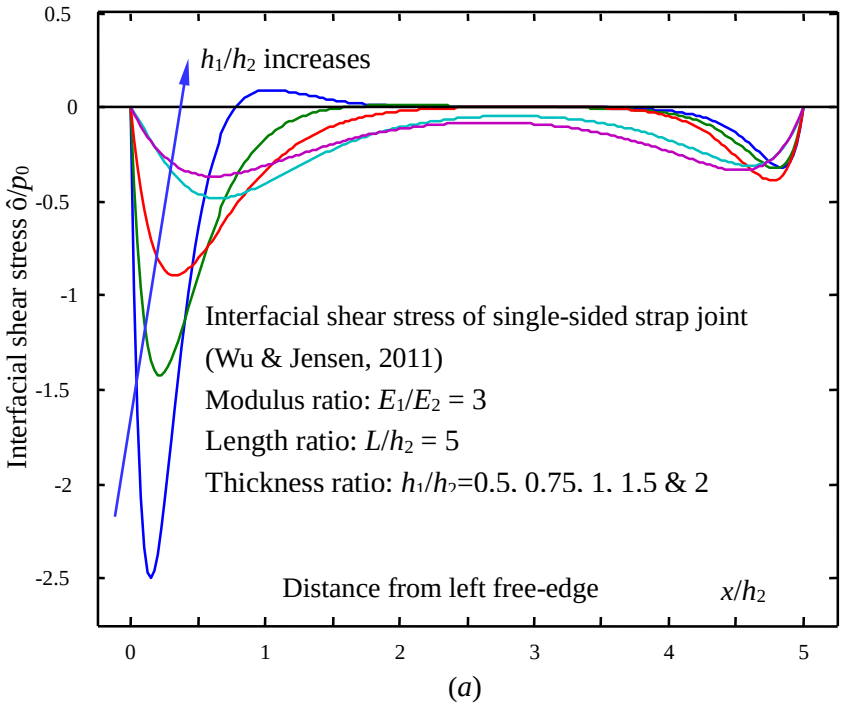


(*a*)

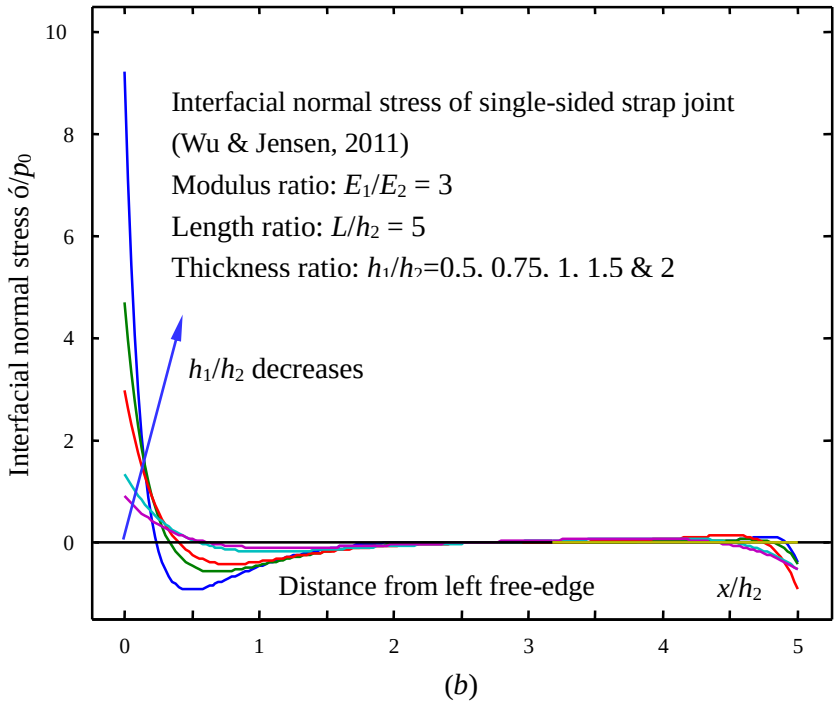


(*b*)

Figure 3.8. Mechanical shear and normal stresses along the interface of single-sided strap joint based on the stress-function variational method (Wu & Jensen, 2011): (*a*) Interfacial shear stresses, (*b*) interfacial normal stresses.

In above figure, all the shear stress components satisfy the shear-free condition at the adherend ends. Figs. 3.9-16 show variations of the dimensionless interfacial shear stress $\tau/p_0$ and normal (peeling) stress $\sigma/p_0$ at the upper and lower interfaces with the dimensionless distance $x/h_2$ from the joint mid-span to the right adherend end at five adherend thickness ratios ($h_1/h_2$ = 0.5, 0.75, 1.0, 1.5, and 2.0), two adhesive thickness ratios ($h_0/h_2$ = 0.2 and 0.5), and two adhesive modulus ratios ($E_0/E_2$ = 1/10 and 1/20), respectively.

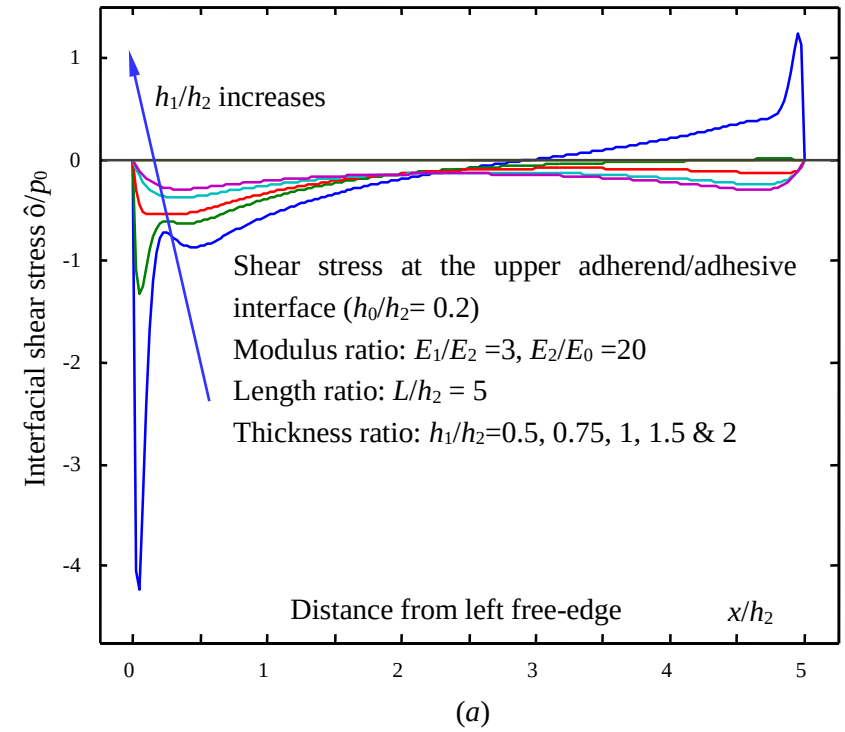


(*a*)

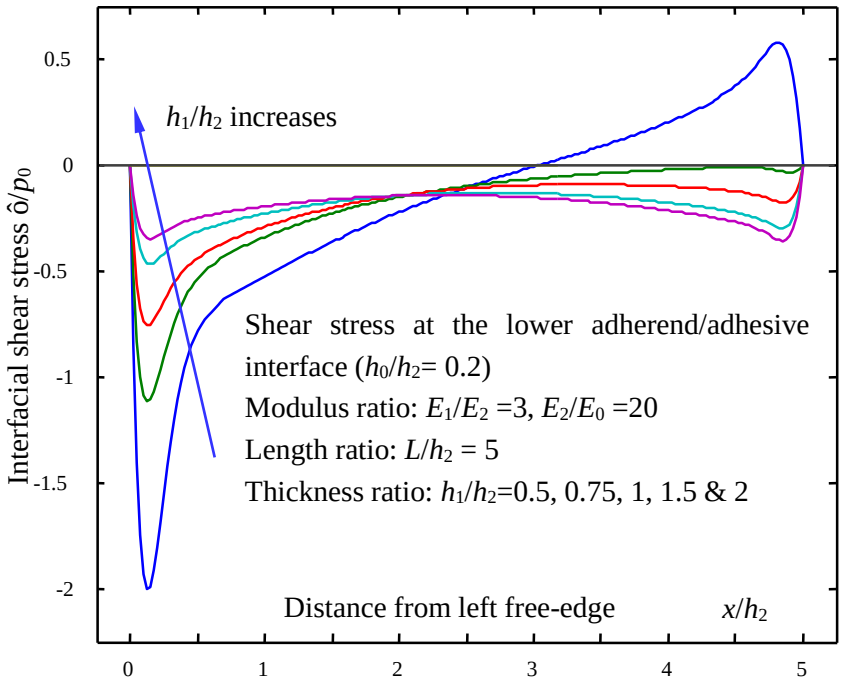


(*b*)

Figure 3.9. Comparison of the variations of the dimensionless interfacial shear stresses in the adhesively single-sided strap joint over the dimensionless distance from the mid-span: (*a*) The shear stress at the upper interface, (*b*) the shear stress at the lower interface. Thickness ratio $h_0/h_2$ = 0.2, Young's modulus ratio $E_2/E_0$ = 20.

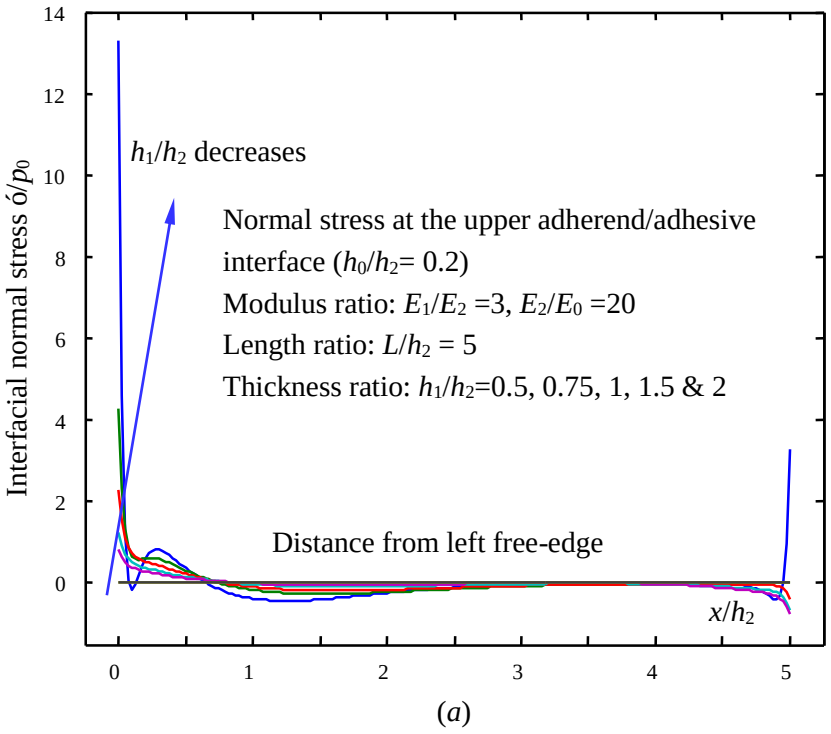


(*a*)

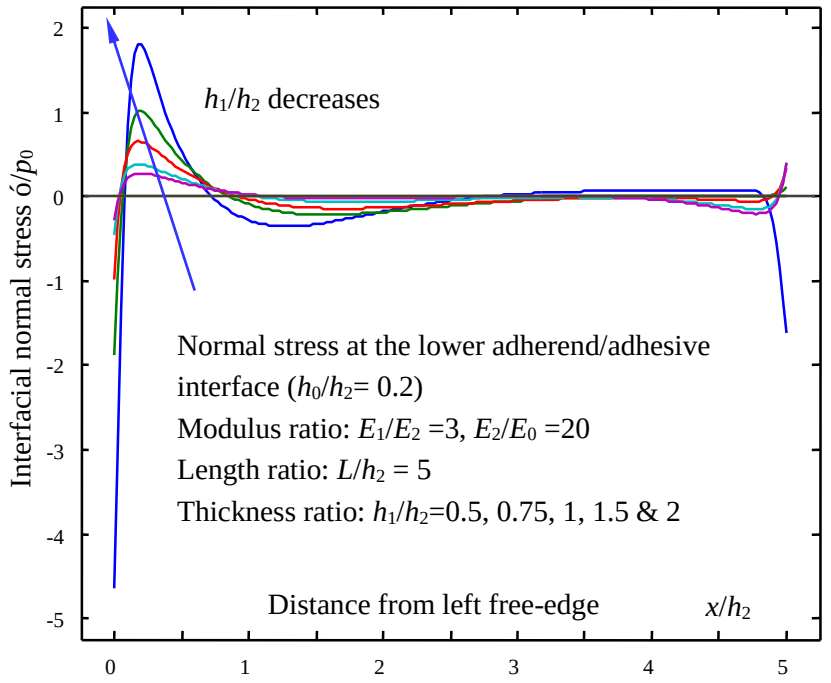


(*b*)

Figure 3.10. Comparison of the variations of the dimensionless interfacial normal stresses in the adhesively single-sided strap joint over the dimensionless distance from the mid-span: (*a*) The normal stress at the upper interface, (*b*) the normal stress at the lower interface. Thickness ratio $h_0/h_2$ = 0.2, Young's modulus ratio $E_2/E_0$ = 20.

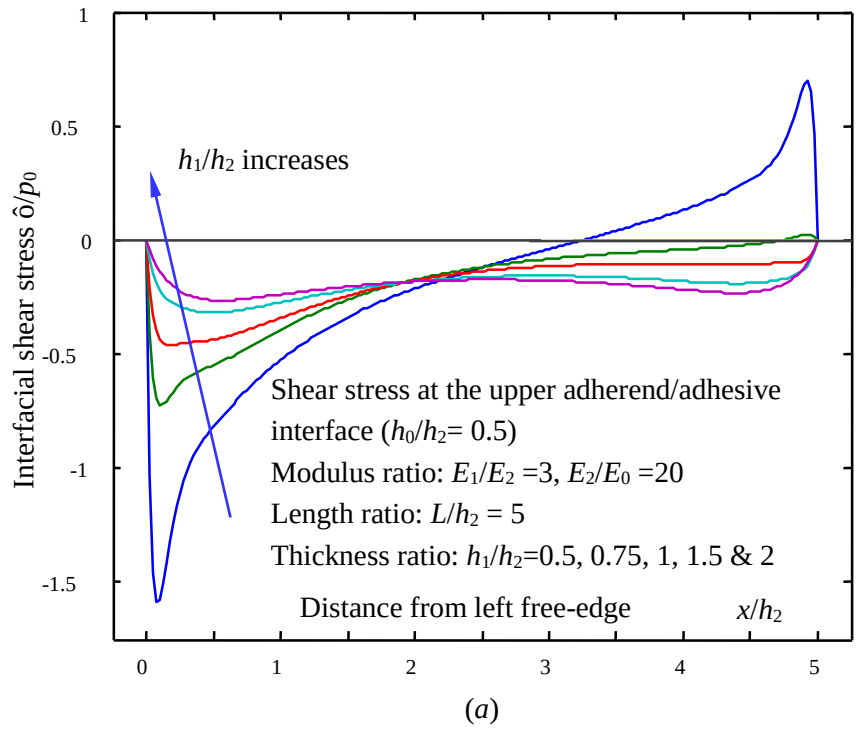


(*a*)

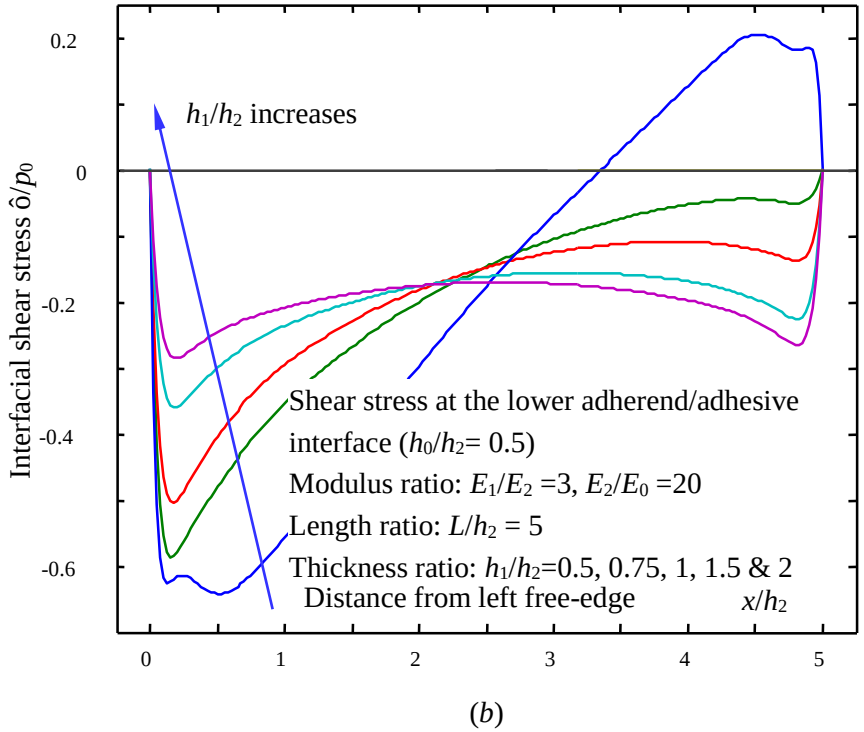


(*b*)

Figure 3.11. Comparison of the variations of the dimensionless interfacial shear stresses in the adhesively single-sided strap joint over the dimensionless distance from the mid-span: (*a*) The shear stress at the upper interface, (*b*) the shear stress at the lower interface. Thickness ratio $h_0/h_2 = 0.5$, Young's modulus ratio $E_2/E_0 = 20$.

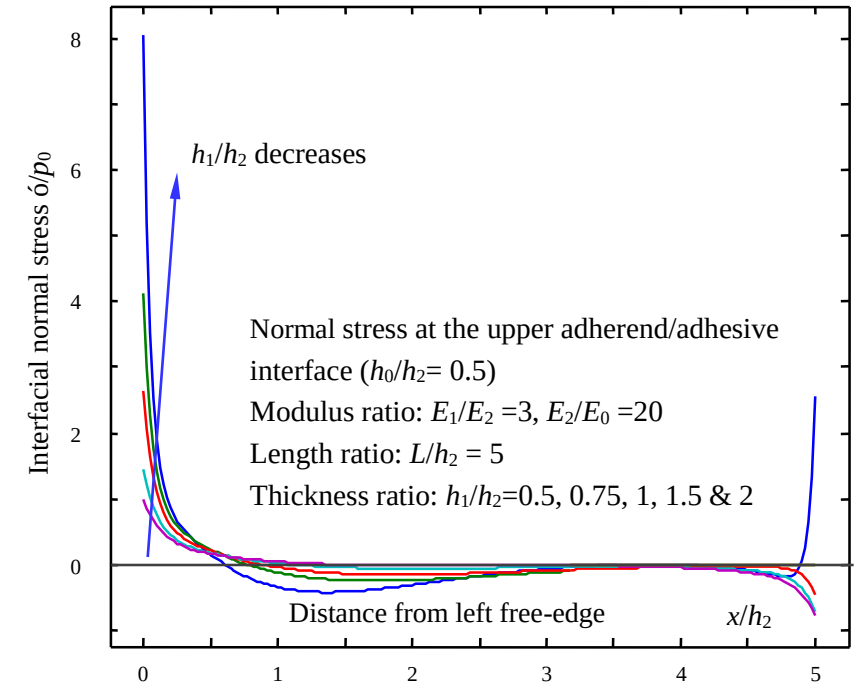


(*a*)

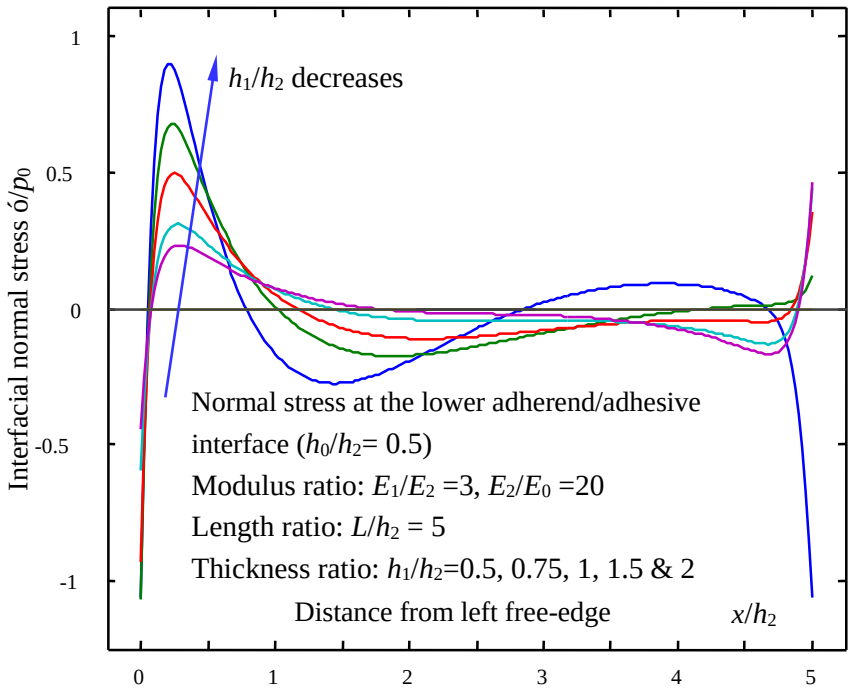


(*b*)

Figure 3.12. Comparison of the variations of the dimensionless interfacial normal stresses in the adhesively single-sided strap joint over dimensionless distance from the mid-span: (*a*) The normal stress at the upper interface, (*b*) the normal stress at the lower interface. Thickness ratio $h_0/h_2$ = 0.5, Young's modulus ratio $E_2/E_0$ = 20.

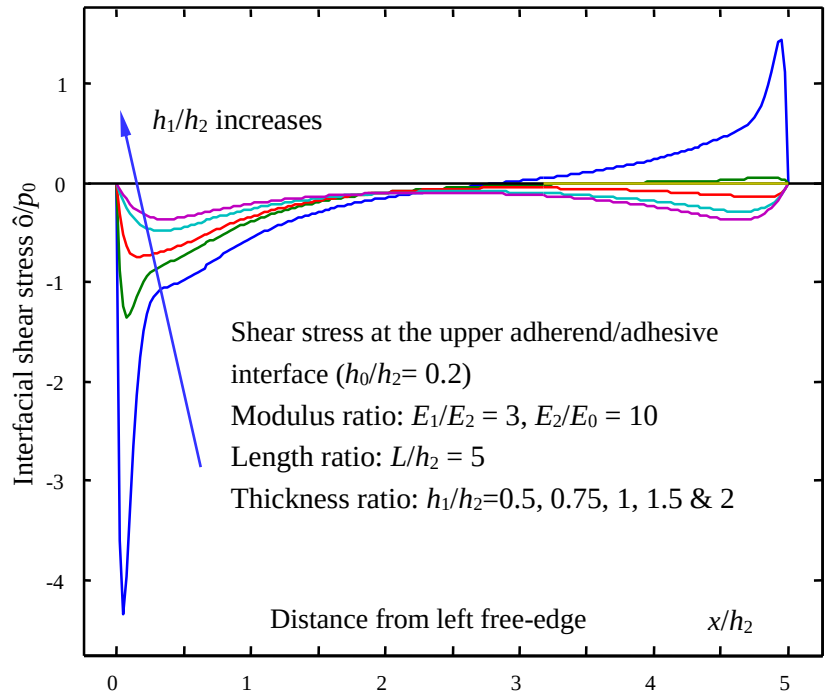


(*a*)

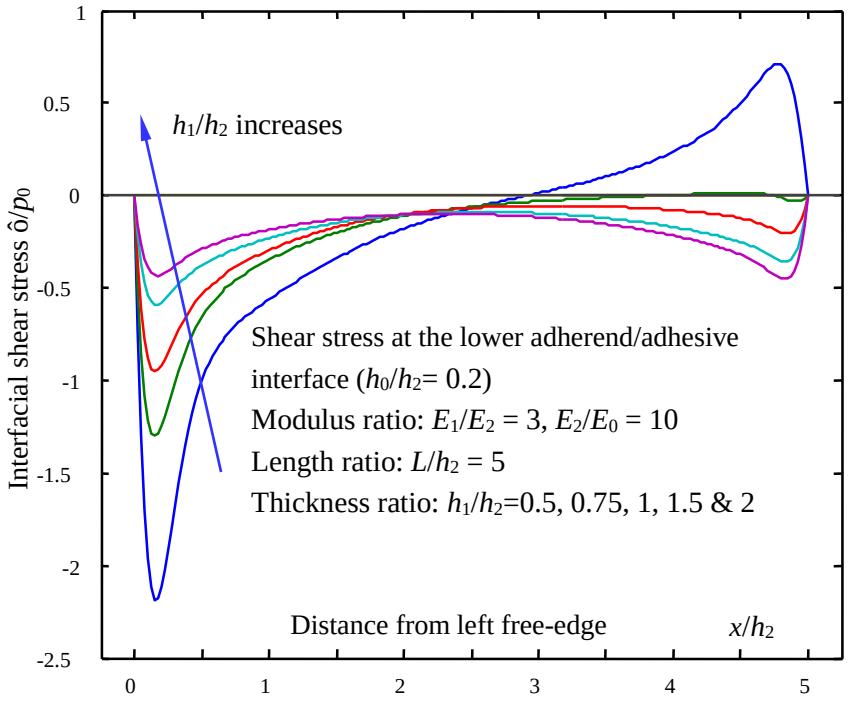


(*b*)

Figure 3.13. Comparison of the variations of the dimensionless interfacial shear stresses in the adhesively single-sided strap joint over the dimensionless distance from the mid-span: (*a*) The shear stress at the upper interface, (*b*) the shear stress at the lower interface. Thickness ratio $h_0/h_2$ = 0.2, Young's modulus ratio $E_2/E_0$ = 10.

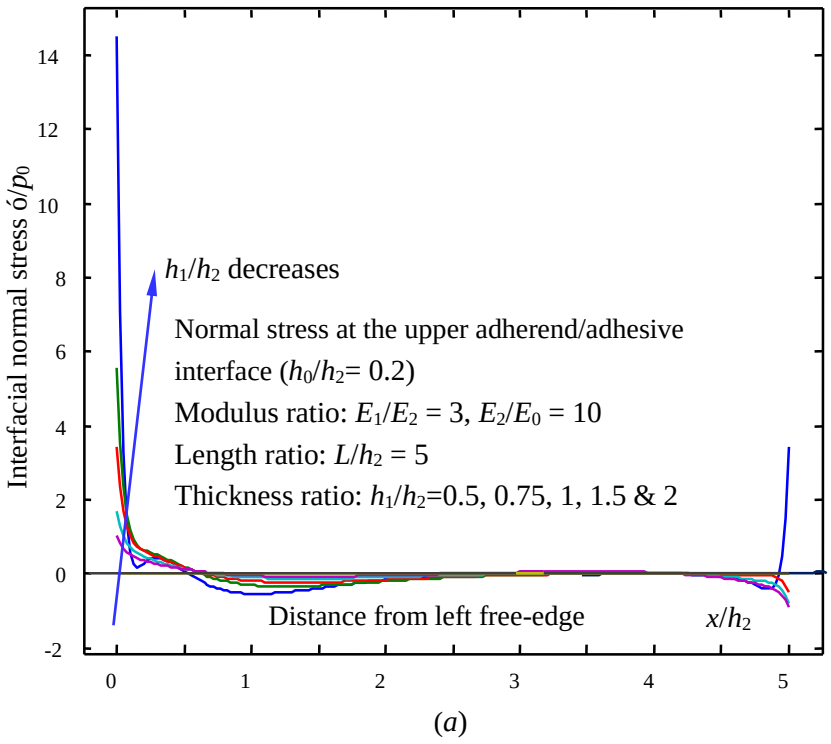


(*a*)

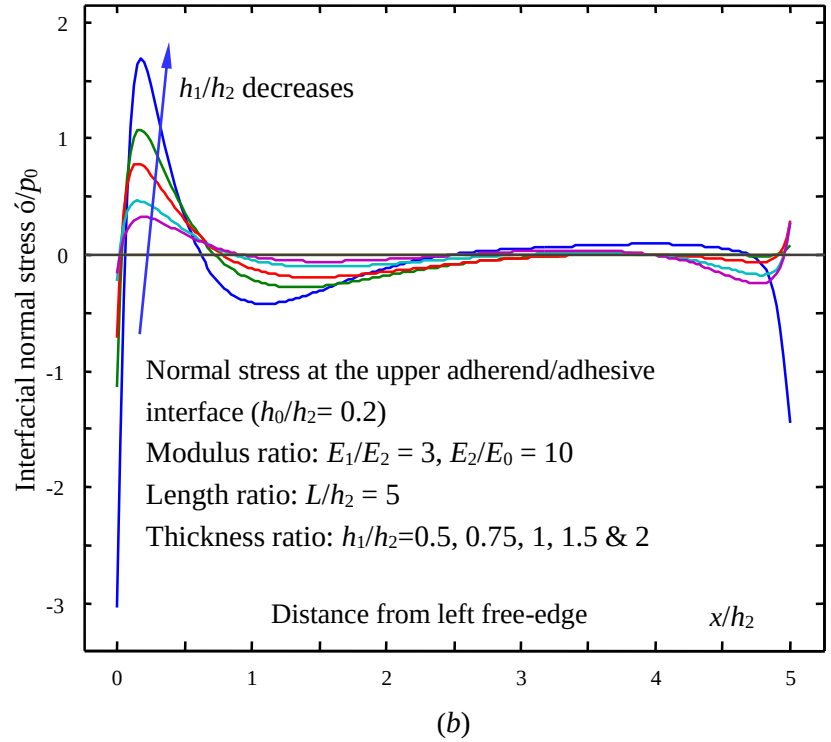


(*b*)

Figure 3.14. Comparison of the variations of the dimensionless interfacial normal stresses in the adhesively single-sided strap joint over the dimensionless distance from the mid-span: (*a*) The normal stress at the upper interface, (*b*) the normal stress at the lower interface. Thickness ratio $h_0/h_2$ = 0.2, Young's modulus ratio $E_2/E_0$ = 10.

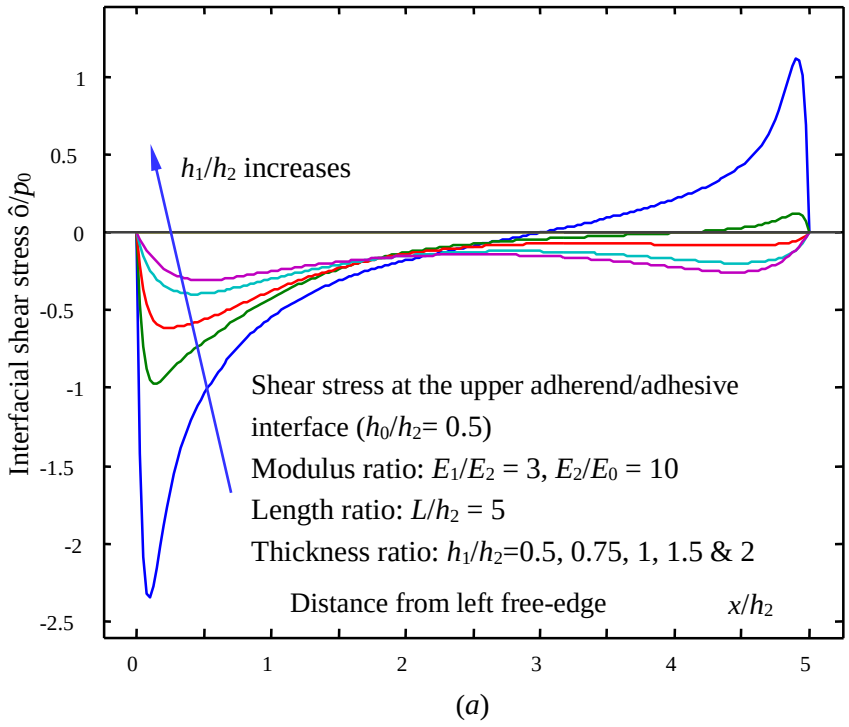


(*a*)

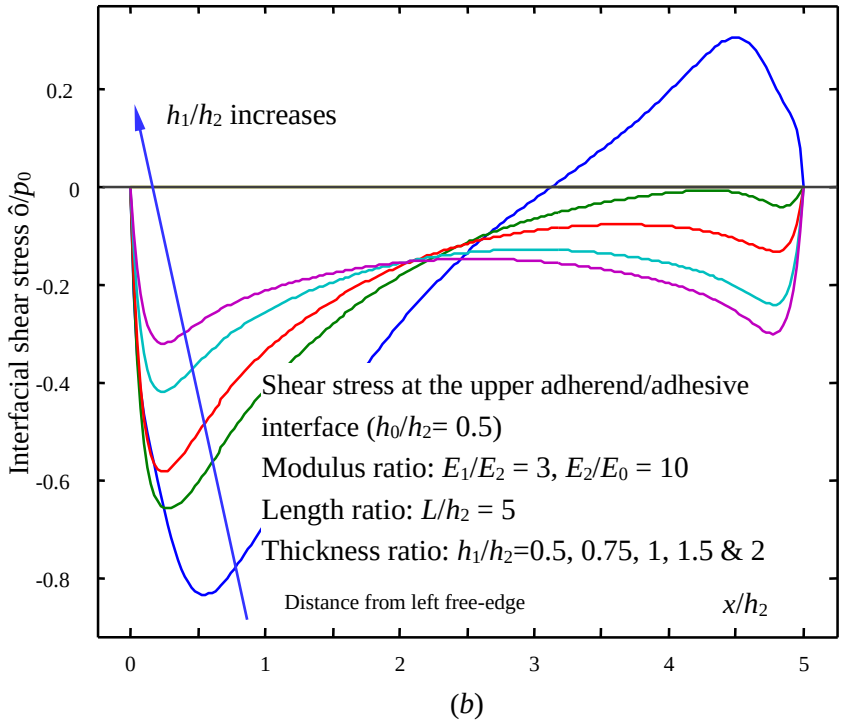


(*b*)

Figure 3.15. Comparison of the variations of the dimensionless interfacial shear stresses in the adhesively single-sided strap joint over the dimensionless distance from the mid-span: (*a*) The shear stress at the upper interface, (*b*) the shear stress at the lower interface. Thickness ratio $h_0/h_2$ = 0.5, Young's modulus ratio $E_2/E_0$ = 10.

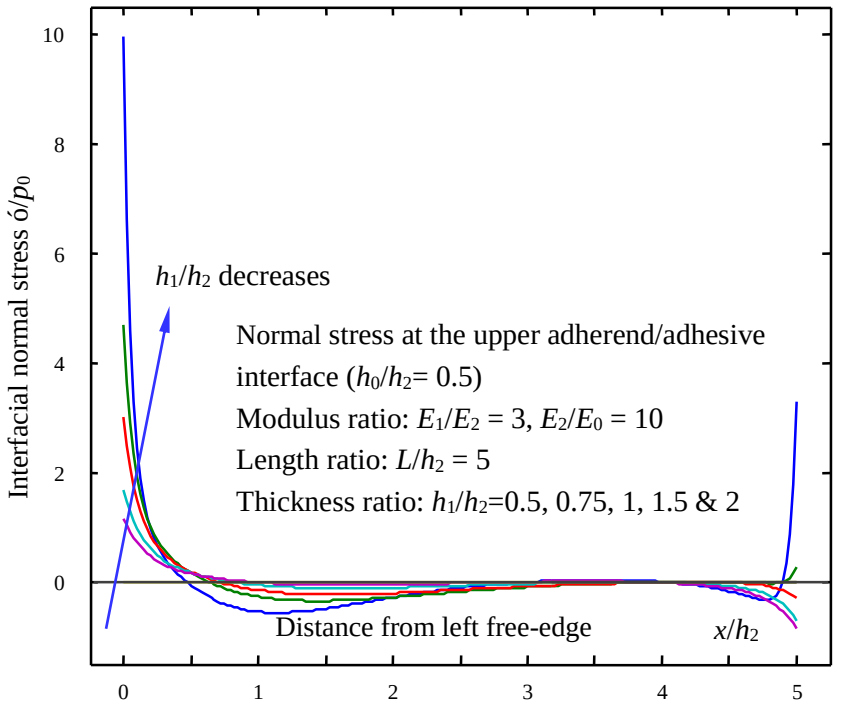


(*a*)

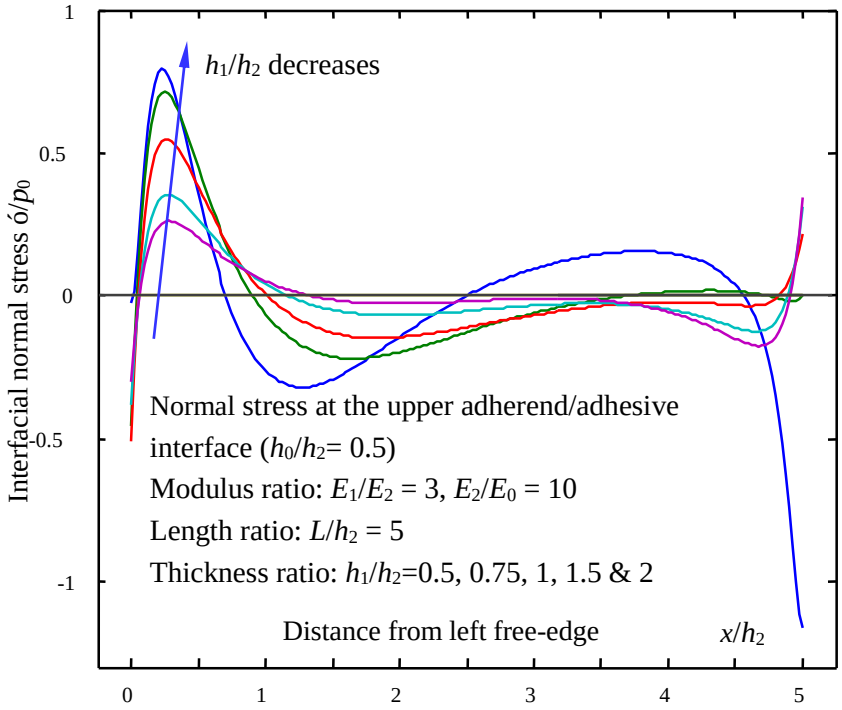


(*b*)

Figure 3.16. Comparison of the variations of the dimensionless interfacial normal stresses in the adhesively single-sided strap joint over the dimensionless distance from the mid-span: (*a*) The normal stress at the upper interface, (*b*) the normal stress at the lower interface. Thickness ratio $h_0/h_2$ = 0.5, Young's modulus ratio $E_2/E_0$ = 10.

It is obvious to observe that high interfacial shear and normal stress concentrations exist near the interior edges of the adherends. For both types of joints with and without the adhesive layer, due to the existence of a bending moment at the mid-span, as illustrated in Fig. 3.1(*b*), the peak value of interfacial normal stress at the interior edges is much larger than that of the shear stress in all the cases under this study. At both the upper and lower surfaces of the adhesive layer, the peak value of the shear stresses decreases with increasing adherend thickness ratio $h_1/h_2$. In particular, the shear stresses at the upper and low surfaces of the adhesive layer have close variation trending along the interface excluding the case of $h_1/h_2 = 0.5$. Also, the interfacial normal stresses at the upper and lower interfaces have very similar variation, both increasing rapidly with the decrease of adherend thickness ratio $h_1/h_2$. This implies that a thicker upper adherend (*i.e.*, larger flexural rigidity of the cover layer) can suppress the joint deflection and flexural stress and therefore suppress the debonding failure. The larger normal stress at the upper surface of the adhesive layer implies that the debonding failure would be pliable to appear along the upper adherend/adhesive interface. The observed varying trends of both the interfacial shear and normal stresses hold for all the cases under this investigation.

## 3.3. Conclusions

The semi-analytic ASSJ model well demonstrated the proposed method for interfacial stress analysis under mechanical or thermomechanical loads. First of all, two unknown interfacial shear and normal stress functions were introduced at each interface of the ASSJ. Secondly, by means of *Euler-Bernoulli* beam theory and 2D linear elasticity, the total stress field was expressed in terms of the interfacial

stress functions. Next, a set of four governing ODEs has been successfully formulated by triggering the theorem of minimum complementary strain energy, which was solved by using eigenfunction method. A semi-analytic solution can be derived for all ABJs made of three layers subjected to tension, shear force, bending moment, and thermomechanical loads. The stress results for each type of joint can be determined by modifying the traction BCs due to the different applications. The interfacial stress results [Fig. 3.3(*a*) & (*b*)] as predicted by the proposed ASSJ model not only satisfy all the traction BCs at the adherend ends and across the interfaces but also are validated by FEA.

By examining the interfacial stresses of thermostat in Figs. 3.6 and 3.7, the adhesive layer carries a large thermal expansion due to its relatively high Poisson's ratio, which is responsible for the higher interfacial stresses at the lower surface constrained by a stiffer adherend. This observation can be understood such that large thickness and low modulus of the adhesive layer could cause large mismatched deformations between the upper and lower adherends owing to the inconsistent thermal expansion.

Furthermore, by scaling analysis, it can be concluded that when letting only one parameter vary and fixing the rest parameters, both the interfacial shear and normal stresses decrease noticeably with increasing thickness of the adhesive layer and also decrease slightly with decreasing elastic modulus of the adhesive layer under the parameters utilized in this study. This observation can be understood such that the thicker and more complaint adhesive layer could provide larger deformation to accommodate the mismatching deformations between the upper and lower adherends and therefore decrease the interfacial stresses. Thus, the above scaling analysis could provide a clear picture on how the joint geometries and material properties influence the interfacial shear and normal stresses. These scaling results can be used to guide reliable and rational design and strength/failure analysis of ABJs.

Consequently, it needs to be emphasized that the theoretical formulation of the present stress-function variational method is within the framework of *Euler-Bernoulli* beam theory and linear elasticity, and no further assumptions were introduced during the above process. Therefore, the present theoretical modeling of stress field in ABJs is theoretically self-consistent; accuracy of the stress field of ABJs based on the present model only relies on the numerical process in solving the resulting set of 16 simultaneous linear algebraic equations [Eqs. 3.64(*a*-*p*)].

The present model can be further exploited for accurate structural design and optimization of ABJs since only one theoretical limitation was in the model assumption such that the axial stress in the joint varies linearly across the thickness. It needs to be noted that except the external stress expression in column {*D*} relevant to the BCs, all the derivations above are independent of the specific configuration of the ABJ. Based on this, the set of governing ODE is suitable for developing robust, high-efficiency methods for stress analysis of other ABJs as to be demonstrated in the following two chapters.

# 4. INTERFACIAL STRESS ANALYSIS OF ADHESIVELY BONDED SINGLE-LAP JOINTS

## 4.1. Introduction

Similar to ASSJ, Fig. 4.1(*a*) shows the configuration of an adhesively bonded single-lap joint (ABSLJ), which illustrates the shear traction applied at the right end of substrate layer. In contrast, at the left side of the cover layer, it is assumed that the joint to be fixed at a designed length far away the bonding area. The geometrical and mechanical parameters are given as: bonding length $L$, thicknesses $h_i$ ($i$ = 0,1,2), Young's modulus $E_i$ ($i$ = 0,1,2), and Poisson's ratio $v_i$ ($i$ = 0,1,2), and coefficients of thermal expansion $\alpha_i$ ($i$ = 0,1,2). The variables carrying subscripts 0, 1 and 2 represent those relating the adhesive layer, cover layer, and substrate layer, respectively. Similarly, the width $b$ of the joint is considered to be unit. The $x$-coordinate in this simplified 2$D$ system starts from the bonding line; the $y$-coordinate is along the vertical direction at the layer edge. In reality, both of the cover and bottom layers have the length much longer than the length of the bonding line. In the process of stress analysis, the left side of the upper layer is assumed to be fixed and the length of the bottom layer is $L$, so that there is only one bending moment resultant acting on the cover layer. In addition, the adhesive layer and two adherends of the ABSLJ are treated as isotropic, linearly thermoelastic materials, respectively. Fig. 4.1(*b*) illustrates the interfacial shear and normal stresses of the joint subjected to a uniform shear traction $\tau_0$ and bending moment resultant $M_1 = \tau_0 L$ at the cover layer. Since singular stresses of the joint appear near the edge of adherends due to mismatched materials boned at a sharp edge, creating a refined mesh in FEA can seize the high stress in the thin adhesive layer, which can demonstrate a reasonable comparison between the stress field predicted by the present stress-function variational method and those predicted by FEA . Fig. 4.1(*c*) displays the geometrical model of the single

lap joint subjected to a uniform shear force, which is used for FEM simulation of the stress field of the joint. In addition, *plane-stress* state is employed in this ABJ. As aforementioned, for the purpose of determining the stress field of the ABJ in the *plane-strain* state, it needs to replace the Young's moduli $E_i$ ($i$ = 1,0,2) by $(1- \upsilon_i^2)/E_i$, Poisson's ratios $\upsilon_i$ ($i$ = 1,0,2) by $\upsilon_i /(1- \upsilon_i)$, and coefficients of thermal expansion $\alpha_i$ ($i$ = 1,0,2) by $(1+ \upsilon_i)\alpha_i$.

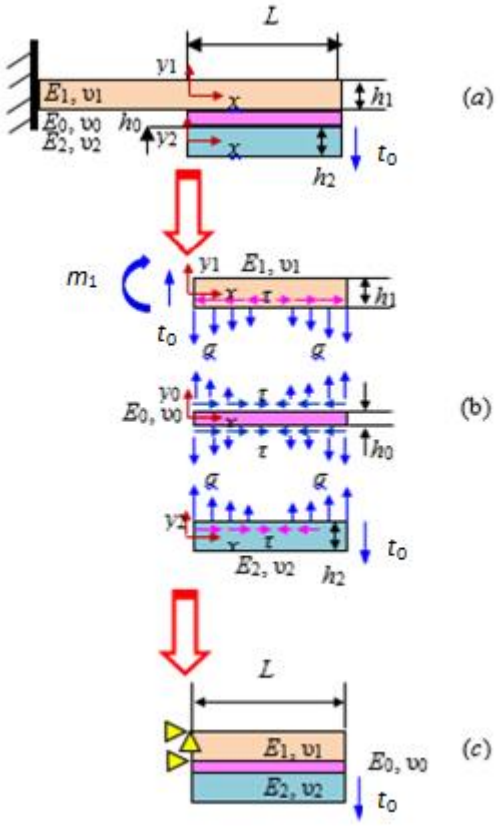


Figure 4.1. Schematic of an adhesively bonded sing-lap joint: (*a*) Geometrical configuration consists of a slender cover layer, an adhesive layer, and a slender substrate layer; (*b*) distribution of interfacial stresses in the joint; (*c*) geometrical model and loads for FEM simulation.

## 4.2. Model Formulation

Following the same process of the ASSJ in Chapter 3, the ABSLJ is assumed to be subjected to a shear traction $t_0$, the physical conditions of the axial force, shear traction, and bending moment of ABSLJ can be conveniently altered from [Figs. 3.2(*a*)-(*c*)] such that

$$S_1(0) = 0, \tag{4.1a}$$

$$S_1(L) = 0, \tag{4.1b}$$

$$Q_1(0) = t_0 b h_2, \tag{4.1c}$$

$$Q_1(L) = 0, \tag{4.1d}$$

$$M_1(0) = b m_1, \tag{4.1e}$$

$$M_1(L) = 0, \tag{4.1f}$$

$$S_2(0) = 0, \tag{4.1g}$$

$$S_2(L) = 0, \tag{4.1h}$$

$$Q_2(0) = 0, \tag{4.1i}$$

$$Q_2(L) = t_0 b h_2, \tag{4.1j}$$

$$M_2(0) = 0, \tag{4.1k}$$

$$M_2(L) = 0, \tag{4.1l}$$

$$S_0(0) = 0, \tag{4.1m}$$

$$S_0(L) = 0, \tag{4.1n}$$

$$Q_0(0) = 0, \tag{4.1o}$$

$$Q_0(L) = 0, \tag{4.1p}$$

$$M_0(0) = 0, \tag{4.1q}$$

$$M_0(L) = 0. \tag{4.1r}$$

where $t_0$ and $m_1$ are the average shear force and bending moment resultant per unit width of the joint. Given the unknown interfacial shear and normal stress functions at the upper and lower interfaces ($\tau_1 = f_1$, $\tau_2 = f_2$, $\sigma_1 = g_1$, $\sigma_2 = g_2$), the axial normal force, shear traction, and bending moment at the ends of the cover layer of the joint are expressed with BCs [Eq. (4.1*a*), Eq. (4.1*c*), and Eq. (4.1*e*)] and integration of Eqs. (3.4-6):

$$S_1(x) = -b\int_0^x f_1(\xi)d\xi, \tag{4.2}$$

$$Q_1(x) = t_0 bh_2 - b\int_0^x g_1(\xi)d\xi, \tag{4.3}$$

$$M_1(0) = bm_1 + t_0 bh_2 x - b\int_0^x \int_0^\zeta g_1(\zeta)d\zeta d\xi - \frac{bh_1}{2}\int_0^\xi f_1(\xi)d\xi, \tag{4.4}$$

Similar to those in Chapter 3, with BCs [Eq. (4.1*m*), Eq. (4.1*o*), and Eq. (4.1*q*)] and integration of Eqs. (3.7-9), the axial normal force, shear traction, and bending moment at the ends of adhesive layer in ABSLJ are written as:

$$S_0(x) = b\int_0^x [f_1(\xi) - f_2(\xi)]d\xi, \tag{4.5}$$

$$Q_0(x) = b\int_0^x [g_1(\xi) - g_2(\xi)]d\xi, \tag{4.6}$$

$$M_0(x) = b\int_0^x \int_0^\zeta [g_1(\zeta) - g_1(\zeta)]d\zeta d\xi - \frac{bh_0}{2}\int_0^x [f_1(\xi) + f_1(\xi)]d\xi. \tag{4.7}$$

Furthermore, with BCs [Eq. (4.1*g*), Eq. (4.1*i*), and Eq. (4.1*k*)] and integration of Eqs. (3.10-12), the axial normal force, shear traction, and bending moment in the bottom adherend of the ABSLJ can be expressed as

$$S_2(x) = b\int_0^x f_2(\xi)d\xi, \tag{4.8}$$

$$Q_2(x) = b\int_0^x g_2(\xi)d\xi, \tag{4.9}$$

$$M_2(x) = b\int_0^x \int_0^\zeta g_2(\zeta)d\zeta d\xi - \frac{bh_2}{2}\int_0^x f_2(\xi)d\xi. \tag{4.10}$$

Since the bending moment superimposed with a uniform shear traction $t_0$ on the cover layer which is caused by the pure shear traction acting on the substrate layer, the axial normal stress can be determined according to the elementary *Euler-Bernoulli* beam theory and 2D static equilibrium equation [Eq. (3.33) & Eq. (3.35)] as

$$\begin{aligned}\sigma_{xx}^{(1)} &= \frac{S_1}{bh_1} - \frac{M_1 y_1}{I_1} = -\frac{1}{h_1}\int_0^x f_1(\xi)d\xi \\ &\quad + \frac{12y_1}{h_1^3}[-m_1 - t_0 h_2 x + \int_0^x \int_0^\zeta g_1(\zeta)d\zeta d\xi + \frac{h_1}{2}\int_0^x f_1(\xi)d\xi],\end{aligned} \tag{4.11}$$

$$\tau_{y_1x}^{(1)} = \frac{1}{h_1}[(\frac{h_1}{2} - y_1) - \frac{3}{h_1}(\frac{h_1^2}{4} - y_1^2)]f_1(x) - \frac{6}{h_1^3}(\frac{h_1^2}{4} - y_1^2)\int_0^x g_1(\xi)d\xi + \frac{6}{h_1^3}(\frac{h_1^2}{4} - y_1^2)t_0 h_2, \tag{4.12}$$

$$\begin{aligned}\sigma_{y_1y_1}^{(1)} &= -\frac{1}{h_1}\{\frac{h_1}{2}(\frac{h_1}{2} - y_1) - \frac{1}{2}(\frac{h_1^2}{4} - y_1^2) - \frac{3}{h_1}[\frac{h_1^2}{4}(\frac{h_1}{2} - y_1) - \frac{1}{3}(\frac{h_1^3}{8} - y_1^3)]\}f_1'(x) \\ &\quad + \frac{6}{h_1^3}[\frac{h_1^2}{4}(\frac{h_1}{2} - y_1) - \frac{1}{3}(\frac{h_1^3}{8} - y_1^3)]g_1(x).\end{aligned} \tag{4.13}$$

$$\begin{aligned}\sigma_{xx}^{(0)} &= \frac{S_0}{bh_0} - \frac{M_0 y_0}{I_0} = \frac{1}{h_0}\int_0^x [f_1(\xi) - f_2(\xi)]d\xi \\ &\quad - \frac{12y_0}{h_0^3}\{\int_0^x \int_0^\zeta [g_1(\zeta) - g_2(\zeta)]d\zeta d\xi - \frac{h_0}{2}\int_0^x [f_1(\xi) + f_1(\xi)]d\xi\},\end{aligned} \tag{4.14}$$

$$\begin{aligned}\tau_{y_0x}^{(0)} &= -f_2(x) - \frac{1}{h_0}(y_0 + \frac{h_0}{2})[f_1(x) - f_2(x)] - \frac{3}{h_0^2}(y_0^2 - \frac{h_0^2}{4})[f_1(x) + f_2(x)] \\ &\quad + \frac{6}{h_0^3}(y_0^2 - \frac{h_0^2}{4})\int_0^x [g_1(\xi) - g_2(\xi)]d\xi,\end{aligned} \tag{4.15}$$

$$\sigma_{y_0y_0}^{(0)} = g_2(x) + (y_0 + \frac{h_0}{2}) f_2'(x) + \frac{1}{h_0}[\frac{1}{2}(y_0^2 - \frac{h_0^2}{4}) + \frac{h_0}{2}(y_0 + \frac{h_0}{2})][f_1'(x) - f_2'(x)]$$
$$+ \frac{3}{h_0^2}[\frac{1}{3}(y_0^3 + \frac{h_0^3}{8}) - \frac{h_0^2}{4}(y_0 + \frac{h_0}{2})][f_1'(x) + f_2'(x)] \quad (4.16)$$
$$- \frac{6}{h_1^3}[\frac{1}{3}(y_0^3 + \frac{h_0^3}{8}) - \frac{h_0^2}{4}(y_0 + \frac{h_0}{2})][g_1(x) - g_1(x)].$$

$$\sigma_{xx}^{(2)} = \frac{S_2}{bh_2} - \frac{M_2 y_2}{I_2} = \frac{1}{h_2}\int_0^x f_2(\xi)d\xi - \frac{12y_2}{h_2^3}[\int_0^x \int_0^\zeta g_2(\zeta)d\zeta d\xi - \frac{h_2}{2}\int_0^x f_2(\xi)d\xi], \quad (4.17)$$

$$\tau_{y_2x}^{(2)} = -\frac{1}{h_2}[(y_2 + \frac{h_2}{2}) + \frac{3}{h_2}(y_2^2 - \frac{h_2^2}{4})] f_2(x) + \frac{6}{h_2^3}(y_2^2 - \frac{h_2^2}{4})\int_0^x g_2(\xi)d\xi, \quad (4.18)$$

$$\sigma_{y_2y_2}^{(2)} = \{\frac{1}{h_2}[\frac{1}{2}(y_2^2 - \frac{h_2^2}{4}) + \frac{h_2}{2}(y_2 + \frac{h_2}{2}) + \frac{3}{h_2^2}[\frac{1}{3}(y_1^3 + \frac{h_2^3}{8}) - \frac{h_1^2}{4}(y_2 + \frac{h_2}{2})]\} f_2'(x)$$
$$- \frac{6}{h_1^3}[\frac{1}{3}(y_2^3 + \frac{h_2^3}{8}) - \frac{h_2^2}{4}(y_2 + \frac{h_2}{2})]g_2(x). \quad (4.19)$$

With the aid of complimentary strain energy functional (3.43) and the theorem of minimum complimentary strain energy, the interfacial stress equations $f_1$, $f_2$, $g_1$, and $g_2$ should satisfy a set of ODEs as

$$[\mathrm{A}]\{\Phi^{(IV)}\} + [\mathrm{B}]\{\Phi''\} + [\mathrm{C}]\{\Phi\} + \{\mathrm{D}\} = \{0\}. \quad (4.20)$$

where $\{\Phi\}$ is a column of dimensionless interfacial stress functions and [*A*], [*B*] and [*C*] are system matrices defined in (3.52), (3.53), and (3.54), respectively. In addition, the dimensionless generalized force column $\{D\}_{4\times1}$ is a function with respect to the shear traction, bending moment resultant, displacement on the bonding patch, and thermomechanical loads, etc., as below

$$
\begin{aligned}
D_1 &= \frac{6m_1 + 6t_0 h_2 x}{h_1^2 E_1} + \frac{\Delta T}{2}(-\alpha_0 + \alpha_1), \\
D_2 &= -\frac{12m_1 + 12t_0 h_2 x}{h_1^3 E_1}, \\
D_3 &= \frac{\Delta T}{2}(-\alpha_2 + \alpha_0), \\
D_4 &= 0.
\end{aligned}
\tag{4.21}
$$

Furthermore, subjected to the shear traction, differentiation of the particular solution with respect to the spatial dimension is:

$$
\frac{d}{d\xi}\{\Phi_0\} = -[C]^{-1}\frac{d}{d\xi}\{D\} = -6h_{12}^{-2}[C]^{-1}\begin{Bmatrix} 1 \\ -2h_{12}^{-1} \end{Bmatrix} t_0 \tag{4.22}
$$

It can be noticed from the above that relation (4.22) is a linear function of *x*. Then, the solution to the interfacial stress functions can be further expressed as

$$
\{\Phi\} = \sum_{k=1}^{8}[\left[c_k\{\Psi_0^k\}\exp(\lambda_k\xi) + d_k\{\Psi_0^k\}\exp(-\lambda_k\xi)\right] + \{\Phi_0(\xi)\} \tag{4.23}
$$

In the present case, the reduced BCs for ABSLJ are:

$$F_1(0) = 0, \tag{4.24a}$$

$$F_1(L/h_2) = 0, \tag{4.24b}$$

$$F_1'(0) = 0, \tag{4.24c}$$

$$F_1'(L/h_2) = 0, \tag{4.24d}$$

$$G_1(0) = 0, \tag{4.24e}$$

$$G_1(L/h_2) = \frac{m_1}{p_0} + \frac{t_0 L}{p_0 h_0}, \tag{4.24f}$$

$$G_1'(0) = 0, \tag{4.24g}$$

$$G_1'(L/h_2)=\frac{t_0}{p_0}, \tag{4.24h}$$

$$F_2(0)=0, \tag{4.24i}$$

$$F_2(L/h_2)=0, \tag{4.24j}$$

$$F_2'(0)=0, \tag{4.24k}$$

$$F_2'(L/h_2)=0, \tag{4.24l}$$

$$G_2(0)=0, \tag{4.24m}$$

$$G_2(L/h_2)=0, \tag{4.24n}$$

$$G_2'(0)=0, \tag{4.24o}$$

$$G_2'(L/h_2)=\frac{t_0}{p_0}. \tag{4.24p}$$

The differentiations of the particular solutions are utilized to form the resulting set of simultaneous linear algebraic equations with the above BCs [Eqs. (4.24*a*-*p*)]:

$$\sum_{k=1}^{8} c_k \Psi_0^{k,1} + \sum_{k=1}^{8} d_k \Psi_0^{k,1} = -\Phi_0^{(1)}, \tag{4.25a}$$

$$\sum_{k=1}^{8} c_k \Psi_0^{k,1} \exp(\lambda_k L/h_2) + \sum_{k=1}^{8} d_k \Psi_0^{k,1} \exp(-\lambda_k L/h_2) = -\Phi_0^{(1)}, \tag{4.25b}$$

$$\sum_{k=1}^{8} c_k \lambda_k \Psi_0^{k,1} - \sum_{k=1}^{8} d_k \lambda_k \Psi_0^{k,1} = -\frac{d\Phi_0^{(1)}}{d\xi}, \tag{4.25c}$$

$$\sum_{k=1}^{8} c_k \lambda_k \Psi_0^{k,1} \exp(\lambda_k L/h_2) - \sum_{k=1}^{8} d_k \lambda_k \Psi_0^{k,1} \exp(-\lambda_k L/h_2) = -\frac{d\Phi_0^{(1)}}{d\xi}, \tag{4.25d}$$

$$\sum_{k=1}^{8} c_k \Psi_0^{k,2} + \sum_{k=1}^{8} d_k \Psi_0^{k,2} = -\Phi_0^{(2)}, \tag{4.25e}$$

$$\sum_{k=1}^{8} c_k \Psi_0^{k,2} \exp(\lambda_k L/h_2) + \sum_{k=1}^{8} d_k \Psi_0^{k,2} \exp(-\lambda_k L/h_2) = \frac{m_1}{p_0} + \frac{t_0 L}{p_0 h_0} - \Phi_0^{(2)}, \quad (4.25f)$$

$$\sum_{k=1}^{8} c_k \lambda_k \Psi_0^{k,2} - \sum_{k=1}^{8} d_k \lambda_k \Psi_0^{k,2} = -\frac{d\Phi_0^{(2)}}{d\xi}, \quad (4.25g)$$

$$\sum_{k=1}^{8} c_k \lambda_k \Psi_0^{k,2} \exp(\lambda_k L/h_2) - \sum_{k=1}^{8} d_k \lambda_k \Psi_0^{k,2} \exp(-\lambda_k L/h_2) = \frac{t_0}{p_0} - \frac{d\Phi_0^{(2)}}{d\xi}, \quad (4.25h)$$

$$\sum_{k=1}^{8} c_k \Psi_0^{k,3} + \sum_{k=1}^{8} d_k \Psi_0^{k,3} = -\Phi_0^{(3)}, \quad (4.25i)$$

$$\sum_{k=1}^{8} c_k \Psi_0^{k,3} \exp(\lambda_k L/h_2) + \sum_{k=1}^{8} d_k \Psi_0^{k,3} \exp(-\lambda_k L/h_2) = h_{02}/2 - \Phi_0^{(3)}, \quad (4.25j)$$

$$\sum_{k=1}^{8} c_k \lambda_k \Psi_0^{k,3} - \sum_{k=1}^{8} d_k \lambda_k \Psi_0^{k,3} = -\frac{d\Phi_0^{(3)}}{d\xi}, \quad (4.25k)$$

$$\sum_{k=1}^{8} c_k \lambda_k \Psi_0^{k,3} \exp(\lambda_k L/h_2) - \sum_{k=1}^{8} d_k \lambda_k \Psi_0^{k,3} \exp(-\lambda_k L/h_2) = -\frac{d\Phi_0^{(3)}}{d\xi}, \quad (4.25l)$$

$$\sum_{k=1}^{8} c_k \Psi_0^{k,4} + \sum_{k=1}^{8} d_k \Psi_0^{k,4} = -\Phi_0^{(4)}, \quad (4.25m)$$

$$\sum_{k=1}^{8} c_k \Psi_0^{k,4} \exp(\lambda_k L/h_2) + \sum_{k=1}^{8} d_k \Psi_0^{k,4} \exp(-\lambda_k L/h_2) = -[h_{02}/4 + \Phi_0^{(4)}], \quad (4.25n)$$

$$\sum_{k=1}^{8} c_k \lambda_k \Psi_0^{k,4} - \sum_{k=1}^{8} d_k \lambda_k \Psi_0^{k,4} = -\frac{d\Phi_0^{(4)}}{d\xi}, \quad (4.25o)$$

$$\sum_{k=1}^{8} c_k \lambda_k \Psi_0^{k,4} \exp(\lambda_k L/h_2) - \sum_{k=1}^{8} d_k \lambda_k \Psi_0^{k,4} \exp(-\lambda_k L/h_2) = \frac{t_0}{p_0} - \frac{d\Phi_0^{(4)}}{d\xi}, \quad (4.25p)$$

where $\Psi_0^{k,1}$, $\Psi_0^{k,2}$, $\Psi_0^{k,3}$, and $\Psi_0^{k,4}$ ($k$ = 1, 2, …, 8) are respectively the 1st to 4th elements of the $k$-th eigenvector, and $\Phi_0^{(1)}$, $\Phi_0^{(2)}$, $\Phi_0^{(3)}$, and $\Phi_0^{(4)}$ are the 1st to 4th elements of the particular solution vector $\{\Phi_0\}$.

Eventually, the interfacial shear stresses [Eqs. (3.48) & (3.50)] have the additional terms of derivation of the corresponding particular solution:

$$f_1(x)/p_0 = -\sum_{k=1}^{8} c_k \lambda_k \Psi_0^{k,1} \exp(\lambda_k x/h_2) + \sum_{k=1}^{8} d_k \lambda_k \Psi_0^{k,1} \exp(-\lambda_k x/h_2) + \frac{d\Phi_0^{(1)}}{d\xi}, \tag{4.26}$$

$$g_1(x)/p_0 = \sum_{k=1}^{8} c_k \lambda_k^2 \Psi_0^{k,2} \exp(\lambda_k x/h_2) + \sum_{k=1}^{8} d_k \lambda_k^2 \Psi_0^{k,2} \exp(-\lambda_k x/h_2), \tag{4.27}$$

$$f_2(x)/p_0 = -\sum_{k=1}^{8} c_k \lambda_k \Psi_0^{k,3} \exp(\lambda_k x/h_2) + \sum_{k=1}^{8} d_k \lambda_k \Psi_0^{k,3} \exp(-\lambda_k x/h_2) + \frac{d\Phi_0^{(3)}}{d\xi}, \tag{4.28}$$

$$g_2(x)/p_0 = \sum_{k=1}^{8} c_k \lambda_k^2 \Psi_0^{k,4} \exp(\lambda_k x/h_2) + \sum_{k=1}^{8} d_k \lambda_k^2 \Psi_0^{k,4} \exp(-\lambda_k x/h_2). \tag{4.29}$$

## 4.3. Model Validation

Subjected to shear traction $t_0$ (1MPa), the stress field of ABSLJ is determined by the proposed semi-analytic stress-function variational method and further compared to numerical solutions based on ANSYS™ (with the 2D plane-stress element type: PLANE182) using two different mesh sizes (0.1 × 0.1 mm and 0.05 × 0.05 mm). The geometrical parameters of the ABSLJ model are taken as: $L$ = 20 mm, $h_1$ = 2.0 mm (steel/cover), $h_2$ = 2.0 mm (aluminum/bottom), and $h_0$ = 0.2 mm (epoxy/adhesive). Parameters of material properties are given as: $E_1$ = 210 GPa, $v_1$ = 0.293 (steel/cover), $E_2$ = 70 GPa, $v_2$ = 0.345 (aluminum/bottom), and $E_0$ = 10 GPa, $v_0$ = 0.40 (epoxy/adhesive). During the FEA simulation using ANSYS™, to constrain the rigid motion of the joint in the horizontal direction under shear traction, a single corner node is constrained as shown in Fig. 4.1(*a*).

During the FEA process of the ABSLJ, the shear traction is selected to distribute evenly to all the nodes on the right edge of the substrate adherend. For instance, the average shear force acting on a node is calculated based on the force resultant of the uniform shear traction 1 MPa acting on an area of the width 1m and thickness 2 mm:

$$t_{node} = \frac{\tau_0 b h_2}{\text{node number} - 1} = \frac{1\text{MPa} \times 1\text{m} \times 2\text{mm}}{21 - 1} = 100\text{N}. \tag{4.30}$$

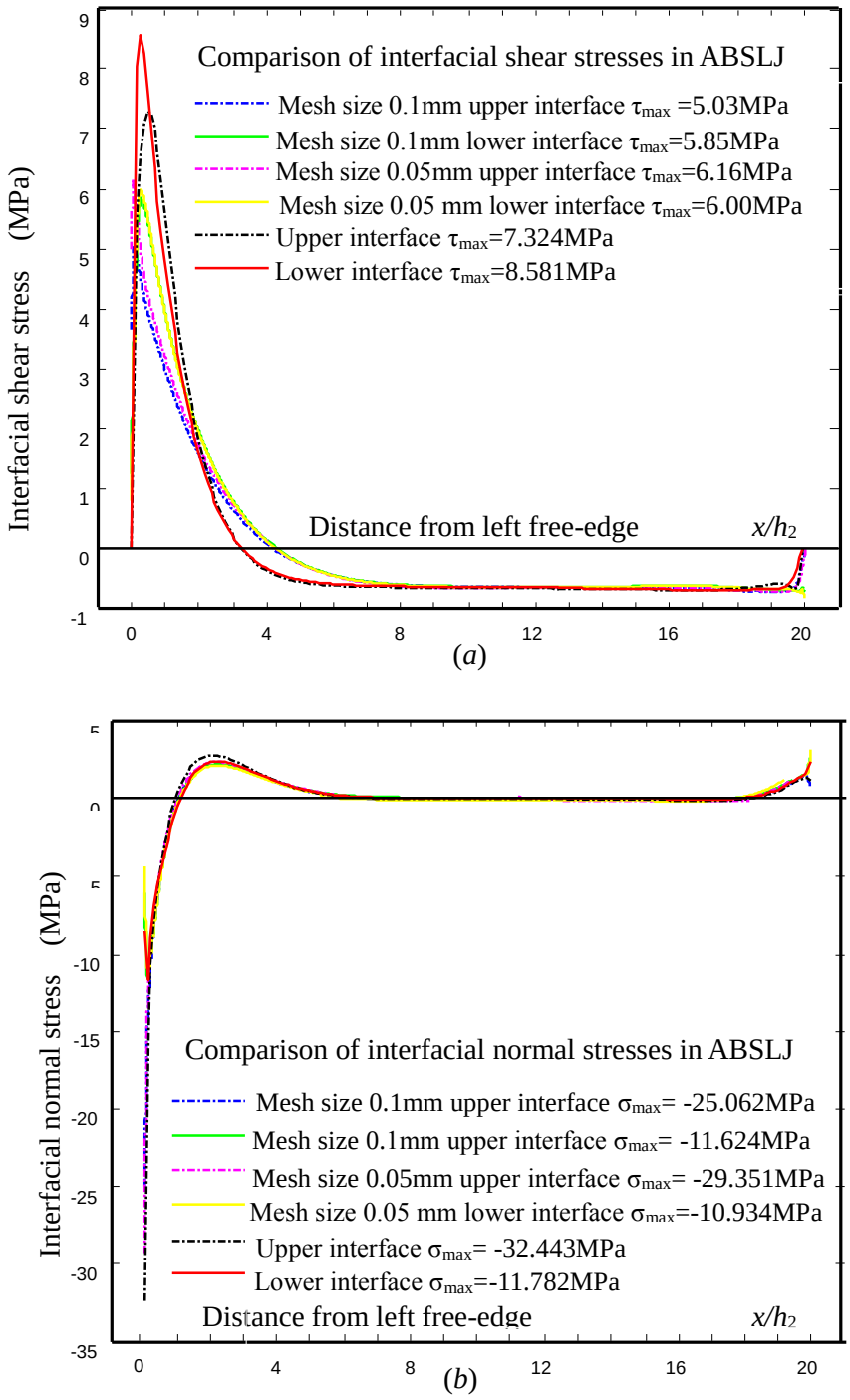


Figure 4.2. Validation of the stress-function variational method for interfacial shear and normal stresses in ABSLJ subjected to shear traction: (*a*) Interfacial shear stress, (*b*) interfacial normal stress.

Shear force with the average force magnitude is applied to the inner nodes of the elements of the joint, while shear force with the half average force magnitude is applied to the first and last edge nodes. Figs. 4.2 (*a*) and (*b*) are the interfacial shear and normal stresses predicted by the present stress-function variational method and related validation by ANSYS™, from which it can be observed that the model predicted shear stresses satisfy the shear-free BCs. Also, the present semi-analytic method and FEM simulation both predict the interfacial normal and shear stresses carrying the same trends along the bonding lines. The shear stresses predicted by the present joint model are slightly higher than those by ANSYS™. Due to the sharp edges responsible for the singular stresses at the joint free-edges, the values of free-edge stresses of the joint predicted by FEA are expected to increase with decreasing mesh size. From the predicted interfacial stresses, it can be found that the normal stress at the upper interface is higher than that at the lower interface, which indicates that debonding failure would most likely initiate at the left edge of this particular ABSLJ.

In addition, Erdogan and his co-workers published an analytic joint model for predicting the interfacial stresses of ABSLJ subjected to tension, shear, or bending moment, or their combinations (Delale et al., 1981). The deficiencies of Erdogan's joint model are ignorance of the thickness effect of adhesive layer and non-satisfaction of the shear-free BCs. As a result, the stress field predicted by Erdogan's joint model has a large deviation from those predicted by FEA and also the present stress-function variational method. Erdogan's joint model is one of the important semi-analytic joint models available in the literature. In Erdogan's ABSLJ model, the interfacial shear and normal (peeling) stresses are given by the following two expressions:

$$\tau(x) = K_0 + K_1 \sinh(\phi_1 x) + K_2 \cosh(\phi_1 x) + K_3 \sinh(\phi_2 x) + K_4 \cosh(\phi_2 x) + K_5 \sinh(\phi_3 x) + K_6 \cosh(\phi_3 x). \tag{4.31}$$

$$\sigma(x) = -\frac{1}{\alpha_2}[(\alpha_1\phi_1 + \phi_1^3)(K_1 \cosh(\phi_1 x) + K_2 \sinh(\phi_1 x) + (\alpha_1\phi_2 + \phi_2^3)(K_3 \cosh(\phi_2 x) + K_4 \sinh(\phi_2 x) + (\alpha_1\phi_3 + \phi_3^3)(K_5 \cosh(\phi_3 x) + K_6 \sinh(\phi_3 x)]. \tag{4.32}$$

where $K_0$, $K_1$, $K_2$, $K_3$, $K_4$, $K_5$, and $K_6$ are the integration constants, $\alpha_1$ and $\alpha_2$ are related to the geometrical parameters, $\varphi_1, \varphi_2,$ and $\varphi_3$ are complex numbers, which are determined to satisfy the multiple traction BCs of the joint.

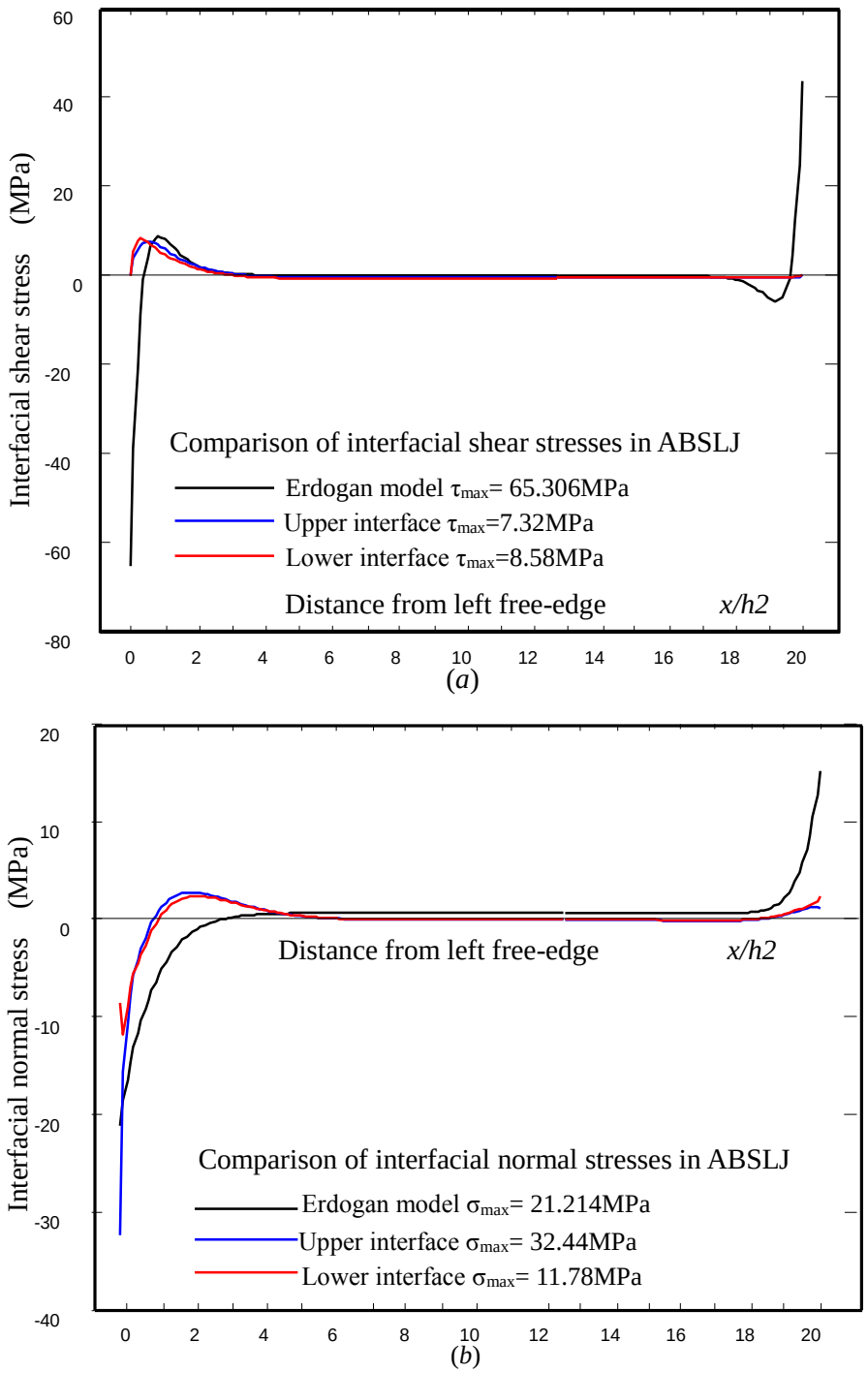


Figure 4.3. Comparison of interfacial stresses predicted by the present stress-function variational method with those by Erdogan's model subjected to shear traction: (*a*) Interfacial shear stress, (*b*) interfacial normal stress.

In Fig. 4.3(*a*), the maximum and minimum values of the interfacial shear stresses according to Eq. (4.31) are overestimated though Erdogan's joint model predicts the similar values of the shear stress as predicted by the current method. On the left side of Fig. 4.3(*b*), the peak values of the interfacial normal stresses at the upper and lower interfaces according to Eq. (4.32) are only close to the medium ones predicted by the present method. However, at the right end, the peak values of the interfacial normal stresses are far higher than those predicted by the present method.

## 4.4. Conclusions

In this chapter, the stress-function variational method has been furthered to determine the stress field of ABSLJ. Similar to those developed in Chapter 3, a semi-analytic solution has been derived by introducing two unknown interfacial shear and normal stress functions at each interface of the ABSLJ. The proposed joint model predicted severe concentration of interfacial stresses at the left end of the joint, which has been validated by commercial FEA package (ANSYS$^{TM}$). The interfacial normal stresses are supposed responsible for debonding failure of the ABJs because their peak values are much larger than those of the shear stresses. The predicted interfacial shear stresses satisfy the shear-free condition at the free edges of adherends, which is normally ignored in the majority of joint models well documented in the literature. In addition, the present semi-analytic stress-function variational method only used two fundamental assumptions of *Euler-Bernoulli* beam theory and 2D linear elasticity, and the accuracy of the stress field of ABJs predicted by the present method only relies on the numerical process in solving the resulting set of 16 simultaneous algebraic Eqs. [4.25(*a*-*p*)].

With the robust numerical stress field predicted by the present ASSJ and ABSLJ models, the stress field of general ABJs or other bonded joints subjected to arbitrary combination of tension, shear traction, bending moment or temperature change can be accurately predicted as the superimposition of the interfacial stresses caused by each load separately.

# 5. APPLICATIONS OF STRESS-FUNCTION VARIATIONAL METHOD FOR INTERFACIAL STRESS ANALYSIS OF OTHER JOINTS

## 5.1. Adhesively Single-sided Bonded Joints

### 5.1.1. Introduction

In this section, the robust, high-efficiency stress-function variational method formulated in Chapter 3 is further used for stress analysis of adhesively single-sided bonded joints (ASSBJs). In this case, the configuration of an ASSBJ is shown in Fig. 5.1(*a*), which consists of a cover layer, an adhesive layer, and a substrate layer from the top to bottom with the uniform width *b* and overlap bonding length *L*. The coordination system is created from the symmetric mid-span of the joint; the *y*-axis is selected perpendicular to *x*-axis. The cover layer carries the thickness $h_1$, Young's modulus $E_1$, and Poisson's ratio $v_1$; the adhesive layer bears the thickness $h_0$, Young's modulus $E_0$, and Poisson's ratio $v_0$; the bottom layer has the thickness $h_2$, Young's modulus $E_2$, and Poisson's ratio $v_2$. In particular, a uniform tension is applied at the two ends of the substrate layer. Besides, illustration of the interfacial stresses is shown in Fig. 5.1(*b*). Since the joint is structurally symmetric with respect to the *y*-axis, only the right half portion of the joint is needed for stress analysis by means of the innovative stress-function variational method formulated in this study and FEM based on the commercial FEA software package (ANSYS$^{TM}$) [Fig. 5.1(*c*)]. As aforementioned, when the joint is loaded in *plane-strain* state, it only needs to replace the Young's moduli $E_i$ ($i$ = 1,0,2) by $(1-\upsilon_i^2)/E_i$, Poisson's ratios $\upsilon_i$ ($i$ = 1,0,2) by $\upsilon_i/(1-\upsilon_i)$, and coefficients of thermal expansion $\alpha_i$ ($i$ = 1,0,2) by $(1+\upsilon_i)\alpha_i$.

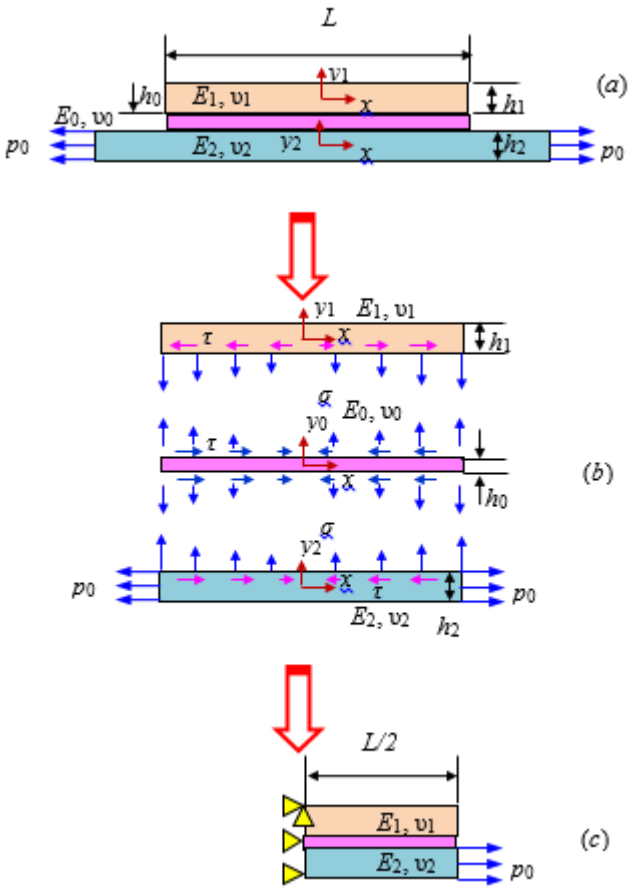


Figure 5.1. Schematic of an adhesively single-sided bonded joint: (*a*) Geometrical configuration consists of an identical substrate layer, an adhesive layer, and a slender cover layer, (*b*) interfacial stress distribution, and (*c*) geometrical model and loads for FEM simulation.

## 5.1.2. Model Formulation

Theoretically, static equilibrium equations of the representative segmental element of the upper adherend, adhesive layer, and lower adherend are the same as those used in the previous two chapters. External mechanical loadings in terms of axial force, shear traction, and bending moment at the ends of the three layers [Figs. 3.2(*a*)-(*c*)] are taken into account. The traction BCs in terms of force and moment resultants are given as

$$S_1(0) = 0, \tag{5.1a}$$

$$S_1(L) = 0, \tag{5.1b}$$

$$Q_1(0) = 0, \tag{5.1c}$$

$$Q_1(L) = 0, \tag{5.1d}$$

$$M_1(0) = 0, \tag{5.1e}$$

$$M_1(L) = 0, \tag{5.1f}$$

$$S_2(0) = p_0 b h_2, \tag{5.1g}$$

$$S_2(L) = p_0 b h_2, \tag{5.1h}$$

$$Q_2(0) = 0, \tag{5.1i}$$

$$Q_2(L) = 0, \tag{5.1j}$$

$$M_2(0) = 0, \tag{5.1k}$$

$$M_2(L) = 0, \tag{5.1l}$$

$$S_0(0) = 0, \tag{5.1m}$$

$$S_0(L) = 0, \tag{5.1n}$$

$$Q_0(0) = 0, \tag{5.1o}$$

$$Q_0(L) = 0, \tag{5.1p}$$

$$M_0(0) = 0, \tag{5.1q}$$

$$M_0(L) = 0. \tag{5.1r}$$

In this case, it is convenient to conduct accurate stress analysis of the ASSBJ model due to its simple geometrical configuration. Similar to the derivations developed in the proceeding Chapters 3 and 4, the static equilibrium equation of the representative segmental elements can be introduced. In the present

model with no external loadings at the cover layer, the normal force, shear traction, and bending moment of the joint can be expressed as

$$S_1(x) = -b\int_0^x f_1(\xi)d\xi, \tag{5.2}$$

$$Q_1(x) = -b\int_0^x g_1(\xi)d\xi, \tag{5.3}$$

$$M_1(x) = -b\int_0^x \int_0^\zeta g_1(\zeta)d\zeta d\xi - \frac{bh_1}{2}\int_0^x f_1(\xi)d\xi. \tag{5.4}$$

Similarly, for the adhesive layer, it reads

$$S_0(x) = b\int_0^x [f_1(\xi) - f_2(\xi)]d\xi, \tag{5.5}$$

$$Q_0(x) = b\int_0^x [g_1(\xi) - g_2(\xi)]d\xi, \tag{5.6}$$

$$M_0(x) = b\int_0^x \int_0^\zeta [g_1(\zeta) - g_1(\zeta)]d\zeta d\xi - \frac{bh_0}{2}\int_0^x [f_1(\xi) + f_1(\xi)]d\xi. \tag{5.7}$$

The external loading $p_0$ is implemented at the edges of the substrate layer, thus

$$S_2(x) = p_0 bh_2 + b\int_0^x f_2(\xi)d\xi, \tag{5.8}$$

$$Q_2(x) = b\int_0^x g_2(\xi)d\xi, \tag{5.9}$$

$$M_2(x) = b\int_0^x \int_0^\zeta g_2(\zeta)d\zeta d\xi - \frac{bh_2}{2}\int_0^x f_2(\xi)d\xi. \tag{5.10}$$

Compared to the previous two joint models (i.e., ASSJ and ASLBJ), the ASSBJ has the uniform axial traction $p_0$ at both the ends of the substrate layer. Similarly, the stress components can be expressed on the basis of the *Euler-Bernoulli* beam theory and 2D elasticity [Eqs. (3.33) & (3.35)].

$$\sigma_{xx}^{(1)} = \frac{S_1}{bh_1} - \frac{M_1 y_1}{I_1} = -\frac{1}{h_1}\int_0^x f_1(\xi)d\xi + \frac{12y_1}{h_1^3}[\int_0^x \int_0^\zeta g_1(\zeta)d\zeta d\xi + \frac{h_1}{2}\int_0^x f_1(\xi)d\xi], \tag{5.11}$$

$$\tau_{y_1 x}^{(1)} = \frac{1}{h_1}[(\frac{h_1}{2} - y_1) - \frac{3}{h_1}(\frac{h_1^2}{4} - y_1^2)]f_1(x) - \frac{6}{h_1^3}(\frac{h_1^2}{4} - y_1^2)\int_0^x g_1(\xi)d\xi, \tag{5.12}$$

$$\sigma_{y_1y_1}^{(1)} = -\frac{1}{h_1}\{\frac{h_1}{2}(\frac{h_1}{2}-y_1)-\frac{1}{2}(\frac{h_1^2}{4}-y_1^2)-\frac{3}{h_1}[\frac{h_1^2}{4}(\frac{h_1}{2}-y_1)-\frac{1}{3}(\frac{h_1^3}{8}-y_1^3)]\}f_1'(x) + \frac{6}{h_1^3}[\frac{h_1^2}{4}(\frac{h_1}{2}-y_1)-\frac{1}{3}(\frac{h_1^3}{8}-y_1^3)]g_1(x). \tag{5.13}$$

$$\sigma_{xx}^{(0)} = \frac{S_0}{bh_0}-\frac{M_0y_0}{I_0} = \frac{1}{h_0}\int_0^x[f_1(\xi)-f_2(\xi)]d\xi-\frac{12y_0}{h_0^3}\{\int_0^x\int_0^\zeta[g_1(\zeta)-g_2(\zeta)]d\zeta d\xi - \frac{h_0}{2}\int_0^x[f_1(\xi)+f_1(\xi)]d\xi\}, \tag{5.14}$$

$$\tau_{y_0x}^{(0)} = -f_2(x)-\frac{1}{h_0}(y_0+\frac{h_0}{2})[f_1(x)-f_2(x)]-\frac{3}{h_0^2}(y_0^2-\frac{h_0^2}{4})[f_1(x)+f_2(x)] + \frac{6}{h_0^3}(y_0^2-\frac{h_0^2}{4})\int_0^x[g_1(\xi)-g_2(\xi)]d\xi, \tag{5.15}$$

$$\sigma_{y_0y_0}^{(0)} = g_2(x)+(y_0+\frac{h_0}{2})f_2'(x)+\frac{1}{h_0}[\frac{1}{2}(y_0^2-\frac{h_0^2}{4})+\frac{h_0}{2}(y_0+\frac{h_0}{2})][f_1'(x)-f_2'(x)] + \frac{3}{h_0^2}[\frac{1}{3}(y_0^3+\frac{h_0^3}{8})-\frac{h_0^2}{4}(y_0+\frac{h_0}{2})][f_1'(x)+f_2'(x)] - \frac{6}{h_1^3}[\frac{1}{3}(y_0^3+\frac{h_0^3}{8})-\frac{h_0^2}{4}(y_0+\frac{h_0}{2})][g_1(x)-g_1(x)]. \tag{5.16}$$

$$\sigma_{xx}^{(2)} = \frac{S_2}{bh_2}-\frac{M_2y_2}{I_2} = p_0+\frac{1}{h_2}\int_0^x f_2(\xi)d\xi-\frac{12y_2}{h_2^3}[\int_0^x\int_0^\zeta g_2(\zeta)d\zeta d\xi-\frac{h_2}{2}\int_0^x f_2(\xi)d\xi], \tag{5.17}$$

$$\tau_{y_2x}^{(2)} = -\frac{1}{h_2}[(y_2+\frac{h_2}{2})+\frac{3}{h_2}(y_2^2-\frac{h_2^2}{4})]f_2(x)+\frac{6}{h_2^3}(y_2^2-\frac{h_2^2}{4})\int_0^x g_2(\xi)d\xi, \tag{5.18}$$

$$\sigma_{y_2y_2}^{(2)} = \{\frac{1}{h_2}[\frac{1}{2}(y_2^2-\frac{h_2^2}{4})+\frac{h_2}{2}(y_2+\frac{h_2}{2})+\frac{3}{h_2^2}[\frac{1}{3}(y_1^3+\frac{h_2^3}{8})-\frac{h_1^2}{4}(y_2+\frac{h_2}{2})]\}f_2'(x) - \frac{6}{h_1^3}[\frac{1}{3}(y_2^3+\frac{h_2^3}{8})-\frac{h_2^2}{4}(y_2+\frac{h_2}{2})]g_2(x). \tag{5.19}$$

In the next step, according to the theorem of minimum complementary strain energy, the strain energy functional (3.43) is further adopted to form a set of governing ODEs in terms of the interfacial stress functions $f_1$, $f_2$, $g_1$, $g_2$ [Eqs. (3.1-2)] over the bonding line. In the form of dimensionless interfacial stress functions, the set of 4$^{th}$-order governing ODEs is

$$[\mathrm{A}]\{\Phi^{(IV)}\}+[\mathrm{B}]\{\Phi''\}+[\mathrm{C}]\{\Phi\}+\{\mathrm{D}\}=\{0\}. \tag{5.20}$$

In the above, $\{\Phi\}=\{F_1(\xi),G_1(\xi),F_2(\xi),G_2(\xi)\}^T$ is the stress function column as defined in Chapter 3, matrixes [A], [B], and [C] are relevant to the structural and material properties as defined in relations (3.52-54), i.e., [A], [B] and [C] are independent of the specific joint type. Generalized dimensionless force column $\{D\}_{4\times1}$ defined in (5.21) is relevant to temperature change, coefficients of thermal expansion, tension, Young's modulus of the substrate layer. In particular, effect of axial tension is investigated in this section and temperature change is set as zero.

$$\begin{aligned} D_1 &= \frac{\Delta T}{2}(-\alpha_0+\alpha_1),\\ D_2 &= 0,\\ D_3 &= -p_0/E_2+\frac{\Delta T}{2}(-\alpha_2+\alpha_0),\\ D_4 &= 0. \end{aligned} \tag{5.21}$$

Thus, traction BCs of the DLBJ can be extracted as

$$F_1(0)=0, \tag{5.22$a$}$$

$$F_1(L/h_2)=0, \tag{5.22$b$}$$

$$F_1'(0)=0, \tag{5.22$c$}$$

$$F_1'(L/h_2)=0, \tag{5.22$d$}$$

$$G_1(0)=0, \tag{5.22$e$}$$

$$G_1(L/h_2)=0, \tag{5.22$f$}$$

$$G_1'(0)=0, \tag{5.22$g$}$$

$$G_1'(L/h_2)=0, \tag{5.22$h$}$$

$$F_2(0)=0, \tag{5.22$i$}$$

$$F_2(L/h_2)=0, \tag{5.22j}$$

$$F_2'(0)=0, \tag{5.22k}$$

$$F_2'(L/h_2)=0, \tag{5.22l}$$

$$G_2(0)=0, \tag{5.22m}$$

$$G_2(L/h_2)=0, \tag{5.22n}$$

$$G_2'(0)=0, \tag{5.22o}$$

$$G_2'(L/h_2)=0. \tag{5.22p}$$

Owing to the structural and loading symmetries, all the right sides of BCs [Eqs. (5.22*a*-*p*)] are set to zero. Then, the set of simultaneous linear algebraic equations can be conveniently expressed as

$$\sum_{k=1}^{8} c_k \Psi_0^{k,1} + \sum_{k=1}^{8} d_k \Psi_0^{k,1} = -\Phi_0^{(1)}, \tag{5.23a}$$

$$\sum_{k=1}^{8} c_k \Psi_0^{k,1} \exp(\lambda_k L/h_2) + \sum_{k=1}^{8} d_k \Psi_0^{k,1} \exp(-\lambda_k L/h_2) = -\Phi_0^{(1)}, \tag{5.23b}$$

$$\sum_{k=1}^{8} c_k \lambda_k \Psi_0^{k,1} - \sum_{k=1}^{8} d_k \lambda_k \Psi_0^{k,1} = 0, \tag{5.23c}$$

$$\sum_{k=1}^{8} c_k \lambda_k \Psi_0^{k,1} \exp(\lambda_k L/h_2) - \sum_{k=1}^{8} d_k \lambda_k \Psi_0^{k,1} \exp(-\lambda_k L/h_2) = 0, \tag{5.23d}$$

$$\sum_{k=1}^{8} c_k \Psi_0^{k,2} + \sum_{k=1}^{8} d_k \Psi_0^{k,2} = -\Phi_0^{(2)}, \tag{5.23e}$$

$$\sum_{k=1}^{8} c_k \Psi_0^{k,2} \exp(\lambda_k L/h_2) + \sum_{k=1}^{8} d_k \Psi_0^{k,2} \exp(-\lambda_k L/h_2) = -\Phi_0^{(2)}, \tag{5.23f}$$

$$\sum_{k=1}^{8} c_k \lambda_k \Psi_0^{k,2} - \sum_{k=1}^{8} d_k \lambda_k \Psi_0^{k,2} = 0, \tag{5.23g}$$

$$\sum_{k=1}^{8} c_k \lambda_k \Psi_0^{k,2} \exp(\lambda_k L / h_2) - \sum_{k=1}^{8} d_k \lambda_k \Psi_0^{k,2} \exp(-\lambda_k L / h_2) = 0, \tag{5.23h}$$

$$\sum_{k=1}^{8} c_k \Psi_0^{k,3} + \sum_{k=1}^{8} d_k \Psi_0^{k,3} = -\Phi_0^{(3)}, \tag{5.23i}$$

$$\sum_{k=1}^{8} c_k \Psi_0^{k,3} \exp(\lambda_k L / h_2) + \sum_{k=1}^{8} d_k \Psi_0^{k,3} \exp(-\lambda_k L / h_2) = -\Phi_0^{(3)}, \tag{5.23j}$$

$$\sum_{k=1}^{8} c_k \lambda_k \Psi_0^{k,3} - \sum_{k=1}^{8} d_k \lambda_k \Psi_0^{k,3} = 0, \tag{5.23k}$$

$$\sum_{k=1}^{8} c_k \lambda_k \Psi_0^{k,3} \exp(\lambda_k L / h_2) - \sum_{k=1}^{8} d_k \lambda_k \Psi_0^{k,3} \exp(-\lambda_k L / h_2) = 0, \tag{5.23l}$$

$$\sum_{k=1}^{8} c_k \Psi_0^{k,4} + \sum_{k=1}^{8} d_k \Psi_0^{k,4} = -\Phi_0^{(4)}, \tag{5.23m}$$

$$\sum_{k=1}^{8} c_k \Psi_0^{k,4} \exp(\lambda_k L / h_2) + \sum_{k=1}^{8} d_k \Psi_0^{k,4} \exp(-\lambda_k L / h_2) = -\Phi_0^{(4)}, \tag{5.23n}$$

$$\sum_{k=1}^{8} c_k \lambda_k \Psi_0^{k,4} - \sum_{k=1}^{8} d_k \lambda_k \Psi_0^{k,4} = 0, \tag{5.23o}$$

$$\sum_{k=1}^{8} c_k \lambda_k \Psi_0^{k,4} \exp(\lambda_k L / h_2) - \sum_{k=1}^{8} d_k \lambda_k \Psi_0^{k,4} \exp(-\lambda_k L / h_2) = 0, \tag{5.23p}$$

where $\Psi_0^{k,1}$, $\Psi_0^{k,2}$, $\Psi_0^{k,3}$, and $\Psi_0^{k,4}$ ($k$ = 1, 2, …, 8) are respectively the 1st to 4th elements of the $k$-th eigenvector, and $\Phi_0^{(1)}$, $\Phi_0^{(2)}$, $\Phi_0^{(3)}$, and $\Phi_0^{(4)}$ are the 1st to 4th elements of the particular solution vector $\{\Phi_0\}$.

The final interfacial shear and normal stresses carry the same formal expressions as those in for ASSJ:

$$f_1(x)/p_0 = -\sum_{k=1}^{8} c_k \lambda_k \Psi_0^{k,1} \exp(\lambda_k x / h_2) + \sum_{k=1}^{8} d_k \lambda_k \Psi_0^{k,1} \exp(-\lambda_k x / h_2), \tag{5.24}$$

$$g_1(x)/p_0 = \sum_{k=1}^{8} c_k \lambda_k^2 \Psi_0^{k,2} \exp(\lambda_k x / h_2) + \sum_{k=1}^{8} d_k \lambda_k^2 \Psi_0^{k,2} \exp(-\lambda_k x / h_2), \tag{5.25}$$

$$f_2(x)/p_0 = -\sum_{k=1}^{8} c_k \lambda_k \Psi_0^{k,3} \exp(\lambda_k x/h_2) + \sum_{k=1}^{8} d_k \lambda_k \Psi_0^{k,3} \exp(-\lambda_k x/h_2), \tag{5.26}$$

$$g_2(x)/p_0 = \sum_{k=1}^{8} c_k \lambda_k^2 \Psi_0^{k,4} \exp(\lambda_k x/h_2) + \sum_{k=1}^{8} d_k \lambda_k^2 \Psi_0^{k,4} \exp(-\lambda_k x/h_2). \tag{5.27}$$

5.1.3. Model Validation

To validate the stress functional variational method for interfacial stress analysis of the proposed joint model, the ASSBJ is assumed under action of uniform axial tension on the substrate layers. In this case, the right half-symmetric portion of the joint is used in the simulation. In the present case, the bonded length used in the joint model is $L/2$ = 10 mm. The rest geometrical and material parameters are selected as: $h_1$ = 2.0 mm, $E_1$ = 210 GPa, $v_1$ = 0.293 (steel cover), $h_2$ = 2.0 mm, $E_2$ = 70 GPa, $v_2$ = 0.345 (aluminum bottom), $h_0$ = 0.2 mm, $E_0$ = 10 GPa, and $v_0$ = 0.40 (epoxy adhesive). The given tension $p_0$ is assumed to be 1 MPa. The stress analysis of the tested joint model is based on the commercial FEA software package (ANSYS$^{TM}$), in which the PLANE182 element type is used as considered in the precious chapters. Two different mesh sizes (0.1 × 0.1 mm and 0.05 × 0.05 mm) are utilized consecutively for the purpose of comparison since at the free edges, the stresses tend to increase rapidly with refining mesh size due to the nature of stress singularity existing at the free-edges of bimaterials. As shown in Fig. 5.1(*c*), to eliminate the vertical rigid motion of the computational joint model for FEA, a single corner node is used to constrain the vertical displacement at the node.

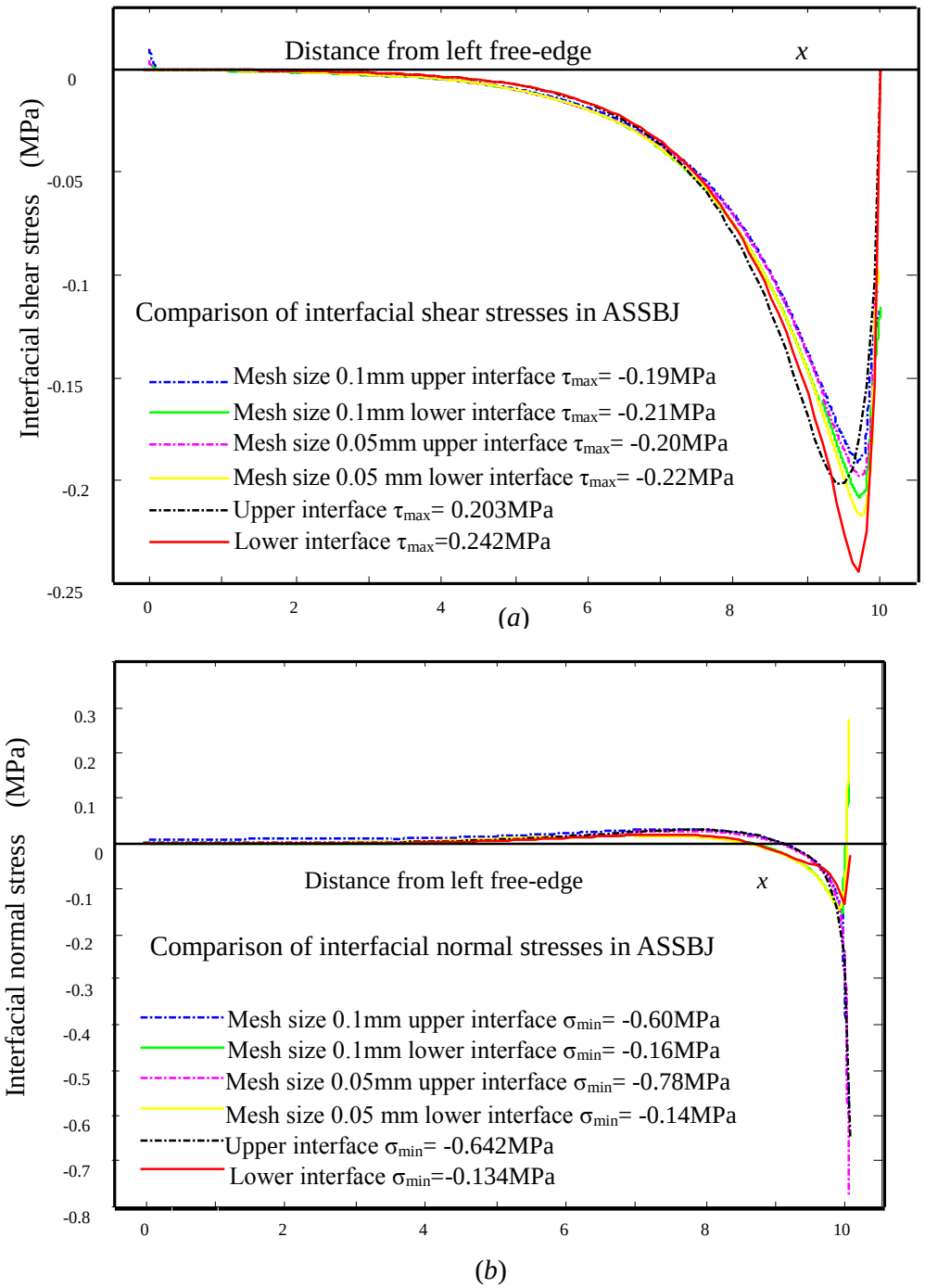


Figure 5.2. Validation of the stress-function variational method for interfacial shear and normal stresses in ASSBJ subjected to uniform axial tension: (*a*) Interfacial shear stress, (*b*) interfacial normal stress.

In Fig. 5.2(*a*), as expected, the interfacial shear stresses determined by the present stress-function variational method exactly satisfy the shear-free BC at the end of $x$ = 10 mm. Obviously, the maximum

peak values of the interfacial shear stress at the lower interface are a little higher than those at the upper interface. In Fig. 5.2(*b*), it can be observed that the high normal stresses are responsible for the debonding failure of ABJs. In contrast, the peak values of the normal stress at the lower interface are much lower than those at the upper interface. Yet, the lower interface stress bounces back near the free edges, nor does the upper interface stress.

### 5.1.4. Conclusions

As the third case study of the present work, the ASSBJ model again demonstrated the robust, high-efficiency stress-function variational method for stress analysis of ABJs. Subjected to uniform axial tension on two sides of the substrate layer, a semi-analytic solution has been derived via introduction of two unknown interfacial shear and normal stress functions at each interface of the ASSBJ and triggering of the theorem of minimum complementary strain energy. In addition, though not performed yet, the thermomechanical effect on the stress analysis of ASSBJ could also be investigated similar to that of ASSJ as demonstrated in Chapter 3. From Fig. 5.2, it can be observed that the concentration of interfacial stresses gained by the present stress-function variational method occurs close to the ends of the joint. Furthermore, the stress field of ASSBJ obtained by the present semi-analytic method has been validated successfully by using two different meshing schemes in computational stress analysis by using FEM (ANSYS$^{TM}$). Within the theoretical framework of *Euler-Bernoulli* beam theory for axial stresses and linear elasticity, the accuracy of stress function variational method for stress analysis of the present ASSBJ model only relies on the numerical process in solving the resulting set of 16 simultaneous algebraic Eqs. 5.23(*a-p*).

## 5.2. Double-Lap Bonded Joints

### 5.2.1. Introduction

Bonded joints, combined with three adherends of the same or dissimilar materials, have also found broad applications in practice. For instance, recently developed flexible electronics are one of the typical examples of such bonded joints, where the rigid silicon islands are bonded onto the compliant polymeric substrates. In such bonded joints, substantial interfacial stress concentrations may cause debonding failure at free ends of the adherends under mechanical or thermomechanical loads. As natural extension of the above studies, the robust, efficient stress-function variational method can be further extended for the stress analysis of such type of bonded joints. In addition, accurate stress analysis of bonded joints can be beneficial to optimal joint design and monitoring structural failure in bonded joints such as progressive cracking.

Without loss of generality, the goal of the upcoming work is to formulate a systematic analytic method in solving the stress distribution in bonded joints based on the well-validated stress-function variational method in the proceeding chapters. Similar to the above theoretical formulation, two interfacial shear and normal stress functions are introduced on each interface of the joint. Then, stress equilibrium equations for each layer are established; expressions of the planar stress components can be constructed based on the elementary *Euler-Bernoulli* beam theory and 2D elasticity. Furthermore, a set of $4^{th}$-order differential equations, resulted from minimization of the complementary strain energy of the bonded joints, can be gained and further solved by using eigenfunctions. Finally, a computational code based on MATLAB$^{TM}$ is designed to implement the semi-analytic method for stress analysis.

Hereafter, the stress-function varational method is utilized for interfacial stress analysis of double-lap bonded joint (DLBJ) as shown in Fig. 5.3(*a*), in which three adherend layers are involved, similar to the

above ABJs. Unlike the other models, DLBJ has a middle layer under uniform tension $p_0$ on the right side, and its top and bottom layers are subjected to a traction $p_1 = p_0 h_0/(2h_1)$ on the left side. The coordinate system is introduced as shown in Fig. 5.3(*a*), in which the *x*-axis is set along the axis of the middle adherend layer while the *y*-axis is established vertically. Schematic distribution of the interfacial stresses is shown in Fig. 5.3(*b*). Fig. 5.3(*c*) shows the geometrical model, loads, and BCs of the half-symmetrical joint to be used for FEA-based computational validation of the stress field predicted by the present stress-function variational method, where structural and loading symmetries have been used.

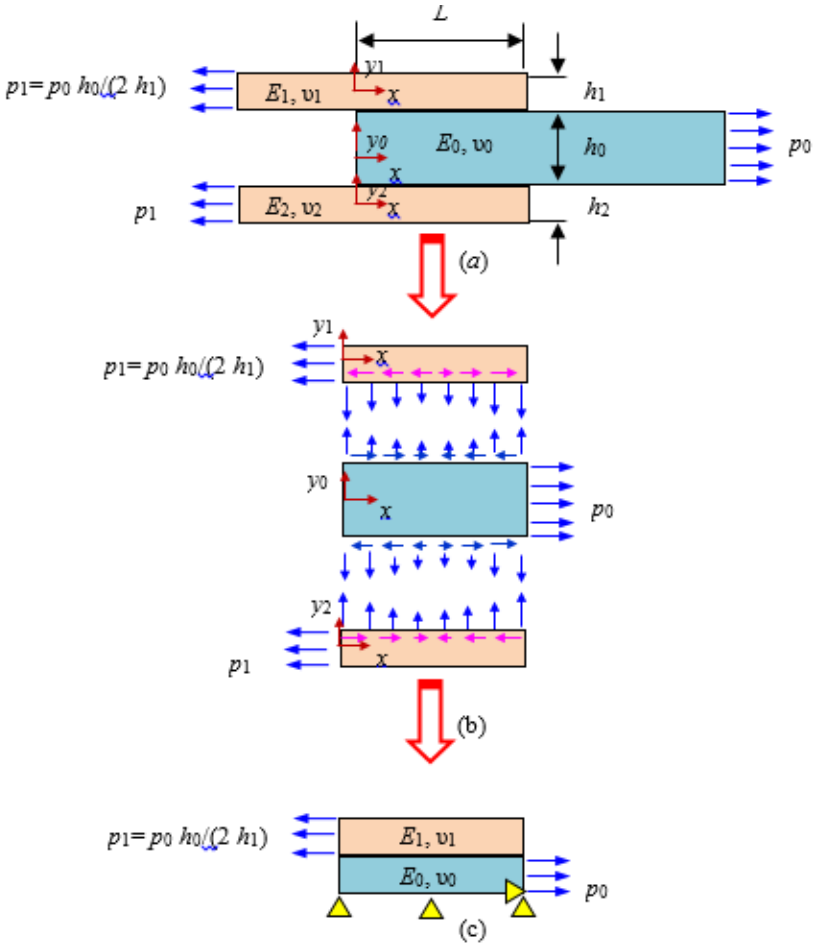


Figure 5.3. Schematic of a double-lap bonded joint: (*a*) Geometrical configuration consisting of an identical substrate layer, an adhesive layer, and a slender cover layer, (*b*) interfacial stress distribution, and (*c*) half symmetrical model for FEA.

5.2.2. Model Formulation

Based on the free body diagrams as shown in Figs. 3.2(*a*-*c*), the given BCs in terms of the axial forces, shear tractions, and bending moments at the ends of the upper, middle, and lower adherends are expressed as

$$S_1(0) = \frac{p_0 b h_0}{2}, \tag{5.28a}$$

$$S_1(L) = 0, \tag{5.28b}$$

$$Q_1(0) = 0, \tag{5.28c}$$

$$Q_1(L) = 0, \tag{5.28d}$$

$$M_1(0) = 0, \tag{5.28e}$$

$$M_1(L) = 0, \tag{5.28f}$$

$$S_2(0) = \frac{p_0 b h_0}{2}, \tag{5.28g}$$

$$S_2(L) = 0, \tag{5.28h}$$

$$Q_2(0) = 0, \tag{5.28i}$$

$$Q_2(L) = 0, \tag{5.28j}$$

$$M_2(0) = 0, \tag{5.28k}$$

$$M_2(L) = 0, \tag{5.28l}$$

$$S_0(0) = 0, \tag{5.28m}$$

$$S_0(L) = p_0 b h_0, \tag{5.28n}$$

$$Q_0(0) = 0, \tag{5.28o}$$

$$Q_0(L) = 0, \tag{5.28p}$$

$$M_0(0) = 0, \tag{5.28q}$$

$$M_0(L) = 0. \tag{5.28r}$$

By introducing four independent unknown interfacial shear and normal stress functions ($f_1$, $g_1$, $f_2$, $g_2$) at the upper and lower interfaces, integration of the internal force equilibrium equations (3.4-6) leads to the stress resultants in the upper layer:

$$S_1(x) = \frac{p_0 b h_0}{2} - b\int_0^x f_1(\xi)d\xi, \tag{5.29}$$

$$Q_1(x) = -b\int_0^x g_1(\xi)d\xi, \tag{5.30}$$

$$M_1(x) = -b\int_0^x \int_0^\zeta g_1(\zeta)d\zeta d\xi - \frac{bh_1}{2}\int_0^x f_1(\xi)d\xi. \tag{5.31}$$

Similarly, integration of internal force equilibrium equations (3.10-12) yields the stress resultants in the bottom layer:

$$S_2(x) = \frac{p_0 b h_0}{2} + b\int_0^x f_2(\xi)d\xi, \tag{5.32}$$

$$Q_2(x) = b\int_0^x g_2(\xi)d\xi, \tag{5.33}$$

$$M_2(x) = b\int_0^x \int_0^\zeta g_2(\zeta)d\zeta d\xi - \frac{bh_2}{2}\int_0^x f_2(\xi)d\xi. \tag{5.34}$$

Consequently, integration of internal force equilibrium equations (3.7-9) results in the stress resultants in the middle layer:

$$S_0(x) = b\int_0^x [f_1(\xi) - f_2(\xi)]d\xi, \tag{5.35}$$

$$Q_0(x) = b\int_0^x [g_1(\xi) - g_2(\xi)]d\xi, \tag{5.36}$$

$$M_0(x) = b\int_0^x \int_0^\zeta [g_1(\zeta) - g_1(\zeta)]d\zeta d\xi - \frac{bh_0}{2}\int_0^x [f_1(\xi) + f_1(\xi)]d\xi. \tag{5.37}$$

Similarly, by assuming that the axial stresses in the adherends follow *Euler-Bernoulli* beam theory and 2D elasticity as used in Chapters 3 and 4, all the planar stress components can be determined in terms of the four unknown interfacial stress functions $f_i$ ($i$ = 1,2) and $g_i$ ($i$ = 1,2) defined at the two interfaces of the DLBJ.

$$\sigma_{xx}^{(1)} = \frac{S_1}{bh_1} - \frac{M_1 y_1}{I_1} = \frac{p_0 h_0}{2h_1} - \frac{1}{h_1}\int_0^x f_1(\xi)d\xi + \frac{12y_1}{h_1^3}[\int_0^x\int_0^\zeta g_1(\zeta)d\zeta d\xi + \frac{h_1}{2}\int_0^x f_1(\xi)d\xi], \quad (5.38)$$

$$\tau_{y_1x}^{(1)} = \frac{1}{h_1}[(\frac{h_1}{2} - y_1) - \frac{3}{h_1}(\frac{h_1^2}{4} - y_1^2)]f_1(x) - \frac{6}{h_1^3}(\frac{h_1^2}{4} - y_1^2)\int_0^x g_1(\xi)d\xi, \quad (5.39)$$

$$\begin{aligned}\sigma_{y_1y_1}^{(1)} = &-\frac{1}{h_1}\{\frac{h_1}{2}(\frac{h_1}{2} - y_1) - \frac{1}{2}(\frac{h_1^2}{4} - y_1^2) - \frac{3}{h_1}[\frac{h_1^2}{4}(\frac{h_1}{2} - y_1) - \frac{1}{3}(\frac{h_1^3}{8} - y_1^3)]\}f_1'(x) \\ &+ \frac{6}{h_1^3}[\frac{h_1^2}{4}(\frac{h_1}{2} - y_1) - \frac{1}{3}(\frac{h_1^3}{8} - y_1^3)]g_1(x).\end{aligned} \quad (5.40)$$

$$\begin{aligned}\sigma_{xx}^{(0)} = &\frac{S_0}{bh_0} - \frac{M_0 y_0}{I_0} = \frac{1}{h_0}\int_0^x [f_1(\xi) - f_2(\xi)]d\xi \\ &- \frac{12y_0}{h_0^3}\{\int_0^x\int_0^\zeta [g_1(\zeta) - g_2(\zeta)]d\zeta d\xi - \frac{h_0}{2}\int_0^x [f_1(\xi) + f_1(\xi)]d\xi\},\end{aligned} \quad (5.41)$$

$$\begin{aligned}\tau_{y_0x}^{(0)} = &-f_2(x) - \frac{1}{h_0}(y_0 + \frac{h_0}{2})[f_1(x) - f_2(x)] - \frac{3}{h_0^2}(y_0^2 - \frac{h_0^2}{4})[f_1(x) + f_2(x)] \\ &+ \frac{6}{h_0^3}(y_0^2 - \frac{h_0^2}{4})\int_0^x [g_1(\xi) - g_2(\xi)]d\xi,\end{aligned} \quad (5.42)$$

$$\begin{aligned}\sigma_{y_0y_0}^{(0)} = &g_2(x) + (y_0 + \frac{h_0}{2})f_2'(x) + \frac{1}{h_0}[\frac{1}{2}(y_0^2 - \frac{h_0^2}{4}) + \frac{h_0}{2}(y_0 + \frac{h_0}{2})][f_1'(x) - f_2'(x)] \\ &+ \frac{3}{h_0^2}[\frac{1}{3}(y_0^3 + \frac{h_0^3}{8}) - \frac{h_0^2}{4}(y_0 + \frac{h_0}{2})][f_1'(x) + f_2'(x)] \\ &- \frac{6}{h_1^3}[\frac{1}{3}(y_0^3 + \frac{h_0^3}{8}) - \frac{h_0^2}{4}(y_0 + \frac{h_0}{2})][g_1(x) - g_1(x)].\end{aligned} \quad (5.43)$$

$$\sigma_{xx}^{(2)} = \frac{S_2}{bh_2} - \frac{M_2 y_2}{I_2} = \frac{p_0 h_0}{2h_2} + \frac{1}{h_2}\int_0^x f_2(\xi)d\xi - \frac{12y_2}{h_2^3}[\int_0^x\int_0^\zeta g_2(\zeta)d\zeta d\xi - \frac{h_2}{2}\int_0^x f_2(\xi)d\xi], \quad (5.44)$$

$$\tau_{y_2x}^{(2)} = -\frac{1}{h_2}[(y_2 + \frac{h_2}{2}) + \frac{3}{h_2}(y_2^2 - \frac{h_2^2}{4})]f_2(x) + \frac{6}{h_2^3}(y_2^2 - \frac{h_2^2}{4})\int_0^x g_2(\xi)d\xi, \tag{5.45}$$

$$\begin{aligned}\sigma_{y_2y_2}^{(2)} = \{&\frac{1}{h_2}[\frac{1}{2}(y_2^2 - \frac{h_2^2}{4}) + \frac{h_2}{2}(y_2 + \frac{h_2}{2}) + \frac{3}{h_2^2}[\frac{1}{3}(y_1^3 + \frac{h_2^3}{8}) - \frac{h_1^2}{4}(y_2 + \frac{h_2}{2})]\} f_2'(x) \\ &- \frac{6}{h_1^3}[\frac{1}{3}(y_2^3 + \frac{h_2^3}{8}) - \frac{h_2^2}{4}(y_2 + \frac{h_2}{2})]g_2(x).\end{aligned} \tag{5.46}$$

By triggering the theorem of minimum complementary strain energy of the DBLJ similar to those formulated in Chapters 3 and 4, a similar set of four 4th-order ODEs (Eq. 5.20) in terms of the four dimensionless stress functions can be determined. In this case, system matrices [*A*], [*B*], and [*C*] are the same as (3.52-54), and the generalized dimensionless force column $\{D\}_{4\times1}$ can be determined in terms of the joint geometries, material properties, mechanical loads and temperature change as

$$\begin{aligned}D_1 &= \frac{p_0 h_0}{2h_1 E_1} + \frac{\Delta T}{2}(-\alpha_0 + \alpha_1), \\ D_2 &= 0, \\ D_3 &= -\frac{p_0 h_0}{2h_2 E_2} + \frac{\Delta T}{2}(-\alpha_2 + \alpha_0), \\ D_4 &= 0.\end{aligned} \tag{5.47}$$

As a result, the above traction BCs of the joint (5.28*a*-*r*) can be reduced in terms of the dimensionless interfacial stress functions as

$$F_1(0) = 0, \tag{5.48a}$$

$$F_1(L/h_2) = -h_{02}/2, \tag{5.48b}$$

$$F_1'(0) = 0, \tag{5.48c}$$

$$F_1'(L/h_2) = 0, \tag{5.48d}$$

$$G_1(0) = 0, \tag{5.48e}$$

$$G_1(L/h_2) = \frac{-h_{12}h_{02}}{4}, \tag{5.48f}$$

$$G_1'(0) = 0, \tag{5.48g}$$

$$G_1'(L/h_2) = 0, \tag{5.48h}$$

$$F_2(0) = 0, \tag{5.48i}$$

$$F_2(L/h_2) = h_{02}/2, \tag{5.48j}$$

$$F_2'(0) = 0, \tag{5.48k}$$

$$F_2'(L/h_2) = 0, \tag{5.48l}$$

$$G_2(0) = 0, \tag{5.48m}$$

$$G_2(L/h_2) = -h_{02}/4, \tag{5.48n}$$

$$G_2'(0) = 0, \tag{5.48o}$$

$$G_2'(L/h_2) = 0. \tag{5.48p}$$

By using the similar procedure as described in Chapter 3, a set of simultaneous linear algebraic equations can be expressed with the above BCs [Eqs. (5.48*a*-*p*)]:

$$\sum_{k=1}^{8} c_k \Psi_0^{k,1} + \sum_{k=1}^{8} d_k \Psi_0^{k,1} = -\Phi_0^{(1)}, \tag{5.49a}$$

$$\sum_{k=1}^{8} c_k \Psi_0^{k,1} \exp(\lambda_k L/h_2) + \sum_{k=1}^{8} d_k \Psi_0^{k,1} \exp(-\lambda_k L/h_2) = -[h_{02}/2 + \Phi_0^{(1)}], \tag{5.49b}$$

$$\sum_{k=1}^{8} c_k \lambda_k \Psi_0^{k,1} - \sum_{k=1}^{8} d_k \lambda_k \Psi_0^{k,1} = 0, \tag{5.49c}$$

$$\sum_{k=1}^{8} c_k \lambda_k \Psi_0^{k,1} \exp(\lambda_k L/h_2) - \sum_{k=1}^{8} d_k \lambda_k \Psi_0^{k,1} \exp(-\lambda_k L/h_2) = 0, \tag{5.49d}$$

$$\sum_{k=1}^{8} c_k \Psi_0^{k,2} + \sum_{k=1}^{8} d_k \Psi_0^{k,2} = -\Phi_0^{(2)}, \tag{5.49e}$$

$$\sum_{k=1}^{8} c_k \Psi_0^{k,2} \exp(\lambda_k L/h_2) + \sum_{k=1}^{8} d_k \Psi_0^{k,2} \exp(-\lambda_k L/h_2) = -[h_{02}h_{12}/4 + \Phi_0^{(2)}], \tag{5.49f}$$

$$\sum_{k=1}^{8} c_k \lambda_k \Psi_0^{k,2} - \sum_{k=1}^{8} d_k \lambda_k \Psi_0^{k,2} = 0, \tag{5.49g}$$

$$\sum_{k=1}^{8} c_k \lambda_k \Psi_0^{k,2} \exp(\lambda_k L/h_2) - \sum_{k=1}^{8} d_k \lambda_k \Psi_0^{k,2} \exp(-\lambda_k L/h_2) = 0, \tag{5.49h}$$

$$\sum_{k=1}^{8} c_k \Psi_0^{k,3} + \sum_{k=1}^{8} d_k \Psi_0^{k,3} = -\Phi_0^{(3)}, \tag{5.49i}$$

$$\sum_{k=1}^{8} c_k \Psi_0^{k,3} \exp(\lambda_k L/h_2) + \sum_{k=1}^{8} d_k \Psi_0^{k,3} \exp(-\lambda_k L/h_2) = h_{02}/2 - \Phi_0^{(3)}, \tag{5.49j}$$

$$\sum_{k=1}^{8} c_k \lambda_k \Psi_0^{k,3} - \sum_{k=1}^{8} d_k \lambda_k \Psi_0^{k,3} = 0, \tag{5.49k}$$

$$\sum_{k=1}^{8} c_k \lambda_k \Psi_0^{k,3} \exp(\lambda_k L/h_2) - \sum_{k=1}^{8} d_k \lambda_k \Psi_0^{k,3} \exp(-\lambda_k L/h_2) = 0, \tag{5.49l}$$

$$\sum_{k=1}^{8} c_k \Psi_0^{k,4} + \sum_{k=1}^{8} d_k \Psi_0^{k,4} = -\Phi_0^{(4)}, \tag{5.49m}$$

$$\sum_{k=1}^{8} c_k \Psi_0^{k,4} \exp(\lambda_k L/h_2) + \sum_{k=1}^{8} d_k \Psi_0^{k,4} \exp(-\lambda_k L/h_2) = -[h_{02}/4 + \Phi_0^{(4)}], \tag{5.49n}$$

$$\sum_{k=1}^{8} c_k \lambda_k \Psi_0^{k,4} - \sum_{k=1}^{8} d_k \lambda_k \Psi_0^{k,4} = 0, \tag{5.49o}$$

$$\sum_{k=1}^{8} c_k \lambda_k \Psi_0^{k,4} \exp(\lambda_k L/h_2) - \sum_{k=1}^{8} d_k \lambda_k \Psi_0^{k,4} \exp(-\lambda_k L/h_2) = 0, \tag{5.49p}$$

where, $\Psi_0^{k,1}$, $\Psi_0^{k,2}$, $\Psi_0^{k,3}$, and $\Psi_0^{k,4}$ ($k$ = 1, 2, …, 8) are respectively the 1st to 4th elements of the $k$-th eigenvector, and $\Phi_0^{(1)}$, $\Phi_0^{(2)}$, $\Phi_0^{(3)}$, and $\Phi_0^{(4)}$ are the 1st to 4th elements of the particular solution vector $\{\Phi_0\}$. Ultimately, the final solutions of interfacial shear and normal stresses can be expressed in the forms similar to solutions (5.24-27).

5.2.3. Model Validation

For model validation, the DLBJ is assumed to be subjected to uniform axial tension on one side of each adherend as shown in Fig. 5.3(*c*). Herein FEM based on commercial FEA software package (ANSYS™) is used to simulate the stress field in the top half-symmetrical portion of the DLBJ model. Plane-stress PLANE182 element is used for the FEM simulation. The FEA results are compared with those gained from the present semi-analytic DLBJ model. Geometrical and material parameters used in the FEM simulation are kept as the same as those used in the proceeding simulations: $L$ = 10 mm, $h_1 = h_2$ = 1.0 mm, $E_1 = E_2$ = 210 GPa, $v_1 = v_2$ = 0.293, $h_0$ = 2 mm, $E_0$ = 70 GPa, and $v_0$ = 0.345. The active tension $p_0$ is fixed as 1 MPa, and the reaction tension $p_1$ = 1 MPa based on $p_1 = p_0 h_0/(2h_1)$ [Fig. 5.3(*b*)]. In FEM simulation of the stress field of the DLBJ based on ANSYS™, two different mesh sizes (0.1 × 0.1 mm and 0.05 × 0.05 mm) are utilized at the two free ends of each adherend layer. A single corner node is used to constrain the horizontal displacement in avoiding the rigid motion of the joint as required in FEA based on ANSYS™.

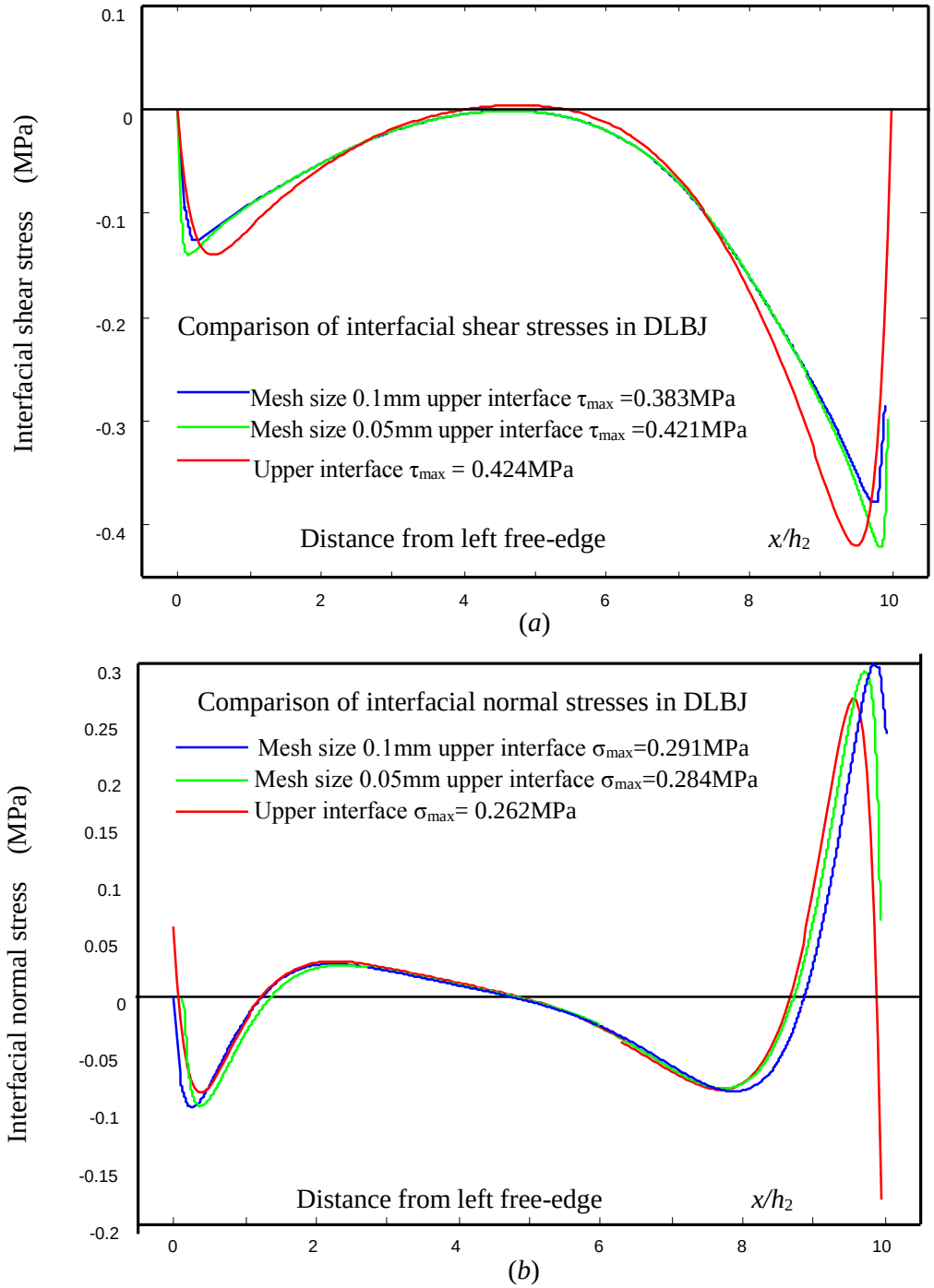


Figure 5.4. Validation of the stress-function variational method for the interfacial shear and normal stresses in double-lap bonded joint subjected to uniaxial tension: (*a*) Interfacial shear stress, (*b*) interfacial normal stress.

Due to adoption of symmetrical conditions of the joint in FEA, the shear and normal stresses at the lower interface have the same values as those at the upper interface. It can be observed from Fig. 5.4(*a*) that two peak values of the interfacial shear stresses appear close to the edges on each side, the first reaches at 0.15 MPa while the second reaches at ~0.42 MPa. In Fig. 5.4(*b*), it can be found that the peak value (0.29 MPa) of the normal stress happens at the right end. Compared to the interfacial shear stresses, the value of interfacial normal stresses is not as high as that of the interfacial shear stresses, to some extent, it is even lower.

### 5.2.4. Conclusions

The stress analysis of the DLBJ further endorses the applicability of the novel stress-function variational method for interfacial stress analysis of bonded joints. It can be concluded that once the middle adherend is regarded as the adhesive layer, in the view of mechanics, the DLBJ can be treated as the same as ASSJ studied in Chapter 3. Technically, the interfacial shear and normal stresses can be expressed in explicit forms. The gained stress field determined by the present stress-function variational method satisfies all the traction BCs, including the shear-free condition at all free-edges of the adherends, which was normally neglected in most ABJ models in the literature. In addition, the model predicted stress field in the DLBJ has been well validated by FEM with the aid of commercial FEA software package (ANSYS$^{TM}$). The close agreement between the results of the proposed stress-function variational method and those obtained by FEM simulations reveal the validity of the proposed method. The highly robust, efficient stress-function variational method can be conveniently implemented for stress analysis of ABJs and bonded joints by designing a concise MATLAB$^{TM}$ code to take into account all the geometries, material properties and

external loads. Thus, the stress function varational method can be conveniently used for optimal design and scaling analysis of ABJs.

## 5.3. Double-sided Bonded Joints

### 5.3.1. Introduction

In this section, double-sided bonded joint (DSBJ) under uniaxial tension as shown in Fig. 5.5(*a*) is considered. The *x*-coordinate is picked from the symmetric mid-span of the joint and extended along the centroidal axis, while the *y*-coordinate is pointed upward from the centroids. The overlap bonding length is defined as $2L$ = 20 mm. In the following, subscripts ($i$ = 1, 2, 0) are adopted to indicate the geometries, material properties, and stresses of the upper, lower, and middle layers, respectively. It is assumed that the joint is doubly symmetric, i.e., the geometries and material properties of the upper and lower strengthening layers are identical. Fig. 5.5(*b*) illustrates the distribution of interfacial stresses. The analytical treatment of DSBJ under uniaxial tension loads can be simplified due to the symmetrical structure. In virtue of the double symmetry, there is no lateral deflection, and symmetric BCs are mandated in Fig. 5.5(*c*) in FEM, simulation for numerical validation of the semi-analytic method for stress analysis of DSBJ.

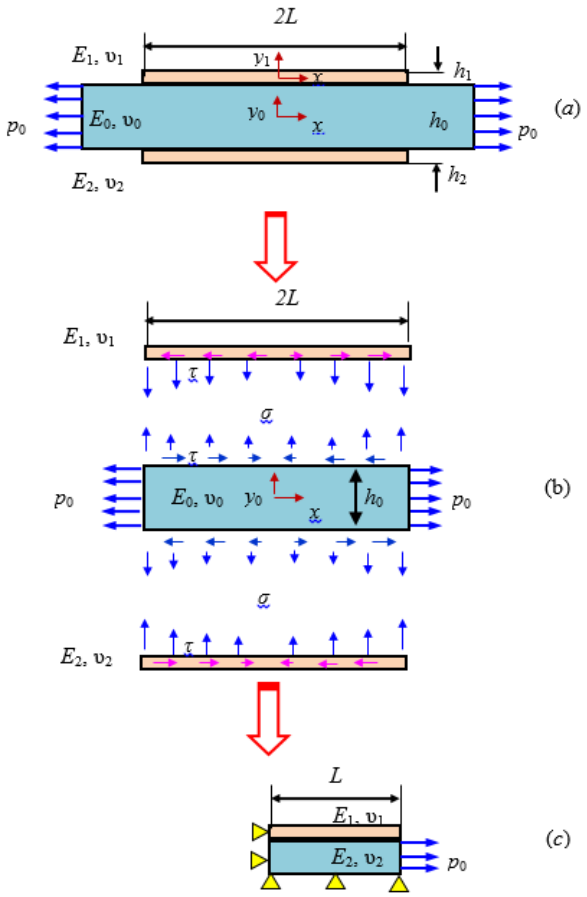


Figure 5.5. Schematic of a double-sided bonded joint: (*a*) Geometrical configuration consists of an identical substrate layer, an adhesive layer, and a slender cover layer, (*b*) interfacial stress distribution, and (*c*) geometrical model, loads and constraints used for FEA.

## 5.3.2. Model Formulation

Uniaxial tension is exerted along the middle layer of the DSBJ. The corresponding traction BCs in terms of axial force, shear traction, and bending moment [Fig. 3.2(*a*-*c*)] are

$$S_1(0) = 0, \tag{5.50a}$$

$$S_1(L) = 0, \tag{5.50b}$$

$$Q_1(0) = 0, \tag{5.50c}$$

$$Q_1(L) = 0, \tag{5.50d}$$

$$M_1(0) = 0, \tag{5.50e}$$

$$M_1(L) = 0, \tag{5.50f}$$

$$S_2(0) = 0, \tag{5.50g}$$

$$S_2(L) = 0, \tag{5.50h}$$

$$Q_2(0) = 0, \tag{5.50i}$$

$$Q_2(L) = 0, \tag{5.50j}$$

$$M_2(0) = 0, \tag{5.50k}$$

$$M_2(L) = 0, \tag{5.50l}$$

$$S_0(0) = p_0 b h_0, \tag{5.50m}$$

$$S_0(L) = p_0 b h_0, \tag{5.50n}$$

$$Q_0(0) = 0, \tag{5.50o}$$

$$Q_0(L) = 0, \tag{5.50p}$$

$$M_0(0) = 0, \tag{5.50q}$$

$$M_0(L) = 0, \tag{5.50r}$$

In DLBJ, only the middle layer is granted with uniaxial tension. Similar to the proceeding procedure, by introducing four independent unknown functions for the interfacial shear and normal stresses ($f_1$, $g_1$, $f_2$, $g_2$), the stress resultants of the upper layer can be derived with BCs [Eq. (5.50*a*), Eq. (5.50*c*), and Eq. (5.50*e*)]:

$$S_1(x) = -b\int_0^x f_1(\xi)d\xi, \tag{5.51}$$

$$Q_1(x) = -b\int_0^x g_1(\xi)d\xi, \tag{5.52}$$

$$M_1(x) = -b\int_0^x \int_0^\zeta g_1(\zeta)d\zeta d\xi - \frac{bh_1}{2}\int_0^x f_1(\xi)d\xi. \tag{5.53}$$

Similarly, with BCs [Eq. (5.50*g*), Eq. (5.50*i*), and Eq. (5.50*k*)], the stress resultants in the bottom layer can be expressed as:

$$S_2(x) = b\int_0^x f_2(\xi)d\xi, \tag{5.54}$$

$$Q_2(x) = b\int_0^x g_2(\xi)d\xi, \tag{5.55}$$

$$M_2(x) = b\int_0^x \int_0^\zeta g_2(\zeta)d\zeta d\xi - \frac{bh_2}{2}\int_0^x f_2(\xi)d\xi. \tag{5.56}$$

Consequently, with BCs [Eq. (5.50*m*), Eq. (5.50*o*), and Eq. (5.50*q*)], the stress resultants in the middle layer can be expressed:

$$S_0(x) = p_0 bh_0 + b\int_0^x [f_1(\xi) - f_2(\xi)]d\xi, \tag{5.57}$$

$$Q_0(x) = b\int_0^x [g_1(\xi) - g_2(\xi)]d\xi, \tag{5.58}$$

$$M_0(x) = b\int_0^x \int_0^\zeta [g_1(\zeta) - g_1(\zeta)]d\zeta d\xi - \frac{bh_0}{2}\int_0^x [f_1(\xi) + f_1(\xi)]d\xi. \tag{5.59}$$

Again, the axial normal stress of the layers is assumed to vary linearly as that of *Euler-Bernoulli* beam theory. In addition, static equilibrium equations in 2D elasticity are used to determine the shear and lateral normal stress components in the three layers of the joint. As a result, the stress components can be expressed as:

$$\sigma_{xx}^{(1)} = \frac{S_1}{bh_1} - \frac{M_1 y_1}{I_1} = -\frac{1}{h_1}\int_0^x f_1(\xi)d\xi + \frac{12y_1}{h_1^3}[\int_0^x \int_0^\zeta g_1(\zeta)d\zeta d\xi + \frac{h_1}{2}\int_0^x f_1(\xi)d\xi], \tag{5.60}$$

$$\tau_{y_1x}^{(1)} = \frac{1}{h_1}[(\frac{h_1}{2} - y_1) - \frac{3}{h_1}(\frac{h_1^2}{4} - y_1^2)]f_1(x) - \frac{6}{h_1^3}(\frac{h_1^2}{4} - y_1^2)\int_0^x g_1(\xi)d\xi, \tag{5.61}$$

$$\begin{aligned}\sigma_{y_1y_1}^{(1)} = &-\frac{1}{h_1}\{\frac{h_1}{2}(\frac{h_1}{2} - y_1) - \frac{1}{2}(\frac{h_1^2}{4} - y_1^2) - \frac{3}{h_1}[\frac{h_1^2}{4}(\frac{h_1}{2} - y_1) - \frac{1}{3}(\frac{h_1^3}{8} - y_1^3)]\}f_1'(x) \\ &+ \frac{6}{h_1^3}[\frac{h_1^2}{4}(\frac{h_1}{2} - y_1) - \frac{1}{3}(\frac{h_1^3}{8} - y_1^3)]g_1(x).\end{aligned} \tag{5.62}$$

$$\begin{aligned}\sigma_{xx}^{(0)} = \frac{S_0}{bh_0} - \frac{M_0y_0}{I_0} = p_0 + \frac{1}{h_0}\int_0^x [f_1(\xi) - f_2(\xi)]d\xi \\ - \frac{12y_0}{h_0^3}\{\int_0^x\int_0^\zeta [g_1(\zeta) - g_2(\zeta)]d\zeta d\xi - \frac{h_0}{2}\int_0^x [f_1(\xi) + f_1(\xi)]d\xi\},\end{aligned} \tag{5.63}$$

$$\begin{aligned}\tau_{y_0x}^{(0)} = &-f_2(x) - \frac{1}{h_0}(y_0 + \frac{h_0}{2})[f_1(x) - f_2(x)] - \frac{3}{h_0^2}(y_0^2 - \frac{h_0^2}{4})[f_1(x) + f_2(x)] \\ &+ \frac{6}{h_0^3}(y_0^2 - \frac{h_0^2}{4})\int_0^x [g_1(\xi) - g_2(\xi)]d\xi,\end{aligned} \tag{5.64}$$

$$\begin{aligned}\sigma_{y_0y_0}^{(0)} = &g_2(x) + (y_0 + \frac{h_0}{2})f_2'(x) + \frac{1}{h_0}[\frac{1}{2}(y_0^2 - \frac{h_0^2}{4}) + \frac{h_0}{2}(y_0 + \frac{h_0}{2})][f_1'(x) - f_2'(x)] \\ &+ \frac{3}{h_0^2}[\frac{1}{3}(y_0^3 + \frac{h_0^3}{8}) - \frac{h_0^2}{4}(y_0 + \frac{h_0}{2})][f_1'(x) + f_2'(x)] \\ &- \frac{6}{h_1^3}[\frac{1}{3}(y_0^3 + \frac{h_0^3}{8}) - \frac{h_0^2}{4}(y_0 + \frac{h_0}{2})][g_1(x) - g_1(x)].\end{aligned} \tag{5.65}$$

$$\sigma_{xx}^{(2)} = \frac{S_2}{bh_2} - \frac{M_2y_2}{I_2} = \frac{1}{h_2}\int_0^x f_2(\xi)d\xi - \frac{12y_2}{h_2^3}[\int_0^x\int_0^\zeta g_2(\zeta)d\zeta d\xi - \frac{h_2}{2}\int_0^x f_2(\xi)d\xi], \tag{5.66}$$

$$\tau_{y_2x}^{(2)} = -\frac{1}{h_2}[(y_2 + \frac{h_2}{2}) + \frac{3}{h_2}(y_2^2 - \frac{h_2^2}{4})]f_2(x) + \frac{6}{h_2^3}(y_2^2 - \frac{h_2^2}{4})\int_0^x g_2(\xi)d\xi, \tag{5.67}$$

$$\begin{aligned}\sigma_{y_2y_2}^{(2)} = &\{\frac{1}{h_2}[\frac{1}{2}(y_2^2 - \frac{h_2^2}{4}) + \frac{h_2}{2}(y_2 + \frac{h_2}{2}) + \frac{3}{h_2^2}[\frac{1}{3}(y_1^3 + \frac{h_2^3}{8}) - \frac{h_1^2}{4}(y_2 + \frac{h_2}{2})]\}f_2'(x) \\ &- \frac{6}{h_1^3}[\frac{1}{3}(y_2^3 + \frac{h_2^3}{8}) - \frac{h_2^2}{4}(y_2 + \frac{h_2}{2})]g_2(x).\end{aligned} \tag{5.68}$$

Moreover, by defining the complimentary strain energy (3.43) of the joint in terms of the stress components of the three layers and triggering the theorem of minimum complimentary strain energy, similar

to Eq. (5.20), a set of four governing ODEs in terms of the four interfacial stress functions is reached. Herein, the generalized dimensionless force column $\{D\}_{4\times1}$ in this particular joint case can be obtained as:

$$\begin{aligned} D_1 &= -p_0 / E_0 + \frac{\Delta T}{2}(-\alpha_0 + \alpha_1), \\ D_2 &= 0, \\ D_3 &= p_0 / E_0 + \frac{\Delta T}{2}(-\alpha_2 + \alpha_0), \\ D_4 &= 0. \end{aligned} \tag{5.69}$$

In the present case, the joint carries the symmetric structure under uniaxial tension. Hence, the traction BCs are equivalent to Eqs. (5.22*a*-*p*). As a result, a set of simultaneous linear algebraic equations similar to Eqs. (5.23*a*-*p*) can be obtained with the proper traction BCs. The final stress expressions can be expressed as the same as Eqs. (5.24-27).

5.3.3. Model Validation

For the reason that DSBJ is doubly symmetric with respect to both *x* and *y* axes, a FEM model [Fig. 5.5(*c*)] is built up with two symmetric boundaries to validate the stress field of the joint predicted by the present stress-function variational method. Due to the nature of double symmetry of the joint, only the quarter-joint needs to be considered. The geometrical parameters for the quarter-DSBJ are taken as: $L$ = 10 mm, $h_1 = h_2$ = 1.0 mm, and $h_0/2$ = 2 mm. Material parameters of the joint are specified as: $E_1 = E_2$ = 400 GPa, $\nu_1 = \nu_2$ = 0.25, $E_0$ = 210 GPa, and $\nu_0$ = 0.293. The uniform tensile traction $p_0$ is fixed as 1 MPa. Quadrilateral elements of the size of 0.1 × 0.1 mm are first generated at the two ends of the middle layer, and refined quadrilateral elements of the size 0.05 × 0.05 mm are further introduced near the free edges.

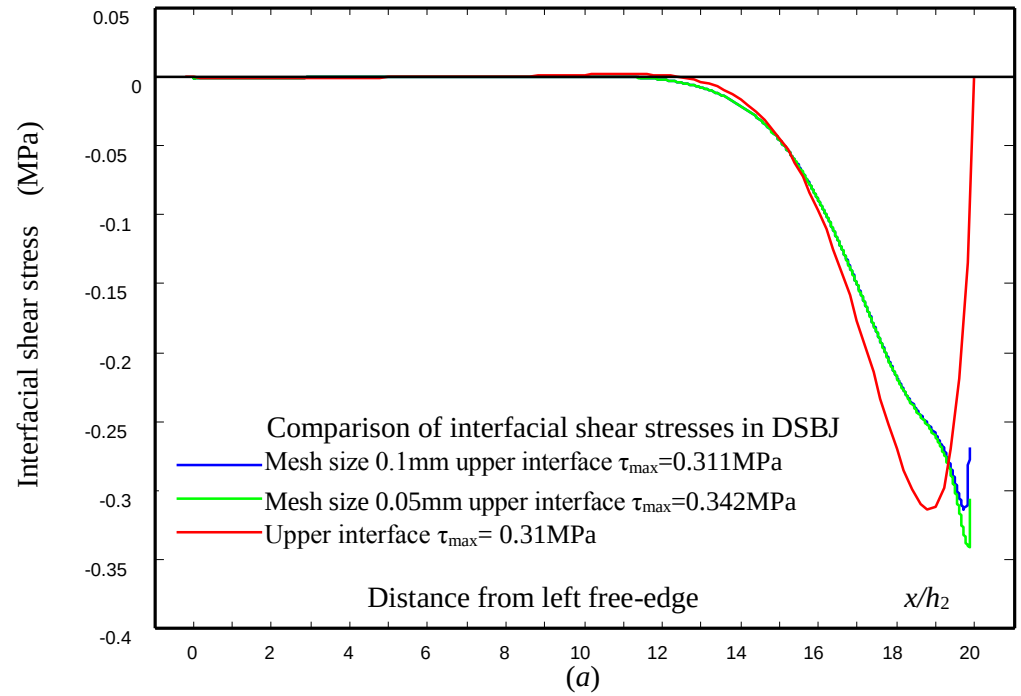


(*a*)

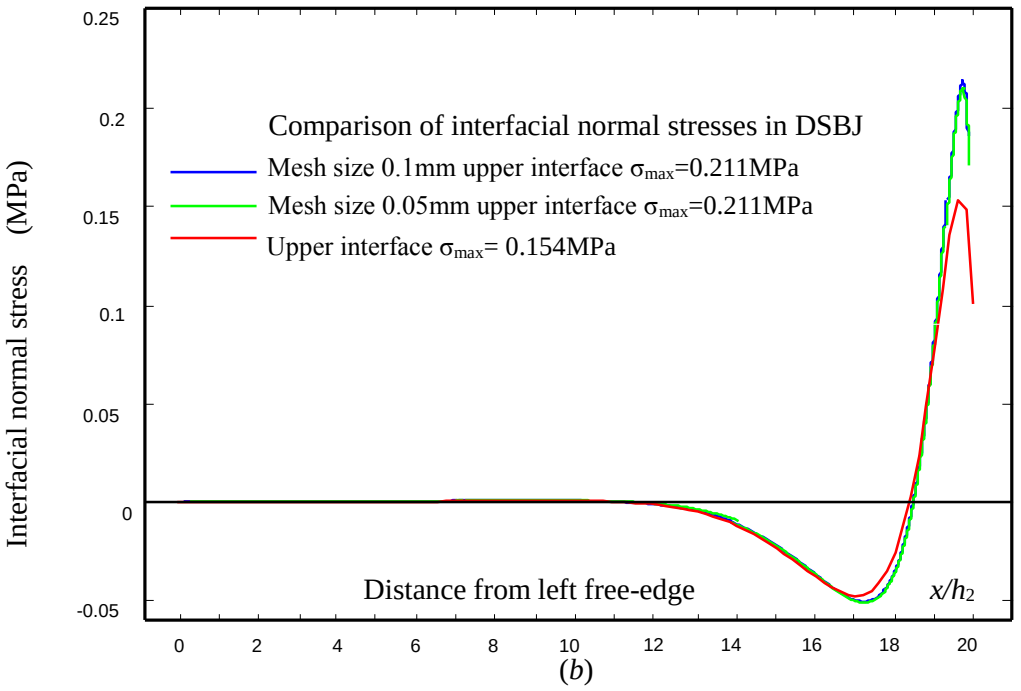


(*b*)

Figure 5.6. Validation of the stress-function variational method for interfacial shear and normal stresses in double-sided bonded joint subjected to axial tension: (*a*) Interfacial shear stress, (*b*) interfacial normal stress.

Due to the double geometrical symmetry, the upper right quarter-portion of the joint is employed for FEA. The interfacial stresses of the upper layer at the right half-length can also represent those at the lower layer or the left half joint. In Fig. 5.6 (*a*), it can be detected that the interfacial shear stress is highly localized within an interval from $x$ = 12 mm to the left free-edge with the peak value around 0.31 MPa. The locus of the peak value of interfacial shear stress predicted by the current method is at $x$ = 19 mm; however, FEM simulation predicts the locus of the peak shear stress at $x$ = 20 mm, almost at the free-end of the joint. In Fig. 5.6 (*b*), it is noticed that the interfacial normal stress also behaves highly localized near the free-edge of the joint. In this case, the peak value of normal stress predicted by the proposed semi-analytic method is 25% lower than that predicted by FEM simulation (ANSYS$^{TM}$). The peak value of the latter is 0.21 MPa as shown in Fig. 5.6(*b*).

5.3.4. Conclusions

DSBJ is another type of commonly used joint models in practice. With the powerful stress-function variational method in this study, two unknown interfacial shear and normal stress functions are introduced at the upper interface of the quarter-joint model. The interfacial shear stresses from the current method exactly satisfy the shear-free condition at the free-end of the joint. By comparison of the model-predicted stress field with those predicted by FEA, the semi-anlytic DSBJ model has been validated. Due to both the shear and normal stresses appear singular near the free-edge of the joint with the close magnitude, the interfacial shear and normal stresses are both responsible for debonding failure of the joint in this case. The deviations of stress results between the ANSYS$^{TM}$ and the present semi-analytic method can be noticed, which implies that some further theoretical refinements could be made in this case.

# 6. CONCLUSIONS

In summary, adhesively bonded joints (ABJs) have been evidenced for use in broad load-carrying aerospace and aeronautical structures, ground vehicles, offshore derricks, etc. Accurate and reliable stress analysis plays a crucial role in optimal design and failure prediction of these ABJs. In this thesis work, by extending Wu and Jenson's seminal work (Wu & Jensen, 2011) on stress-function variational method for stress analysis of bonded joints, this accurate and high-efficiency method has been successfully implemented for stress analysis of ABJs and other three-layered bonded joints. Several theoretical results have been accomplished as follows.

1. By introducing two interfacial shear and normal stress functions on each interface and assuming the linear-varying axial stress across the adherends (*Euler-Bernoulli beam theory*), the entire stress field of three-layered ABJs and bonded joints can be expressed explicitly in terms of the unknown interfacial stress functions. Such formal stress field satisfies all the multiple traction BCs. In particular, the shear-free conditions at the edges of these three-layered ABJs and bonded joints, which have been commonly neglected in most literature ABJ models.
2. The set of governing ODEs (Eq. 3.47) of three-layered ABJs and bonded joints is determined via triggering the theorem of minimum complimentary strain energy, which has been uniformly solved by eigenfunction method. Also, the system matrices [$A$], [$B$], and [$C$] of the ODEs are universal to all the three-layered ABJs and bonded joints, while different type of joints only corresponds to the its specific generalized force column {$D$}.

3. The stress fields of all the three-layered ABJs and bonded joints predicted by the present stress-function variational method in this thesis study have been validated successfully by detailed FEA based on ANSYS$^{TM}$. Comparative studies (Chapters 3, 4 and 5) indicate that the present stress-function variational method is a highly reliable, accurate and efficient semi-analytic method for stress analysis of all three-layered ABJs and bonded joints.
4. The present stress-function varational method also indicates that due to the very high shear and normal stresses near the edges of ABJs (Chapter 3), the stress variation across the thin adhesive layer is noticeable. However, in the majority of the ABJ models in the literature, the stress variation across the adhesive layer is ignored.
5. The theoretical formalism of stress function variational method can be conveniently extended for stress analysis of multi-layered joints and adhesively bonded composite joints, which lays the theoretical basis for universal stress analysis of adhesively multi-material bonded joints.

Furthermore, with the success of the present theoretical study on stress-function varational method for stress analysis of three-layered ABJs and bonded joints, further advanced applications of the present method could be initiated as follows.

1. Formulation of a universal, reliable, high-efficiency stress-function variational method for stress analysis of multi-layered composite joints and related computational code development.
2. Extension of the present stress-function variational method for failure and fracture analysis of joints and composites such as progressive cracking in multilayered coatings and laminated composites, debonding and delamination of ABJs and composite joints, etc.

3. Potential applications of the present stress-function variational method for nondestructive evaluation (NDE) of multilayered structures such as coatings and laminated composites, including static and dynamic methods.
4. Development of reliable finite-strip method for static and dynamic analysis of layered structures, in which all the physical quantities could be potentially expressed as functions of the physical quantities at the surfaces or interfaces by extending the present stress-function variational method.

## REFERENCES


Beer, F., Johnston, E.R., Dewolf, J.T., Mazurek, D.F., 2011. Mechanics of Materials (7th edition). McGraw Hill, New York, USA.

Chataigner, S., Caron, J.F., Diaz, A.D., Aubagna, C., Benzarti, K., 2010. Non-linear failure criteria for a double lap bonded jont. Int. J. Adhes. Adhes. 30, 10-20.

Chen, D., Cheng, S., 1983. An analysis of adhesive-bonded single-lap joints. J. Appl. Mech. Trans. ASME 50, 109-115.

Chen, W.T., Nelson, C.W., 1979. Thermal stress in bonded joints. IBM J. Res. Develop. 23, 179-188.

da Silva, L.F.M., Adams, R.D., 2006. Joint strength predictions for adhesive joints to be used over a wide temperature range. Int. J. Adhes. Adhes. 04:227-35.

Delale, F., Erdogan, F., Aydinoglu, M.N., 1981. Stress in adhesively bonded joints: a closed-form solution. J. Compos. Mater. 15, 249-271.

Diaz, A.D., Hady-Ahmed, R., Foret, G., Ehrlacher, A., 2009. Stress analysis in a classical double lap, adhesively bonded joint with a layerwise model. Int. J. Adhes. Adhes. 29, 67-76.

Eischen, J.W., Chuang, C., Kim, J.H., 1990. Realistic modeling of edge effect stresses in bimetallic elements. J. Electron. Packag. 112, 16-23.

Frostig, Y., Thomsen, O.T., Mortensen, F., 1997. Analysis of adhesive bonded joints, square-end and spew-fillet: higher-order theory approach. J. Eng. Mech., 125(11), 1298-307.

Goland, M., Reissner, E., 1944. The stresses in cemented joints. J. Appl. Mech. Trans. ASME 11, A17-A27.

Goncalves, J.P.M., de Moura, M.F.S.F., de Castro, P.M.S.T., 2002. A three-dimensional finite element model for stress analysis of adhesive joints. Int. J. Adhe. Adhe. 22, 357-65.

Her, S.C., 1999. Stress analysis of adhesively-bonded lap joints. Compos. Struct. 47, 673-8.

Heslehurst, R.B., Hart-Smith, L., 2002. The science and art of structural adhesive bonding. SAMPLE Journal. 60-71.

Higgins, A., 2000. Adhesive bonding of aircraft structures. Int. J. Adhe. Adhe. 20, 367-76.

Jiang, H.Q., Khang, D.Y., Fei, H.Y., Kim, H., Huang, Y.G., Xiao, J.L., Rogers, J.A., 2008. Finite width effect of thin-films buckling on compliant substrate: experimental and theoretical studies. J. Mech. Phys. Solids. 56, 2585-2598.

Kadioglu, F., 2003. Some considerations on the adhesively-bonded joints under environmental conditions. J. Adv. Mater. 35, 61-5.

Keller, T., Valle'e, T., 2004. Adhesively bonded lap joints from Pultruded GFRP profiles. Part I: Stress-strain Analysis and failure modes. Composites B: Eng. 36, 331-340.

Kim, D.H., Rogers, J.A., 2008. Stretchable electronics: Material strategies and devices. Adv. Mater. 20, 1-6.

Kumar, S., Scanlan, J.P., 2013. On axisymmetric adhesive joints with graded interface stiffness. Int. J. Adhes. Adhes. 41, 57-72.

Lee, J., Kim, H., 2005. Stress analysis of generally asymmetric single lap adhesively bonded joints. J. Adhesion. 81,443-472.

Lu, N.S., Yoon, J., Suo, Z.G., 2007. Delamination of stiff islands patterned on stretchable substrates. Int. J. Mater. Res. 98, 717-722.

Mazza, P.P.A., Martini, F., Sala, B., Magi, M., Colombini, M.P., Giachi, G., Landucci, F., Lemorini, C., Modugno, F. and Ribechini, E., 2006. J. Archaeological Sci. 3, 1310-18.

Mortensen, F., Thomsen, O.T., 2002. Analysis of adhesive bonded joints: a unified approach. Compos. Sci. Tech.. 62, 1011-1131.

Ozel, A., Yazici, B., Akpinar, S., Aydin, M.D.A., Temiz, S., 2014. A study on the strength of adhesively bonded joints with different adherends. Composites: B 62, 167-74.

Racker, B., 2004. Bonding processes in airbus in: 2004 FAA Workshop on Adhesive Bonding, Sussex, UK.

Renton, J., Vinson, J.R., 1975. The efficient design of adhesive bonded joints. J. Adhesion. 7,175-193.

Sayman, O., 2012. Elasto-plastic stress analysis in an adhesively bonded single-lap joint. Composites: B 43,204-9.

Seltzer, S.S., Klang, E.C., 2003. Proceeding of the 18th Annual Technical Conference. American Society for Composites. Gainesville, FL, USA.

Suhir, E., 1989. Interfacial stresses in bimaterial thermostats. J. Appl. Mech.-Trans. ASME. 56,595-600.

Suhir, E., 1989. Thermally induced interfacial stresses in elongated bimaterial plates. Appl. Mech. Rev. 42, S253-S262.

Sun, J.Y., Lu, N.S., Oh, K.H., Suo, Z.G., Vlassak, J.J., 2013. Islands stretch test for measuring the interfacial fracture energy between a hard film and a soft substrate. J. Appl. Phys. 113, 223702.

Suo, Z.G., 2012. Mechanics of stretchable electronics and soft machines. MRS Bull. 37, 218-225.

Suo, Z.G., 2003. Reliability of interconnect structures in: Gerbeich, W., Yang, W., Interfacial and Nanoscale Failure. Elsevier, Amsterdam, Netherland, 265-324.

Timoshenko, S., 1915. Analysis of bi-metal thermostats. J. Optical Soc. Amer. 11, 233-255.

Tomblin,J., Davies, C., 2004. Bonded structures industry survey in: 204 PAA workshop on Bonded Structures, Seattle, WA, 2004, June.

Volkersen, O., 1938. Die Nietkraftverleitung in zugbeanspruchten Nietverbindungen mit konstanten Laschenquerschnitten. Luftfahrtforschung 15, 41-47.

Wu, X.F., Jenson, R.A., 2011. Stress-function variational method for stress analysis of bonded joints under mechanical and thermal loads. Int. J. Eng. Sci. 49, 279-294.

Wu, X.F., Jenson, R.A., Zhao, Y., 2014 Stress-function variational method approach to the interfacial stresses and progressive cracking in surface coatings. Mech. Mater. 69, 195-203.

Wu, X.F., Zhao, Y., 2013. Stress-function variational method for interfacial stress analysis of adhesively bonded joints. Int. J. Solids. Struct. 50, 4305-4319.

Xiao, X., Foss, P.H., Schroeder, J.A., 2004. Stiffness prediction of the double lap shear joint. Part 1: analytical bonded joints. Compos. Struct. 65, 499-510.

Yang, C., Huang, H., Tomblin, J.S., Sun W., 2004. Elastic-plastic model of adhesive bonded single-lap composite joints. J. Compos. Mater. 38, 293.

Yang, C., Pang, S.S., 1996. Stress-strain relation of single lap composite joints under tension. J. Eng. Mater. Tech. Trans. ASME 118, 247-255.

Yousefsani, S.A., Tahani, M., 2013a. Accurate determination of stress distribution in adhesively bonded homogenous and heterogeneous double-lap joints. Eur. J. Mech. A 39, 197-208.

Yousefsani, S.A., Tahani, M., 2013b. Analytic solution for adhesively bonded composite single-lap joints under mechanical loadings using full layerwise theory. Int. J. Adhes. Adhes. 43, 32-41.